

# Study on the Formation Processes of Wormlike Micelles Derived from Peptide Amphiphiles

ペプチド両親媒性分子の紐状ミセル形成過程に関する研究

February 2012

Waseda University

Graduate school of Advanced Science and Engineering

Major in Inorganic Synthetic Chemistry,

Research on Prof. Kazuyuki Kuroda

Tomoko Shimada

島田 智子

**Promoter:**

Prof. Kazuyuki Kuroda (Waseda University)

**Referees:**

Prof. Hiroyuki Nishide (Waseda University)

Prof. Yoshiyuki Sugahara (Waseda University)

Pritzker Director, Matthew Tirrell (University of Chicago)

## Preface

Peptide Amphiphiles (PA) are surfactants that have hydrophilic peptides and hydrophobic alkyl tails in the molecules. PA have many advantages as compared to conventional surfactants, including highly ordered structures (i.e. peptide secondary structures), bioactivity and wide-spread freedom of design in the peptide region. The self-assembled structures of PA such as bi-layers, vesicles and spherical micelles receive much attention as drug carriers and nano-reactors. Especially, wormlike micelles, unidirectionally long extended micelles, of PA are actively studied because the gel formed of the wormlike micelles is a promising candidate for new-functionalized scaffolds in regenerative medicine. Though the manipulation of the wormlike micelle formation and gelation is required to get the functional gel in an appropriate timing, at appropriate place, the mechanism of the micelle formation has not been fully understood because it is affected by various non-covalent interactions including hydrophobic interactions, electrostatic interactions, and hydrogen bonding. Further, most of the previously reported PA have been designed to have bio-functional amino sequences derived from proteins, and formation of the PA wormlike micelles requires some triggers, such as pH change, which makes it difficult to analyze the detailed structural changes during the formation process.

Therefore, in this thesis, the author especially focuses on the design of novel peptide amphiphile (C16-W3K) that form wormlike micelles with “simple structure”, at “slow formation speed” and in the “absence of a need

for a specific trigger”, and studies the time-dependent structural changes of peptide secondary structure, self-assembled structure, and mechanical property of the solution with various analytical methods. Chapter 1 describes recapitulation of peptide amphiphiles and summary of previous papers about PA wormlike micelles. Chapter 2 and 3 show the design and synthesis of C16-W3K and structural changes during the wormlike micelle formation. Chapter 4 and 5 describe the control of the structural changes by simple mechanical shear and addition of a fluoro-alcohol, respectively. In Chapter 6, the author proposes a new preparative method of silica nanotubes with templates of C16-W3K wormlike micelles, as an example for potential applications of the PA wormlike micelles. The last chapter concludes this thesis and the future prospects are summarized.

# Contents

## Chapter 1: General Introduction

1.1 What is Peptide Amphiphiles (PA)?	2
1.2 Synthesis of Peptide Amphiphiles	3
1.3 Structures of Peptide Amphiphiles	4
1.3.1 Molecular structures	4
1.3.2 Peptide secondary structures	5
1.3.3 Self-assembled structures	6
1.4 PA wormlike micelles	8
1.4.1 List of the previously reported PA	8
1.4.2 Applications of PA wormlike micelles	13
1) PA wormlike micelles as materials for scaffolds	13
2) PA wormlike micelles for delivery	22
3) PA wormlike micelles as templates for biomineralization	24
4) PA wormlike micelles for surface modification and patterning	25
5) Other potential applications	29
1.4.3 Structural analysis on PA wormlike micelles	32
1) Effect of alkyl tail length	32
2) Role of $\beta$ -sheet structure	32
3) Effect of electrostatic interaction	35
4) Simulation	36
5) Inner environment of PA wormlike micelles	38
1.5 Motivation for the thesis	39
References	40

## **Chapter 2:**

### **Wormlike Micelle Formation in Peptide Amphiphile Driven by**

#### **Secondary Structure Transformation of the Headgroups**

2.1 Introduction .....	44
2.2 Experimental methods .....	46
2.2.1 Design and synthesis of the peptide amphiphile; C16-W3K .....	46
2.2.2 Sample analysis .....	47
2.3 Results .....	48
2.3.1 Self-assembled structure .....	48
2.3.2 Peptide secondary structure .....	49
2.3.3 Effect of temperature on the peptide transition .....	51
2.3.4 Effect of PA alkyl tail length on the peptide transition .....	51
2.3.5 Effect of initial micelle formation on the peptide transition .....	52
2.4 Discussion .....	53
2.5 Conclusion .....	55
References .....	56

## **Chapter 3:**

### **Self-Assembly Process of Peptide Amphiphile Wormlike Micelles**

3.1 Introduction .....	68
3.2 Experimental methods .....	69
3.2.1 Design and synthesis of the peptide amphiphile; C16-W3K .....	69
3.2.2 SANS measurements .....	70
3.2.3 AFM measurements .....	70

3.3 Results and discussion .....	71
3.4 Conclusion .....	76
References .....	77

## **Chapter 4:**

### **Wormlike Micelle formation of Peptide Amphiphiles Induced by Fluid**

#### **Mechanical Shear**

4.1 Introduction .....	87
4.2 Experimental methods .....	89
4.2.1 Synthesis and material preparation .....	89
4.2.2 Rheological measurements .....	90
4.2.3 Cryogenic transmission electron microscopy .....	90
4.2.4 Atomic force microscopy .....	91
4.2.5 Circular dichroism .....	91
4.2.6 Infrared spectroscopy .....	92
4.3 Results .....	92
4.3.1 Rheological testing .....	92
4.3.2 Micellar structures .....	94
4.3.3 Peptide secondary structures .....	95
4.4 Discussion .....	96
4.5 Conclusion .....	98
References .....	99

## **Chapter 5:**

### **Disassembly of Peptide Amphiphile Wormlike Micelles Induced by Trifluoro Ethanol**

5.1 Introduction.....	111
5.2 Experimental methods.....	112
5.3 Results.....	113
5.3.1 Effect of TFE on the peptide secondary structure.....	113
5.3.2 Effect of TFE on the micelle structure.....	113
5.4 Discussion.....	114
5.5 Conclusion.....	116
References.....	117

## **Chapter 6:**

### **A Novel Method of Silica Nanotubes by Utilizing Self-Assembly and Disassembly of Peptide Amphiphiles**

6.1 Introduction.....	122
6.2 Experimental methods.....	123
6.3 Results and discussion.....	125
6.4 Conclusion.....	129
References.....	130



## **Chapter 7: Conclusions and Future Prospects**

7.1 Conclusions .....	137
7.2 Future prospects.....	140

List of publications and oral presentations

Acknowledgement

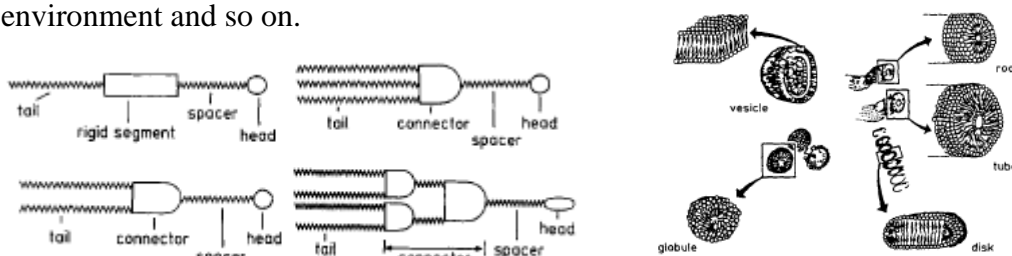
# **Chapter 1**

## **General Introduction**

## 1.1 What is Peptide-amphiphiles?

Peptide amphiphiles (PA) are amphiphilic molecules with a hydrophilic peptide head-group and a hydrophobic alkyl tail in one molecule. Due to the amphiphilicity, the PA self-assemble into various structures like conventional surfactants. However, the PA have some unique features because of the peptide head-group, designed from free combination and order of the amino acids. A peptide chain of PA could form secondary structures ( $\alpha$ -helix,  $\beta$ -sheet, random coil) and provide a bioactivity to the molecule. In contrast, a hydrophobic alkyl tail works to align the peptides by tethering, drive self-assembly of the molecules due to its hydrophobic interactions, and induce and/or stabilizes the secondary structure of the peptide. Recently, many PA were designed to have some specific bioactivities for potential applications in medical fields.

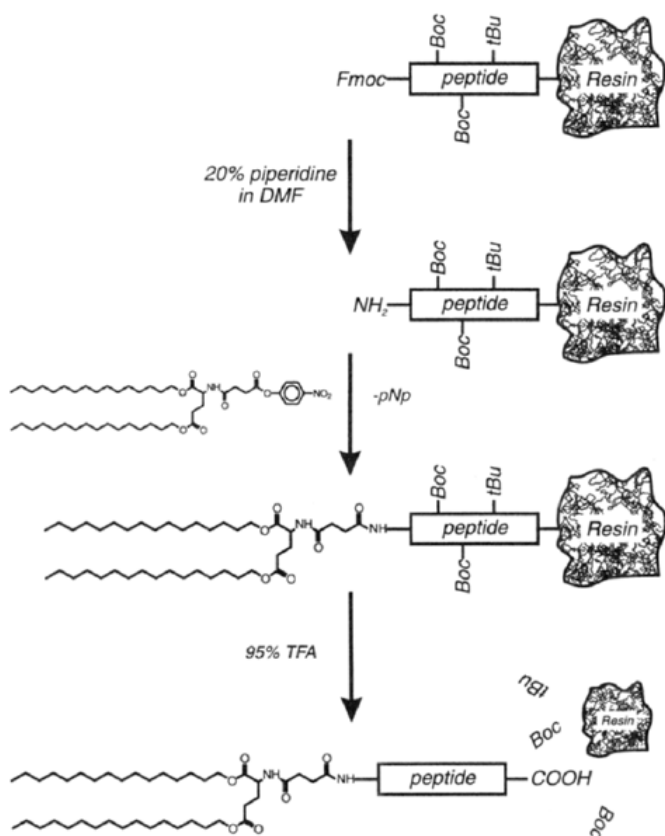
Originally, Kunitake proposed the first concept of peptide-amphiphiles in 1992, composed of a hydrophilic head-group, a spacer, a connector and an alkyl tail<sup>1</sup> (Figure 1-1). He synthesized various types of amphiphiles and exhibited that the assembled structures can be controlled by changing the structure of the amphiphiles. From these findings, many peptide amphiphiles were synthesized and the assembled structure of the PA were studied and controlled by changing the peptide sequence, alkyl tail length, the environment and so on.



**Figure 1-1.** Schematic drawing of the amphiphilic molecules and assembled structures of the amphiphilic molecules.<sup>1</sup>

## 1.2 Synthesis of Peptide Amphiphiles

The method for PA synthesis was firstly reported by M. Tirrell et al as shown in Figure 1-2<sup>2</sup>.



**Figure 1-2.** Synthesis process of peptide amphiphiles by a modification of solid-phase Fmoc method.

At first, designed peptides were synthesized by solid-phase Fmoc method using commercially available resin. Then after removal of the N-terminal Fmoc group with 20% piperidine in dimethylformamide (DMF), the tail compound was coupled to the protected peptide on the resin in dichloromethane (DCM) and DMF for hours. Next, deprotection and cleavage from the resin were performed by adding 95% trifluoroacetic acid to the solution. The resultant peptide amphiphile was precipitated with cold ether, and purified by HPLC with a C4 reversed-phase column.

### **1.3 Structures of Peptide Amphiphiles**

The most important feature of the PA structures is its well-ordered hierarchical structure, including a peptide secondary structure and an assembled structure. In this section, the PA structures in different scales are explained.

#### **1.3.1 Molecular structures**

- **Peptide region**

The most prominent feature of peptide amphiphiles is a peptide region that can be designed from free selection and combination of more than twenty amino acids. A peptide secondary structure is basically determined by the amino sequence of the peptide. Since every amino acid has a unique feature, categorized to an acidic amino acid such as aspartic acid, a basic amino acid including lysine and histidine, the amino acid with benzene ring etc., it is important to design an appropriate amino sequence to have desirable bio activity or micelle structures. Some amino sequences in proteins are known to have specific bio activities, which are often incorporated in the peptide of PA.

- **Alkyl tail**

Alkyl tails of PA provide hydrophobic interactions, which is the most common driving force for self-assembly<sup>3</sup>. A number of the alkyl tails and an alkyl tail length in PA can be easily modified by changing the tail compounds, leading various typed of self-assembled structures.

### 1.3.2 Peptide secondary structures

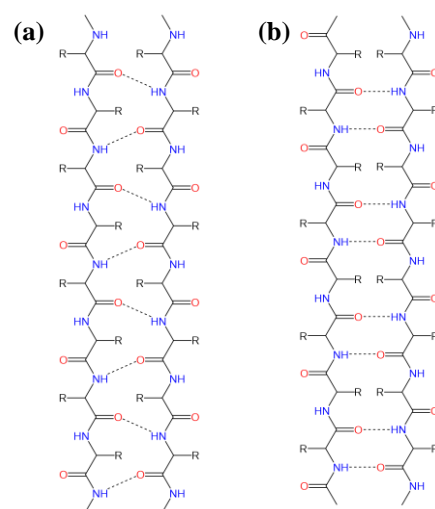
Peptides form secondary structures, highly organized structures, defined by patterns of hydrogen bonding of peptides. There are two main types of secondary structures;  $\alpha$ -helix and  $\beta$ -sheet.

- **$\alpha$ -helix**

An  $\alpha$ -helix is the most prevalent secondary structure in proteins and polypeptides. The  $\alpha$ -helical structure is a right-handed spiral conformation, in which a N-H group in the peptide backbone provides a hydrogen bonding to a C=O group of the amino acid four residues earlier. Different amino acid sequences have different propensities to form  $\alpha$ -helical structure. For example, methionine, alanine, leucine, and lysine are known to have high  $\alpha$ -helical propensities, whereas proline and glycine have poor helical propensities.

- **$\beta$ -sheet**

A  $\beta$ -sheet structure consists of almost fully extended peptide chains connected laterally by intermolecular hydrogen bonding. There are two major types of  $\beta$ -sheet structure; parallel and anti-parallel. In the parallel  $\beta$ -sheet, two peptide chains run in the same direction, while the anti-parallel  $\beta$ -sheet is characterized by two peptides running in opposite directions as shown in Figure 1-3 (a) and (b), respectively.



**Figure 1-3.** Two structures of  $\beta$ -sheet; parallel and anti-parallel

### 1.3.3 Self-assembled structures

In an aqueous solution, surfactants, including peptide amphiphiles, self-assemble into a variety of spatially organized structures, such as spherical micelles, cylindrical micelles and bilayers. The self-assembly of surfactants is mainly driven by relatively weak non-covalent bonding.






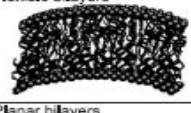
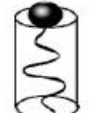


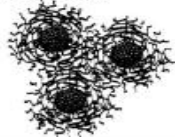
A commonly used method to evaluate and predict the type of self-assembled structures is a packing parameter  $P$ <sup>4</sup>;

$$P = v/a_0l$$

, where  $v$  is a volume of a tail group,  $a_0$  is an area of a head group, and  $l$  is a length of an alkyl tail. By using the packing parameter, morphology of assembled structures can be predicted as shown in Table 1-1.

For controlling the packing parameter to obtain an applicable assembled structure, manipulation of the tail group (changing the tail length or the number of tails) is one of the simplest ways. Further, manipulating the head-group is also an effective way, especially for peptide amphiphiles because the peptide head group can be designed easily and freely as described above. However, the assembled structure of PA does not only depend on the space filling dimension as a packing parameter, but various other

**Table 1-1.** Packing parameter and micelle structures<sup>4</sup>

Critical Packing parameter ( $v/a_0l$ )	Critical packing shape	Structure Formed
$<1/3$	Cone 	Spherical micelle 
$1/3 - 1/2$	Truncated cone 	Cylindrical micelle 
$1/2 - 1$	Truncated cone 	Flexible bilayers 
$\sim 1$	Cylinder 	Planar bilayers 
$>1$	Inverted truncated cone 	Inverted micelles 

interactions. There are three major interactions that govern self-assembly of PA in water: hydrophobic interactions among alkyl tails, hydrogen bonding between the peptides and peptide-water, and electrostatic interactions between the charged amino acids in the peptides. For example, the charged amino acid residues repelled each other increase the head group area  $a_0$ , generally leading the formation of spherical micelles. To obtain cylindrical micelles with such PA, electrolytes are often added to screen the electrostatic interactions. The final assembled structure is determined by a delicate balance of all the interactions.

Further, it has been reported that the self-assembly of PA correlates with induction and stabilization of the secondary structure in the peptides in some peptide amphiphiles. The previous studies in the Tirrell's group<sup>5,6</sup> showed that peptides in the PA can adopt ordered secondary structures, both triple-helix and  $\alpha$ -helix, when the PA form micelle structures, while the peptides without alkyl tails did not form ordered structure. The induction of ordered secondary structure may be due to the configurational constraints imposed by a combination of elevated local peptide concentration in the shell of the micelle, and the reduction in translational and rotational degrees of freedom caused by peptide tethering.



## **1.4 PA wormlike micelles**

### **1.4.1 List of the previously reported PA**

Among the various types of self-assembled structures of PA, a wormlike micelle of PA is one of the most attractive structures for many applications because of its homogeneous and tunable diameter and the peptides on the surface that can form secondary structures and exhibit bioactivity.

Recently, W. Hamley reviewed almost all the PA that have been reported to form wormlike micelles (Table 1-2)<sup>7</sup>. Though the list clearly exhibits that many PA that have various functional peptides derived from proteins were synthesized and studied recently for bio-applications, a number of the PA is still limited and there are few systematic studies to elucidate the mechanism of the formation of PA wormlike micelles.

**Table 1-2.** The list of PA systems previously reported <sup>7</sup>

Amphiphilic peptide	Peptide design	Nature of study	Reference
<i>Surfactant-like peptides</i>			
A <sub>6</sub> D, V <sub>6</sub> D, V <sub>6</sub> D <sub>2</sub> , L <sub>6</sub> D <sub>2</sub>	<i>de novo</i> design	Nanotube formation	15
G <sub>4</sub> D <sub>2</sub> , G <sub>6</sub> D <sub>2</sub> , G <sub>8</sub> D <sub>2</sub> , G <sub>10</sub> D <sub>2</sub>	<i>de novo</i> design	Nanotube and vesicle formation	16
V <sub>6</sub> K, V <sub>6</sub> K <sub>2</sub> , V <sub>3</sub> K	<i>de novo</i> design	Adsorption at the air/solid interface, DNA immobilization	17
V <sub>6</sub> K <sub>2</sub> , L <sub>6</sub> K <sub>2</sub> , A <sub>6</sub> K, V <sub>6</sub> H, V <sub>6</sub> K, H <sub>2</sub> V <sub>6</sub> , KV <sub>6</sub>	<i>de novo</i> design	Nanotube and vesicle formation	18
Ac-A <sub>6</sub> D-COOH and Ac-A <sub>6</sub> K-COOH	<i>de novo</i> design	Self-assembly and cac determination	19
Mixtures of Ac-A <sub>6</sub> D-OH and Ac-A <sub>6</sub> K-NH <sub>2</sub>	<i>de novo</i> design	Synergistic effects on cac, and observation of twisted fibrils	20
Ac-GAVILRR-NH <sub>2</sub>	<i>de novo</i> design	Formation of "nanodonut" structures	23
I <sub>6</sub> K <sub>2</sub> , L <sub>6</sub> K <sub>2</sub> , V <sub>6</sub> K <sub>2</sub>	<i>de novo</i> design	Self-assembled morphology correlated to secondary structure	24
V <sub>6</sub> D <sub>2</sub> , V <sub>3</sub> DVD, V <sub>4</sub> D <sub>2</sub> V <sub>2</sub>	<i>de novo</i> design	Influence of sequence and purity on self-assembly	25
A <sub>3</sub> K, A <sub>6</sub> K, A <sub>9</sub> K	<i>de novo</i> design	Determination of cmc, self-assembled structures	26
A <sub>6</sub> K	<i>de novo</i> design	Antibacterial properties	27
Ac-A <sub>2</sub> V <sub>2</sub> L <sub>2</sub> WG <sub>2</sub> -COOH and Ac-A <sub>2</sub> V <sub>2</sub> L <sub>2</sub> WG <sub>7</sub> -COOH	<i>de novo</i> design	Nanotube formation	28
chol-H <sub>3</sub> R <sub>10</sub> , chol-H <sub>10</sub> R <sub>10</sub> , chol denotes cholesterol	<i>de novo</i> design	Nanotube structure	29
A <sub>12</sub> H <sub>5</sub> K <sub>10</sub> , A <sub>12</sub> H <sub>5</sub> K <sub>15</sub> and H <sub>3</sub> K <sub>10</sub> (non-amphiphilic control)	<i>de novo</i> design	Formation of vesicles	40
Ac-(AF) <sub>6</sub> H <sub>3</sub> K <sub>15</sub> -NH <sub>2</sub>	<i>de novo</i> design	Gene delivery	104
NH <sub>2</sub> -I <sub>3</sub> H <sub>4</sub> R <sub>8</sub> -CONH <sub>2</sub> , NH <sub>2</sub> -F <sub>3</sub> H <sub>4</sub> R <sub>8</sub> -CONH <sub>2</sub> , NH <sub>2</sub> -W <sub>3</sub> H <sub>4</sub> R <sub>8</sub> -CONH <sub>2</sub> , NH <sub>2</sub> -H <sub>4</sub> R <sub>8</sub> -CONH <sub>2</sub> , chol-G <sub>3</sub> R <sub>6</sub> TAT, TAT = YGRKKRRQRRR	<i>de novo</i> design	Gene delivery	105
A <sub>6</sub> D and A <sub>6</sub> K	Contains TAT sequence	Co-delivery of drug and DNA (gene delivery)	106
A <sub>6</sub> D and A <sub>6</sub> K	<i>de novo</i> design	Gene delivery	107
Ac-V <sub>6</sub> R <sub>2</sub> -NH <sub>2</sub> , Ac-V <sub>6</sub> K <sub>2</sub> -NH <sub>2</sub> , Ac-A <sub>6</sub> K-NH <sub>2</sub> , Ac-I <sub>6</sub> K <sub>2</sub> -NH <sub>2</sub> , Ac-A <sub>6</sub> K-OH, DA <sub>6</sub> -NH <sub>2</sub> , Ac-V <sub>6</sub> D <sub>2</sub> -NH <sub>2</sub> , Ac-A <sub>6</sub> D-OH, K <sub>A6</sub> -NH <sub>2</sub>	<i>de novo</i> design	Antimicrobial properties	112
H-K <sub>3</sub> -[W <sup>D</sup> L] <sub>3</sub> -W-NH <sub>2</sub> , H-CK <sub>3</sub> -[W <sup>D</sup> L] <sub>3</sub> -W-NH <sub>2</sub> , Ac-[K(Ac)] <sub>3</sub> -W-[W <sup>D</sup> L] <sub>3</sub> -W-NH <sub>2</sub> , Ac-C[K(Ac)] <sub>3</sub> -W-[W <sup>D</sup> L] <sub>3</sub> -W-NH <sub>2</sub> , Ac-C(sI)[K(Ac)] <sub>3</sub> -W-[W <sup>D</sup> L] <sub>3</sub> -W-NH <sub>2</sub> , sI denotes the spin label acetamidopropyl	<i>de novo</i> design	Stabilization of G-protein coupled receptor bovine rhodopsin against denaturing	118
A <sub>6</sub> D and A <sub>6</sub> K	<i>de novo</i> design	Stabilization of protein complex Photosystem-I and enhancement of activity	119–121
H-K <sub>3</sub> -[W <sup>D</sup> L] <sub>3</sub> -W-NH <sub>2</sub> , H-CK <sub>3</sub> -[W <sup>D</sup> L] <sub>3</sub> -W-NH <sub>2</sub> , Ac-[K(Ac)] <sub>3</sub> -W-[W <sup>D</sup> L] <sub>3</sub> -W-NH <sub>2</sub> , Ac-C[K(Ac)] <sub>3</sub> -W-[W <sup>D</sup> L] <sub>3</sub> -W-NH <sub>2</sub> , Ac-C(sI)[K(Ac)] <sub>3</sub> -W-[W <sup>D</sup> L] <sub>3</sub> -W-NH <sub>2</sub> , sI denotes the spin label acetamidopropyl	<i>de novo</i> design	Micelle aggregation and formation of particles and beads	42
<i>Lipidated peptides</i>			
C <sub>n</sub> -C <sub>4</sub> G <sub>3</sub> S(Phos)RGD n = 6, 10, 16, 22, C <sub>n</sub> -A <sub>4</sub> G <sub>3</sub> S(Phos)RGD n = 10, 16, C <sub>16</sub> -C <sub>4</sub> G <sub>3</sub> S(Phos), C <sub>16</sub> -C <sub>4</sub> G <sub>3</sub> S(Phos)KGE, C <sub>16</sub> -C <sub>4</sub> G <sub>3</sub> S(Phos)RGDS, C <sub>16</sub> -C <sub>4</sub> G <sub>3</sub> SRGD, C <sub>16</sub> -C <sub>4</sub> G <sub>3</sub> EIKVAV, S(Phos) denotes phosphorylated serine	<i>de novo</i> design	Influence of PA structure on self-assembly, and covalent capture by disulfide cross-linking	43
C <sub>16</sub> O-V <sub>3</sub> A <sub>3</sub> E <sub>3</sub> , C <sub>16</sub> O-V <sub>2</sub> A <sub>2</sub> E <sub>3</sub> , C <sub>16</sub> O-V <sub>4</sub> A <sub>4</sub> E <sub>3</sub> , C <sub>16</sub> O-V <sub>2</sub> A <sub>4</sub> E <sub>3</sub> , C <sub>16</sub> O-V <sub>4</sub> A <sub>2</sub> E <sub>3</sub> , C <sub>16</sub> O-A <sub>3</sub> V <sub>3</sub> E <sub>3</sub>	<i>de novo</i> design	Mechanical properties of hydrogels	44
C <sub>16</sub> O-V <sub>3</sub> A <sub>3</sub> E <sub>3</sub> , C <sub>16</sub> O-V <sub>2</sub> A <sub>2</sub> E <sub>3</sub> , C <sub>16</sub> O-V <sub>4</sub> A <sub>4</sub> E <sub>3</sub> , C <sub>16</sub> O-V <sub>2</sub> A <sub>4</sub> E <sub>3</sub> , C <sub>16</sub> O-V <sub>4</sub> A <sub>2</sub> E <sub>3</sub> , C <sub>16</sub> O-A <sub>3</sub> V <sub>3</sub> E <sub>3</sub>	<i>de novo</i> design	Influence of sequence on hydrogen bond alignment, fibril twisting and gel stiffness	45
GWVAVKIEG <sub>3</sub> A <sub>4</sub> -OC <sub>16</sub> , VAVKIEG <sub>3</sub> A <sub>4</sub> W-OC <sub>16</sub> , VAVKIEG <sub>3</sub> A <sub>4</sub> -COC <sub>3</sub> H <sub>6</sub> -Pyrene, G(K-COCH <sub>2</sub> Pyrene) EVAVKIEG <sub>3</sub> A <sub>4</sub> -OC <sub>16</sub> , VAVKIEG <sub>3</sub> A <sub>4</sub> (K-COCH <sub>2</sub> Pyrene)-OC <sub>16</sub> , VAVKIEG <sub>3</sub> A <sub>4</sub> -OC <sub>16</sub>	<i>de novo</i> design	Tryptophan and pyrene fluorescence of solvation of PA fibrils	46
C <sub>16</sub> ONH-A <sub>4</sub> G <sub>3</sub> EIKVAV-COOH, C <sub>16</sub> ONH-A <sub>4</sub> G <sub>3</sub> KYIGSR-CONH <sub>2</sub> , C <sub>16</sub> ONH-C <sub>4</sub> G <sub>3</sub> S(Phos)RGDS-COOH, C <sub>16</sub> ONH-C <sub>4</sub> G <sub>3</sub> KIKVAV-CONH <sub>2</sub>	<i>de novo</i> design	Coassembly of PAs with oppositely charged peptide sequences	47

Amphiphilic peptide	Peptide design	Nature of study	Reference
C <sub>16</sub> ONH-V <sub>3</sub> A <sub>3</sub> K <sub>3</sub> -COOH, C <sub>16</sub> ONH-V <sub>3</sub> A <sub>3</sub> E <sub>3</sub> -COOH, C <sub>12</sub> ONHCO-CH <sub>2</sub> CH(CCONH <sub>2</sub> )V <sub>6</sub> K <sub>3</sub> -NH <sub>2</sub> , C <sub>12</sub> ONHCO-CH <sub>2</sub> CH(CCONH <sub>2</sub> )V <sub>3</sub> A <sub>3</sub> E <sub>3</sub> -NH <sub>2</sub>	<i>de novo</i> design	Mixing of PAs with free C- and N-termini	48
COOH-GE <sub>3</sub> L <sub>3</sub> -COC <sub>5</sub> H <sub>10</sub> -(urea oligomer), COOH-GE <sub>3</sub> L <sub>3</sub> -COC <sub>5</sub> H <sub>10</sub> -(urea oligomer), COOH-E <sub>3</sub> L <sub>3</sub> -COC <sub>5</sub> H <sub>10</sub> -(urea oligomer)	<i>de novo</i> design	Nanofibril formation by asymmetric peptide bolaamphiphiles	49
C <sub>16</sub> -V <sub>3</sub> A <sub>3</sub> K <sub>3</sub>	<i>de novo</i> design	Formation of macroscopic gels and membranes at the interface of PA and hyaluronic acid solutions	50
C <sub>16</sub> O-VEVE and C <sub>16</sub> O-VEVEGRGD	<i>de novo</i> design	Nanobelt formation	52
C <sub>16</sub> O-F <sub>3</sub> E <sub>3</sub> , C <sub>16</sub> O-A <sub>3</sub> E <sub>3</sub>	<i>de novo</i> design	Twisted ribbon to helical ribbon transition	53
WRGDSG <sub>3</sub> A <sub>3</sub> (K)-C <sub>16</sub> O, K(WRGDS-K)KX <sub>3</sub> A <sub>3</sub> (K)-C <sub>16</sub> O; X = G or VCH <sub>3</sub> , K(RGDSW-K)KX <sub>3</sub> A <sub>3</sub> (K)-C <sub>16</sub> O; X = G or VCH <sub>3</sub> , RGDSG <sub>3</sub> A <sub>3</sub> (K)-C <sub>16</sub> O, K(RGDS-K)KL <sub>3</sub> A <sub>3</sub> (K)-C <sub>16</sub> O, (RGDS-K)K(K-RGDS)L <sub>3</sub> A <sub>3</sub> (K)-C <sub>16</sub> O, <sup>15</sup> D(RGDS-D)KL <sub>3</sub> A <sub>3</sub> (K)-C <sub>16</sub> O, K(GRSDSD-K)KL <sub>3</sub> A <sub>3</sub> (K)-C <sub>16</sub> O, RGDSD denotes cyclic peptide	<i>de novo</i> designs incorporating RGDS cell adhesion motif	Influence of branching on PA self-assembly	54
C <sub>12</sub> COOH(CH <sub>2</sub> ) <sub>2</sub> D(C <sub>12</sub> )A <sub>2</sub> -C <sub>10</sub> N(CH <sub>3</sub> ) <sup>3+</sup> Br <sup>-</sup> , Thy-C <sub>12</sub> COOH(CH <sub>2</sub> ) <sub>2</sub> D(C <sub>12</sub> )F <sub>2</sub> -C <sub>10</sub> N(CH <sub>3</sub> ) <sup>3+</sup> Br <sup>-</sup> , Thy denotes thymine	<i>de novo</i> designs	Use of PA nanofibrils to attach gold nanoparticles via complementary interactions	55
C <sub>16</sub> -A <sub>6</sub> E <sub>3</sub> , C <sub>16</sub> -V <sub>2</sub> A <sub>2</sub> E <sub>2</sub> G <sub>2</sub> REDKETV, C <sub>16</sub> -V <sub>2</sub> A <sub>2</sub> E <sub>2</sub> G <sub>2</sub> TKRE <sub>2</sub> VD, C <sub>16</sub> -A <sub>2</sub> E <sub>2</sub> G <sub>2</sub> REDKETV	<i>de novo</i> design	X-Ray induced ordering	56
C <sub>16</sub> -V <sub>3</sub> A <sub>3</sub> E <sub>3</sub> and others	<i>de novo</i> design	Formation of aligned monodomain strings	57
C <sub>n</sub> -KTVIII-NH <sub>2</sub> ; n = 6, 8, 10, 12, 14, 16	<i>de novo</i> design	Thermal stability as a function of alkyl chain length	59
C <sub>n</sub> O-KTVIIE-NH(CH <sub>2</sub> ) <sub>2</sub> -(EO) <sub>68</sub> -OH; n = 6, 8, 10, 12, 14, C <sub>18</sub> ONHCO(nitrobenz)-KTVIIE-NH(CH <sub>2</sub> ) <sub>2</sub> -(EO) <sub>68</sub> -OH, EO denotes ethylene oxide, nitrobenz denotes a nitrobenzyl unit with linker	<i>de novo</i> design	Balance between hydrophobic/hydrophilic self-assembly by attachment of PEG. UV-induced disassembly	60
C <sub>n</sub> -GANPNAAG; n = 6, 8, 10, 12, 14, 16	Derived from protein of the malaria parasite <i>Plasmodium falciparum</i>	Formation of β-sheet structure for sufficiently long alkyl chain, and thermal stabilization of β-sheet	61
C <sub>24</sub> CO-GANPNAAG, C <sub>24</sub> chain contains diacetylene at 4,6- 10,12- or 16,18-positions,	Derived from protein of the malaria parasite <i>P. falciparum</i>	Influence of cross-linking polymerization of hydrophobic chains on chromatic properties	62
(10,12-derivative)		Patterning using polarization holography	63
C <sub>16</sub> -G <sub>7</sub> with <sup>15</sup> N-G substitution in 0–6 positions, C <sub>16</sub> -(G <sub>6</sub> A)ERGDS with A position varied	<i>de novo</i> design	Fibril secondary structure and β-sheet packing motif	65
C <sub>16</sub> O-A <sub>4</sub> K <sub>4</sub> , C <sub>16</sub> O-A <sub>4</sub> H <sub>4</sub> , C <sub>16</sub> O-A <sub>4</sub> E <sub>4</sub> , C <sub>16</sub> O-A <sub>8</sub> K <sub>4</sub> , C <sub>16</sub> O-A <sub>12</sub> K <sub>4</sub>	<i>de novo</i> design	Templating of silica nanotubes by PA nanofibrils	66
C <sub>8</sub> -KLVFFAE	Amyloid β peptide sequence Aβ(16–22).	Influence of lipidation on β-sheet structure	67
(C <sub>16</sub> ) <sub>2</sub> -EC <sub>2</sub> -X; X = G, A, V, K, COOH, AOEt, AOBz, IV-H1, IV-H1-GP <sup>0</sup> PGP <sup>0</sup> PGP <sup>0</sup> PP, [IV-H1] = GNKGNGPWPGAP is a type IV collagen sequence	<i>de novo</i> designs and modified type IV collagen sequence	Formation of monolayers at the air/water interface, and packing within the monolayer	68
DOPE-(LG) <sub>2</sub> , DOPE-(LG) <sub>3</sub> , DOPE-(LG) <sub>4</sub> , DOPE = dioleoylphosphatidyl ethanolamine	<i>de novo</i> design	Ordering of β-sheets in monolayers at the air/water interface	69
C <sub>12</sub> -EVHHQKL	Amyloid β peptide sequence Aβ(11–17).	Amyloid fibrillisation	70
NH <sub>2</sub> -SDDFGAIV-SO <sub>2</sub> -N(C <sub>n</sub> )(CH <sub>2</sub> OH)SCONH <sub>2</sub> n = 12, 15, 16, 18	Modified amylin(20–29) peptide	Fibrillisation	71
(C <sub>16</sub> ) <sub>2</sub> -GC <sub>2</sub> G, (C <sub>16</sub> ) <sub>2</sub> -GC <sub>2</sub> -[IV-H1]-Y, (C <sub>16</sub> ) <sub>2</sub> -GC <sub>2</sub> -(GPHyp) <sub>4</sub> -[IV-H1], (C <sub>14</sub> ) <sub>2</sub> -GC <sub>2</sub> -[IV-H1]-(GPHyp) <sub>4</sub>	Modified type IV collagen sequence and control	Formation of triple-helical structure and enhanced thermal stability compared to unlipidated peptides	72
C <sub>6</sub> - C <sub>8</sub> -, C <sub>10</sub> -, C <sub>12</sub> - C <sub>14</sub> - & C <sub>16</sub> - & (C <sub>12</sub> ) <sub>2</sub> -, (GPHyp) <sub>4</sub> -[IV-H1]-(GPHyp) <sub>4</sub>	Modified type IV collagen sequence	Stabilization of polypro II triple helical structures	73
C <sub>6</sub> - & C <sub>16</sub> - & (C <sub>12</sub> ) <sub>2</sub> -G-C <sub>2</sub> -KA[GIGALKA] <sub>2</sub> , KA[GIGALKA] <sub>2</sub> ,	<i>de novo</i> 16-residue coiled coil peptide	Influence of alkyl chain on helical secondary structure formation, and thermal stability	74
C <sub>6</sub> -, C <sub>8</sub> -, C <sub>10</sub> -, C <sub>12</sub> - C <sub>14</sub> - & C <sub>16</sub> - & (C <sub>12</sub> ) <sub>2</sub> -G-C <sub>2</sub> -, [GPG] <sub>4</sub> (GVKGNKGNPWPGAP)[GPG] <sub>4</sub>	Collagen-derived		
* C <sub>16</sub> -WAAAAAKAAAAAKA	<i>de novo</i> design	Transformation from spherical to wormlike micelles with development of β-sheet structure	75

\*the author's

Amphiphilic peptide	Peptide design	Nature of study	Reference
C <sub>11</sub> ONH-VRGDV, C <sub>12</sub> ONH-VRGDV, C <sub>12</sub> ONH-ERGD, Fmoc-VRGDV	RGD cell adhesion motif	pH effect on self-assembly	76
NH <sub>2</sub> (CH <sub>2</sub> ) <sub>4</sub> CHNH <sub>2</sub> CO-GPAALKRARNYEAARRSRARKLQRMKQLE-(EIEALKA)-K $\epsilon$ -C <sub>12</sub> -MMA, MMA denotes methyl methacrylate	DNA binding sequence and coiled-coil septet	Self-assembly	77
(C <sub>18</sub> ) <sup>2</sup> OCO(CH <sub>2</sub> ) <sub>2</sub> CH(COOC <sub>18</sub> )( $\beta$ A)RGD-COOH, (C <sub>18</sub> ) <sup>2</sup> OCO(CH <sub>2</sub> ) <sub>2</sub> CH(COOC <sub>18</sub> )( $\beta$ A)DGR-NH <sub>2</sub> , (C <sub>18</sub> ) <sup>2</sup> OCO(CH <sub>2</sub> ) <sub>2</sub> CH(COOC <sub>18</sub> )( $\beta$ A)DGR( $\beta$ A), CH(COOC <sub>18</sub> )(CH <sub>2</sub> ) <sub>2</sub> (COOC <sub>18</sub> )	RGD cell adhesion motif	Cell spreading	78
C <sub>16</sub> O-RGDS-OC <sub>16</sub> , C <sub>15</sub> O-RGDS, GRGDS-OCO-C <sub>15</sub> , HOCOCH <sub>2</sub> CH <sub>2</sub> CO-RGDS-OCH <sub>2</sub> CH(OC <sub>14</sub> )(CH <sub>2</sub> OC <sub>14</sub> ), and analogues with substituted alkyl chains	RGD cell adhesion motif	Inhibition of metastasis	79
C <sub>n</sub> -16r-Y-SPARC <sub>119-122</sub> ; n = 6, 10, 14, 16, 18, 18:1 and 18:1-OH, 16r denotes KAEIEALKAEIEALKA, SPARC <sub>119-122</sub> denotes KHGK-NH <sub>2</sub>	SPARC <sub>119-122</sub> sequence and 16-residue coiled coil sequence	Cell adhesion and self-assembly	82
C <sub>16</sub> O-NH-GTAGLIGQES-COOH, C <sub>16</sub> O-NH-GTAGLIGQERGDS-COOH, C <sub>16</sub> O-NH-GTAGLIGQERRDGS	RGDS cell adhesion motif (or scrambled control) and MMP degradable sequence	Neural cell growth, biodegradability of PA network, mechanical properties of hydrogels	83
C <sub>16</sub> O-A <sub>4</sub> G <sub>3</sub> EIKVAV	IKVAV cell adhesion motif	Selective differentiation of neural progenitor cells	84
C <sub>16</sub> O-V <sub>3</sub> A <sub>3</sub> K <sub>3</sub> RGDS, C <sub>16</sub> O-V <sub>3</sub> A <sub>3</sub> K <sub>3</sub> DGSR and C <sub>16</sub> O-V <sub>3</sub> A <sub>3</sub> K <sub>3</sub> , C <sub>16</sub> O-V <sub>3</sub> A <sub>3</sub> R <sub>3</sub> , C <sub>16</sub> O-V <sub>3</sub> A <sub>3</sub> E <sub>3</sub> (diluent)	RGDS cell adhesion motif, scrambled control and diluent PAs	Treatment of spinal cord injury	85
HSNGLPLG <sub>3</sub> E <sub>3</sub> A <sub>3</sub> V <sub>3</sub> (K)-COC <sub>11</sub> H <sub>23</sub> , C <sub>16</sub> O-V <sub>3</sub> A <sub>3</sub> E <sub>3</sub>	HSNGLPL TGF- $\beta$ 1 domain	Growth of bone marrow stem and progenitor cells	86
C <sub>16</sub> O-LRKKLGGKA	Heparin-binding sequence	Cartilage regeneration	87
RGDSKKLLA(K)-C <sub>9</sub> O-diacetylene-C <sub>12</sub> with KKLLA(K)-C <sub>9</sub> O-diacetylene-C <sub>12</sub> as diluent	RGDS cell adhesion motif	Angiogenesis	88
C <sub>16</sub> O-A <sub>4</sub> G <sub>3</sub> S(Phos)RGD, C <sub>16</sub> O-A <sub>4</sub> G <sub>3</sub> EIKVAV	RGD/IKVAV cell adhesion motifs	Alignment of stem cells using soft lithographic photopatterning methods	89
(C <sub>16</sub> ) <sub>2</sub> NCICH(EO) <sub>4</sub> RGDF(K), (C <sub>16</sub> ) <sub>2</sub> N-chalcone-(EO) <sub>3</sub> RGDF(K), EO indicates ethylene oxide, chalcone is a chromophore unit employed in ref. 80	RGD cell adhesion motif	Alignment of fibrils by soft lithography	90
C <sub>16</sub> -KTTKS	Matrikine from propeptide $\alpha$ 1(I) collagen <sub>212-216</sub>	RGD-functionalized vesicles—adhesion to endothelial cells	91,92 and 95
C <sub>16</sub> -KTTKS, C <sub>16</sub> -GHK, C <sub>16</sub> -GQPR	Collagen-stimulating peptides	RGD-functionalized vesicles—adhesion to integrins	96
(C <sub>16</sub> ) <sub>2</sub> -GC <sub>2</sub> -KAbuGRGDSPAbuK, (C <sub>16</sub> ) <sub>2</sub> -GC <sub>2</sub> -KAbuGRGDSPAbuK-C <sub>2</sub> -G-(C <sub>16</sub> ) <sub>2</sub> , (C <sub>16</sub> ) <sub>2</sub> -GC <sub>2</sub> -KAbuGRGESPAbuK-C <sub>2</sub> -G-(C <sub>16</sub> ) <sub>2</sub> , (C <sub>16</sub> ) <sub>2</sub> -GC <sub>2</sub> -PHSRN, (C <sub>16</sub> ) <sub>2</sub> -GC <sub>2</sub> -PHSRN(SG) <sub>3</sub> -SGRGDSP, (C <sub>16</sub> ) <sub>2</sub> -GC <sub>2</sub> -GRGESP	Contain synergy domain PHSRN and/or RGDS cell adhesion motif	Collagen production, application in skincare products	93
(C <sub>16</sub> ) <sub>2</sub> -GC <sub>2</sub> -GRGDSP, (C <sub>16</sub> ) <sub>2</sub> -GC <sub>2</sub> -GRGESP, (C <sub>16</sub> ) <sub>2</sub> -GC <sub>2</sub> -PHSRN, (C <sub>16</sub> ) <sub>2</sub> -GC <sub>2</sub> -PHSRN(SG) <sub>4</sub> RGDSP, (C <sub>16</sub> ) <sub>2</sub> -GC <sub>2</sub> -KSSPHSRN(SG) <sub>3</sub> RGDSP	Contain synergy domain PHSRN and/or RGD(E)S cell adhesion motif	Self-assembly	96
(C <sub>16</sub> ) <sub>2</sub> -GC <sub>2</sub> -PHSRN(SG) <sub>4</sub> RGDSP, (C <sub>16</sub> ) <sub>2</sub> -GC <sub>2</sub> -K(S) <sub>2</sub> PHSRN(SG) <sub>3</sub> RGDSP, (C <sub>16</sub> ) <sub>2</sub> -GC <sub>2</sub> -K(S) <sub>2</sub> PHSRN(SG) <sub>10</sub> RGDSP, (C <sub>16</sub> ) <sub>2</sub> -GC <sub>2</sub> -K(S) <sub>2</sub> PHSRN(S) <sub>10</sub> RGDSP, (C <sub>16</sub> ) <sub>2</sub> -GC <sub>2</sub> -PHSRN(SG) <sub>3</sub> RGDSP, (C <sub>16</sub> ) <sub>2</sub> -GC <sub>2</sub> -K(S) <sub>2</sub> PHSRN(SG) <sub>3</sub> RGDSP	Contain synergy domain PHSRN and RGDS cell adhesion motif	LC mass spectroscopy to monitor PA content in anti-wrinkle cosmetics	93
C <sub>16</sub> -(G) <sub>3</sub> (S) <sub>2</sub> PHSRN(SG) <sub>3</sub> RGDSP	Contains synergy domain PHSRN and RGDS cell adhesion motif	Interaction between PAs and $\alpha$ 5 $\beta$ 1 integrin probed by AFM	97 and 98
C <sub>16</sub> OWG[(CH <sub>2</sub> ) <sub>4</sub> NHCOC <sub>15</sub> ]G(LRKLKRLLR) <sub>2</sub> -NH <sub>2</sub>	Binding sites for LDL receptor and proteoglycans	Influence of motif and linker on adhesion and proliferation of HUVEC cells and fibronectin production	99
C <sub>16</sub> -LSQETFSDLWKLLEN and C <sub>16</sub> -K(rho)LSQETFSDLWKLLEN, rho denotes a rhodamine derivative	p53 tumor suppressor protein sequence p53 <sub>14-29</sub>	Influence of linker on adhesion between PAs and $\alpha$ 5 $\beta$ 1 integrin probed by AFM	100
C <sub>16</sub> ONH-GTAGLIGQRGDS-COOH	Contains MMP-2 sensitive (and RGDS-containing) sequence	Nanofibril formation, hydrogelation and growth/proliferation of HUVEC cells	101
DOPE-PEG <sub>12</sub> -G(EIAALEK) <sub>3</sub> -NH <sub>2</sub> , DOPE-PEG <sub>12</sub> -G(KIAALEK) <sub>3</sub> -GW-NH <sub>2</sub>	SNARE protein mimics	Internalization within cells	102
		Mechanism of internalization in cells	103
		Enzymatic release of cisplatin from hydrogel	108
		Membrane fusion induced by complementary coiled coil peptides	109

Amphiphilic peptide	Peptide design	Nature of study	Reference
C <sub>12</sub> O-YGAAKKA AAKKA AAKAA, C <sub>12</sub> O-YGAKAKAAKAAKAAKAA, C <sub>12</sub> O-KLFKRHLKWKII	Cationic peptides—two designed and one biomimetic	Antimicrobial activity and eukaryotic cell toxicity	110
C <sub>16</sub> -KAK, C <sub>16</sub> -KGGK, C <sub>16</sub> -KKK, G <sub>16</sub> -K(PK)K, C <sub>16</sub> -KLLK, C <sub>16</sub> -K(PK), C <sub>16</sub> -K	<i>de novo</i> design	Antimicrobial properties	111
C <sub>n</sub> O-GCKPTFRRLKWKTKCG-NH <sub>2</sub> , C <sub>16</sub> O-IKISGKWKAAQKRFLKM, C <sub>16</sub> O-QALNVEIRGYVIKIP, italic denotes a cyclic peptide (linked through cysteine S-S)	LPS-binding peptides	LPS-neutralizing activity and self-assembly	114
C <sub>16</sub> -C <sub>4</sub> G <sub>3</sub> S(Phos)RGD	RGD cell adhesion motif	Nanofibril formation and templating of artificial bone mineralization	115
C <sub>16</sub> -(SV) <sub>2</sub> G <sub>3</sub> S(Phos)RGD, S(Phos) denotes phosphorylated serine	RGD cell adhesion motif	Templating of artificial bone mineralization	116
DOPE-(LG) <sub>4</sub>	<i>de novo</i> design	Biomimetic mineralization of CaCO <sub>3</sub>	117
[C <sub>15</sub> COO(CH <sub>2</sub> ) <sub>2</sub> CHPO <sub>4</sub> <sup>-</sup> (CH <sub>2</sub> ) <sub>2</sub> NHCO(CH <sub>2</sub> ) <sub>2</sub> CO-[HR1(A153-Q202)]. The peptide contains a sequence from heptad repeat region 1 (HR1) from the F <sub>1</sub> glycoprotein of respiratory syncytial virus	HR1 sequence	Synthetic virus-like particle stimulating antibody production	122
Ac-A(Ox)AEAAEKAAKYAAEAAEKAAKA(Ox)A-NH <sub>2</sub> , Ox denotes ornithine or ornithine-C <sub>m</sub> , <i>n</i> = 12, 14, 16, 18, 20	<i>de novo</i> design	Denaturing agents	123
(C <sub>18</sub> ) <sub>2</sub> AhOH-Lys(DTPAGlu)-(AhOH) <sub>2</sub> -octreotide, (C <sub>18</sub> ) <sub>2</sub> AhOH-Lys(DOTA)-(AhOH) <sub>2</sub> -octreotide, AhOH = 4,7,10,13,16,-19-hexaoheneicosanoic acid, DOTA and DTPAGlu denote chelating agents, octreotide = <sup>D</sup> FCF <sup>W</sup> KTCT(ol) italics denotes cyclic peptide	Octreotide peptide	MRI contrast agents for cancer detection	124
DβA(K-βADCOOH)L <sub>2</sub> C <sub>4</sub> (K)OC <sub>16</sub> , K(K-KNH <sub>2</sub> )L <sub>2</sub> C <sub>4</sub> (K)OC <sub>16</sub> , DβA(K-DSDGR)L <sub>3</sub> A <sub>3</sub> (K)OC <sub>16</sub> , βA denotes β-alanine	<i>de novo</i> branched designs, and incorporation of RGD cell adhesion motif	Encapsulation of carbon nanotubes	125
Biotin-RGDSK G <sub>3</sub> A <sub>3</sub> (K)OC <sub>16</sub> , K(K-Biotin-RGDS)X <sub>3</sub> A <sub>3</sub> (K)OC <sub>16</sub> , (K-Biotin-RGDS)(K-Biotin-RGDS)X <sub>3</sub> A <sub>3</sub> (K)OC <sub>16</sub> , X = G or VCH <sub>3</sub>	<i>de novo</i> branched designs incorporating RGDS and biotin	Presentation of biotin on PA nanofibrils	126
C <sub>n</sub> -KTVIII; <i>n</i> = 6, 8, 10, 12, 14, 16	Model amyloid forming peptide	Stabilization of β-sheet structure	129

<sup>a</sup> The difference between C<sub>n</sub> labelling of alkyl chain and C denoting cysteine within a peptide sequence should be evident from the structure.

### **1.4.2 Applications of PA wormlike micelles**

As Table 1-2 showed, most of the PA have been designed for some specific applications. Here, I introduce some examples of the studies on the PA for the potential applications for scaffolds in regenerative medicine, carriers to deliver drugs and carbon-nanotubes, and surface modifications.

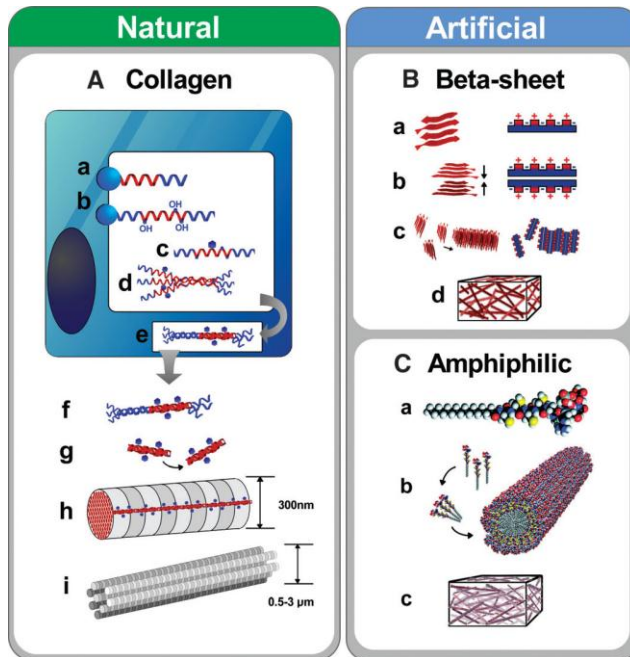
#### **1) PA wormlike micelles as materials for scaffolds**

The most promising potential applications for the PA wormlike micelles are materials for scaffolds in regenerative medicine and tissue engineering. In this section, the newly designed PA that form wormlike micelles for the applications as scaffolds are illustrated.

Cells are inherently sensitive to their surroundings. To regenerate tissue, artificial scaffolds play host to cells. Thus, controlling structure of the scaffold materials in nano-scale is important to bring out the cell behavior. Conventionally, the scaffold materials have been designed in macro-scale to have mechanical properties similar to natural tissue, for example hard for bone<sup>8</sup> and elastic for arteries<sup>9</sup>. Whereafter, Pattison et al. found that the roughness of the materials in nano-scale enhanced the cell attachment, proliferation<sup>10</sup>. The results implied that further control of the structures of the scaffold materials in nano-scale and incorporation of biological activities into the scaffold should be rewarding.

Figure 1-4 shows the images of self-assembled structures of natural bone (A), and artificial scaffolds composed of  $\beta$ -sheet peptides (B) and of wormlike micelles of PA (C)<sup>11</sup>. In the natural bone, the scaffold is made of collagen fibers formed by

aggregates of fibrils, self-assembled procollagen. The structures of the artificial scaffold composed of self-assembled wormlike micelles of PA is similar to the hierarchical structures of the natural bone scaffold in scales.



**Figure 1-4.** Natural and artificial fiber self-assembly.

Further, the wormlike micelles of PA can be customized through the amino sequence for specific cell response. Some specific amino sequences were incorporated into PA for enhancing the cell response. RGD (arginine-glycine-asparagic acid) and IKVAV (isoleucine-lysine-valine-alanine-valine), well-known to be the especially attractive sequences in some proteins, were incorporated into the PA for the applications.



- **PA with RGD sequence**

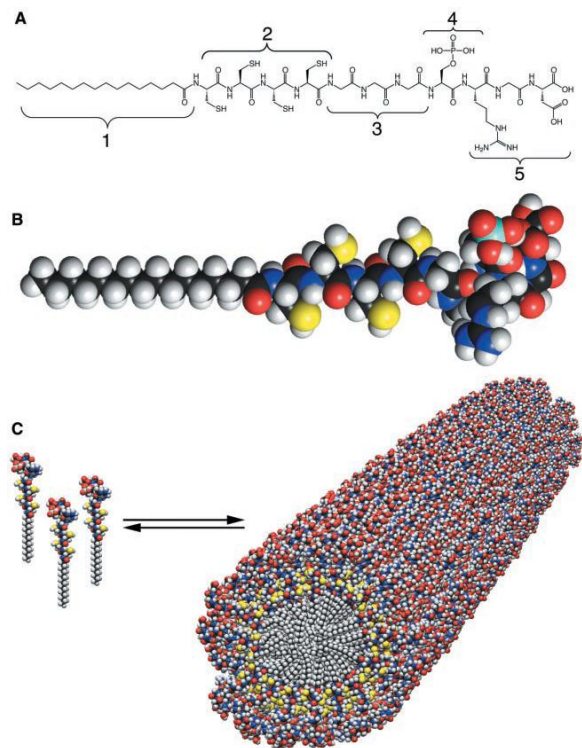
For the scaffold application, the peptides that promote cell adhesion are frequently incorporated into PA. RGD is known to be the most common cell adhesion sequence in the natural tissue scaffolds of proteins, notably fibronectin. The incorporation of the cell adhesion sequences into networks of PA wormlike micelles brings both structural and functional mimicry of native scaffolds.

Stupp et al. used pH-induced wormlike micelle formation of PA with RGD to make a nano-structured fibrous scaffold as an artificial extracellular matrix for bone <sup>12</sup>. Their designed PA has three features in the peptides as shown in Figure 1-5 (A). Region 2 is composed of four consecutive cysteine residues for covalent capture of micelles by disulfide bonds through oxidation, leading to the robust wormlike micelles.

Region 3 is a flexible linker, and region 4 is a phosphorylated serine

residue that plays a key role for the formation of calcium phosphate minerals.

In addition, RGD is incorporated in a region 5 for promoting the adhesion and growth of cells on the micelle surfaces.

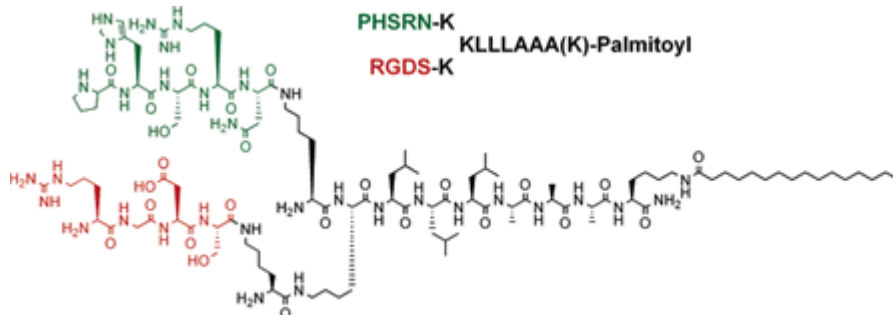


**Figure 1-5.** (A) chemical structure of the PA with RGD. (B) molecular structure of the PA with RGD. (C) self-assembled structure of the PA.



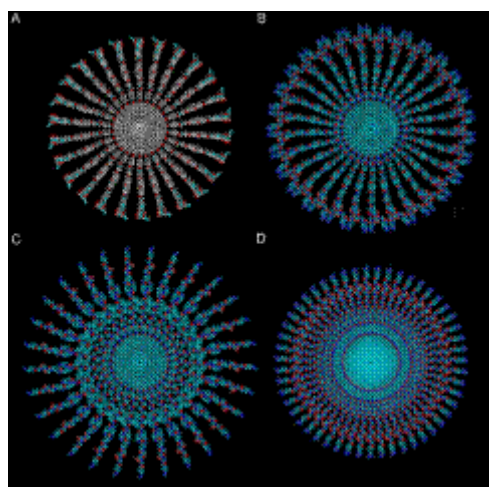
In their study, the PA wormlike micelles directed mineralization of hydroxyapatite to form a composite material. In the composite, hydroxyapatites were aligned with long axes of the micelles, which is similar to the relation between collagen fibrils and hydroxyapatite crystals in natural bone.

Branched PA with RGD (Figure 1-6) was also studied for potential use as scaffolds for regenerative medicine by Guler et al <sup>13</sup>. The branched architecture of the peptide allows the presentation of more than one epitope in a single PA and enhances accessibility of epitopes for protein binding. The branched PA self-assembled into wormlike micelles, resulting in gel formation in the presence of physiological fluids and other biological macromolecules including synovial fluid and DNA.



**Figure 1-6.** Structure of branched PA with RGD

They also found that the branched PA exhibited improvement of cell attachment and migration, even though the PA with branched architectures form wormlike micelles with lower packing efficiency as compared to the linear PA as shown in Figure 1-7 <sup>14</sup>. It was presumed that the lower packing efficiency make an additional space for epitope motion, which improves signaling for cell adhesion, spreading, and migration.



**Figure 1-7.** Cross-sections of PA wormlike micelles formed from branched and linear PA. Branched PA with one cyclic RGDS epitope (A), branched PA with two RGDS epitopes (B), branched PA with one RGDS epitope (C), and linear PA with one RGD epitope (D).

Beniash et al found that a class of PA with RGD or IKVAV sequence (Table 1-3) self-assembled into wormlike micelles and formed gel under physiological conditions in the presence of metal ions, such as  $Mg^{2+}$ ,  $Ca^{2+}$  and  $Ba^{2+}$ <sup>15</sup>.

**Table1-3.** Gelation of various PA with metal ions.

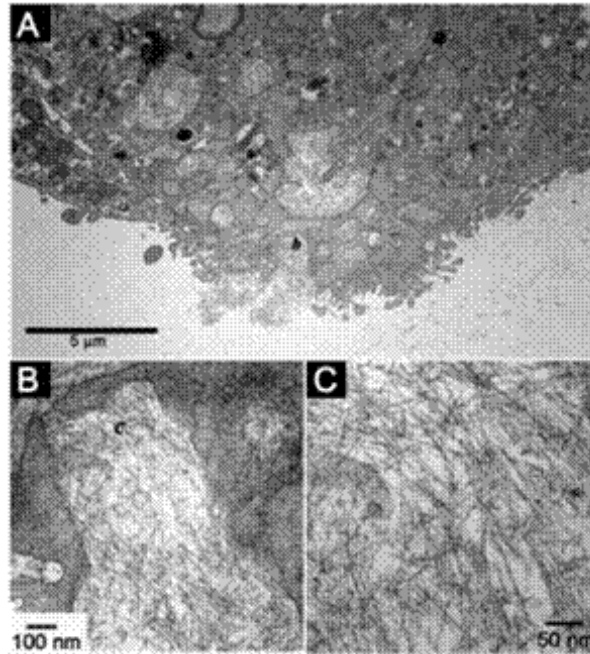
PA	Sequence	Charge	$K^{+a}$	$Mg^{2+b}$	$Ca^{2+}$	$Ba^{2+}$	$Cu^{2+}$	$Zn^{2+}$	$Gd^{3+}$
1	Alkyl- $C_4G_3S^{(P)}$ RGD-COOH	3	Viscous liquid	Gel	Gel	Gel	N/A	Gel	Gel
2	Alkyl- $A_4G_3S^{(P)}$ RGD-COOH	3	Viscous liquid	Gel	Gel	Gel	Gel	Gel	Gel
3	Alkyl- $A_4G_3S^{(P)}$ KGE-COOH	3	Viscous liquid	Gel	Gel	Gel	Gel	Gel	Gel
4	Alkyl- $C_4G_3SRGD$ -COOH	1	Viscous liquid	Viscous liquid	Gel	Gel	N/A	Gel	Gel
5	Alkyl- $A_3G_2EQS$ -COOH	2	Viscous liquid	Gel	Gel	Gel	Gel	Gel	Gel
6	Alkyl- $A_4G_3ERGD$ S-COOH	2	Viscous liquid	Viscous liquid	Viscous liquid	Viscous liquid	N/A	Gel	Gel
7	Alkyl- $C_4G_3EIKVAV$ -COOH	1	Gel	Gel	Gel	N/A	N/A	Gel	Gel
8	Alkyl- $C_4G_3KIKVAV$ -NH <sub>2</sub>	+2	Gel	Viscous liquid	Viscous liquid	Viscous liquid	N/A	Viscous liquid	Viscous liquid

<sup>a</sup> 200 mM KCl.

<sup>b</sup> 20 mM for all polyvalent cations.

Cells entrapped within the network of PA wormlike micelles were found to survive for at least three weeks and proliferate. The TEM images in Figure 1-8 (A-C) showed internalization of the PA wormlike micelles by the encapsulated cells, and

results of biochemical assays provided evidence of PA metabolism. The results show the application possibility of PA wormlike micelles matrices as an artificial extra cellular matrix.



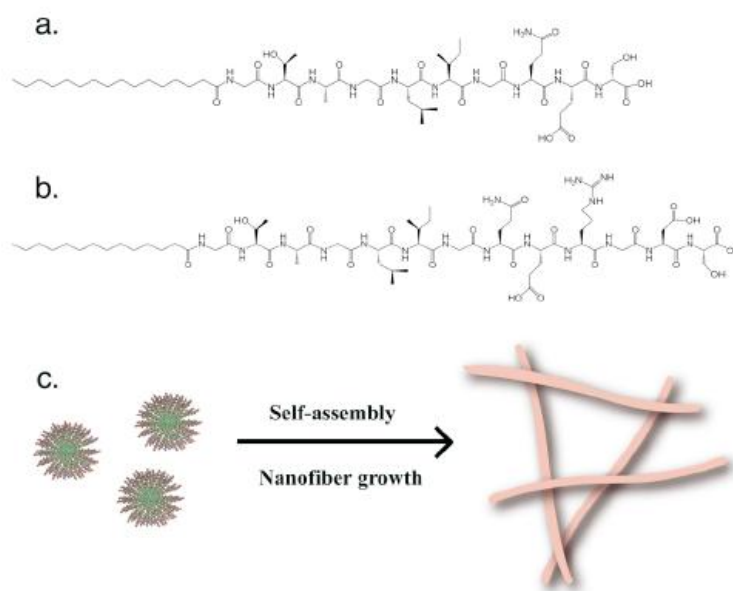
**Figure 1-8.** (A) TEM image of a cell entrapped in the matrix of PA wormlike micelles. (B) Intermediate magnification of the region marked b in (A). (C) High magnification of the nano-fibers in the area marked c in (B).

Co-assembly of the PA with RGD and PA with different peptide sequences can produce combination of two features or enhancement of the features.

Hartgerink et al found co-assembled PA wormlike micelles, whose bioactivity, degradability, and mechanical properties can be controlled<sup>16</sup>. In their system, though the mixed two PA with different mechanical and biological properties formed small aggregates at neutral pH, they changed the structure from the small aggregates to wormlike micelles by adding divalent ions to the PA solution, as shown in Figure 1-9 and 1-10.

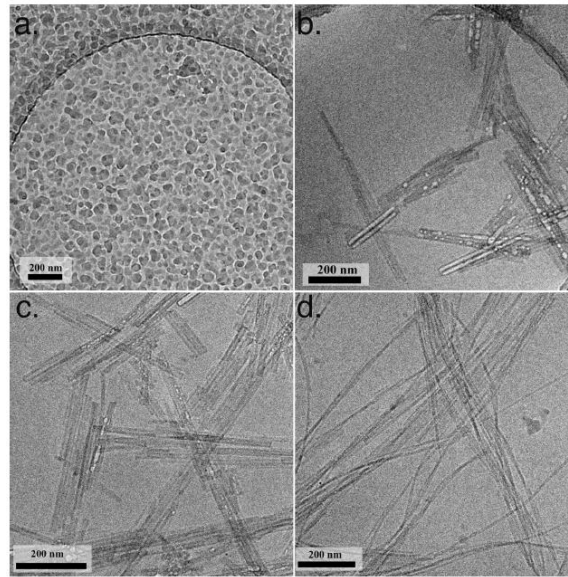
PA1 [CH<sub>3</sub> (CH<sub>2</sub>)<sub>14</sub>CONH-GTAGLIGQES-COOH] contains a proteolytically degradable sequence, Gly-Thr-Ala-Gly-Leu-Ile-Gly-Gln (GTAGLIGQ), specific for a matrix metalloproteinase 2.

PA2 [CH<sub>3</sub>(CH<sub>2</sub>)<sub>14</sub>CONH-GTAGLIGQERGDS-COOH] has additionally a cell adhesion sequence RGDS. The RGDS sequence in PA2 led to good cell spreading and proliferation and enhanced the expression of MMP2 to degrade the gel composed of wormlike micelles by cleaving the PA into two pieces, while PA1 enhances mechanical properties.



**Figure 1-9.** Structures of PA and mechanism of self-assembly into wormlike micelles.

(a) Chemical structure of PA1 (C16-MMP-ES), (b) Chemical structure of PA2 (C14-MMP-E-RGDS). (c) The small aggregates of PA at neutral pH were changed to the wormlike micelles by addition of divalent ions.



**Figure 1-10.** cryo-TEM images of PA. (a) 1 wt% of PA2 without calcium ions at neutral pH. (b) PA1, (c) PA1/PA2 (50/50) and (d) PA2 at  $M_r = 2$ .

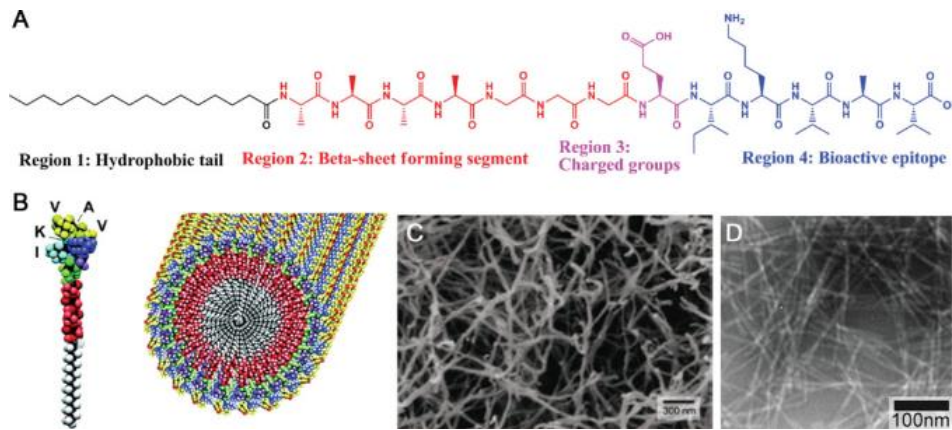
All PA presented here show that they need external stimuli to form wormlike micelles.

- **IKVAV**

Another popular functional amino sequence is a laminin-derived IKVAV (isolucine-lysine-valine-alanine-valine) which is crucial for cell attachment, migration, and neurite outgrowth. The IKVAV sequence has been specifically incorporated into PA for the scaffold of neuron cells.

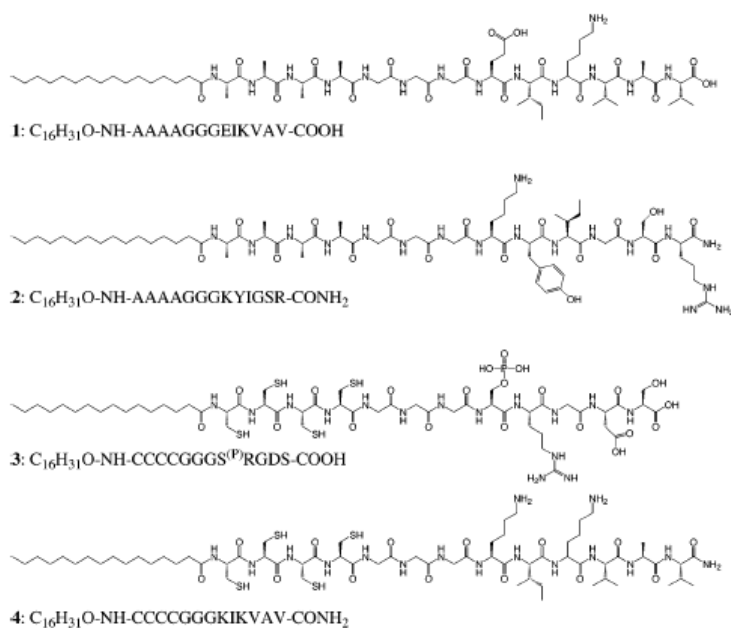
Silva et al synthesized a new PA that contains an IKVAV known to promote neurite sprouting and to direct neurite growth as shown in Figure 1-11<sup>17</sup>. The PA self-assembled into wormlike micelles, triggered by addition of cell suspension to PA solution. The scaffold formed of the PA wormlike micelles induced differentiation of

cells into neurons, while suppressed the astrocyte differentiation, which reveals that the PA scaffold can direct the selective differentiation of cells.



**Figure 1-11.** Chemical structure of the PA (A), self-assembled structure of the PA (B), SEM image of the assembled structure (C) and cryo-TEM image of the assembled structure (D).

Niece et al. also synthesized four PA that have IKVAV, RGD and YIGSR (Figure 1-12) and studied the co-assembly effect of the PA<sup>18</sup>. YIGSR is also known to interact with neurons. PA 1 and PA 3 have a negative charge, whereas PA 2 and PA 4 have net positive charge at neutral pH. The study showed that the mixed samples of PA 1 and PA 2, PA 3 and PA 4 co-assembled into wormlike micelles, driven by electrostatic interaction of opposite charged peptides. The wormlike micelles composed of two different PAs can provide two biological signals to cells.



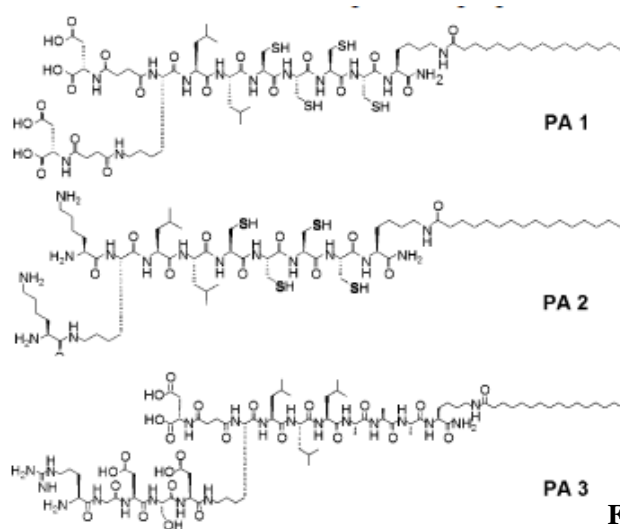
**Figure 1-12.** Chemical structures of the four PA. PA **1** and **3** self-assembled at acidic pH, and PA **2** and **4** self-assembled at basic pH, while combination of PA **1/2** and **3/4** co-assembled at neutral pH.

## 2) PA wormlike micelles for delivery

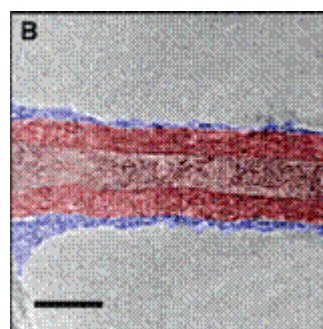
Another potential application of PA is encapsulation of hydrophobic molecules such as carbon nanotubes and drugs. PA wormlike micelles should act as smart carriers that can encapsulate and release the molecules depending on the environment.

### ● Dispersion and modification of carbon nanotubes

Stupp et al proposed a new PA application for dispersion of carbon nanotubes in water<sup>19</sup>. The PA in Figure 1-13 self-assembled on carbon nanotubes and the coating of PA dispersed and functionalized the carbon nanotubes. In the TEM image of a multi-walled carbon nanotube with the peptide amphiphile PA2 (Figure 1-14), an organic film was observed on the outer surface of a nanotube. The PA molecules on the surface of carbon nanotubes have potential for adding bio-functionality to nanotubes.



**Figure 1-13.** Structures of PA1, PA2 and PA3.

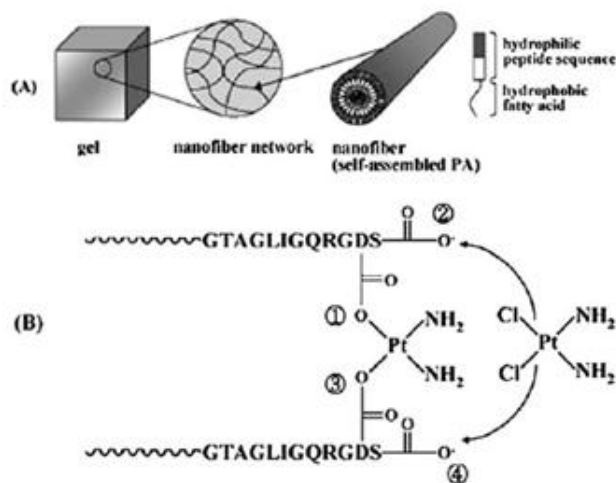


**Figure 1-14.** TEM image of a carbon nanotube with PA 2. Scale bar, 10nm.

- **Anticancer agent delivery system**

Kim et al reported a bio-responsive cisplatin (CDDP) delivery system with PA containing a cell-adhesive matrix metalloproteinase-2 (MMP-2)-sensitive amino sequence GTAGLIGQRGDS in the peptide region <sup>20</sup>. The PA self-assembled into wormlike micelles by incubation at 37°C for 5 hours and CDDP are loaded in the PA gel. They presumed that the wormlike micelle formation of the PA was induced by complexation of Pt in CDDP with the carboxylic group of aspartic acid or C-terminus of the PA as shown in Figure 1-15(B). Release of CDDP by enzymatic cleavage of the MMP-2 sensitive sequence was demonstrated, which should be useful for a bio-responsive anticancer drug delivery system.





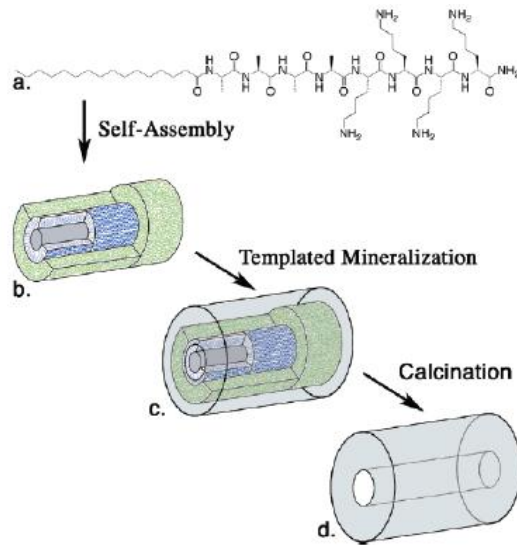
**Figure 1-15.** Schematic illustration of the PA gel. Scheme of self-assembled structures (A) and mechanism of cross-linking in the system (B).

### 3) PA wormlike micelles as templates for biomineralization

Another important potential application of PA wormlike micelles is utilization of its charged surface to template inorganic mineralization.

The study that showed the formation of a composite with PA wormlike micelles and hydroxyapatite <sup>12</sup> is one of the examples exhibiting direct mineralization utilizing the PA wormlike micelles as templates.

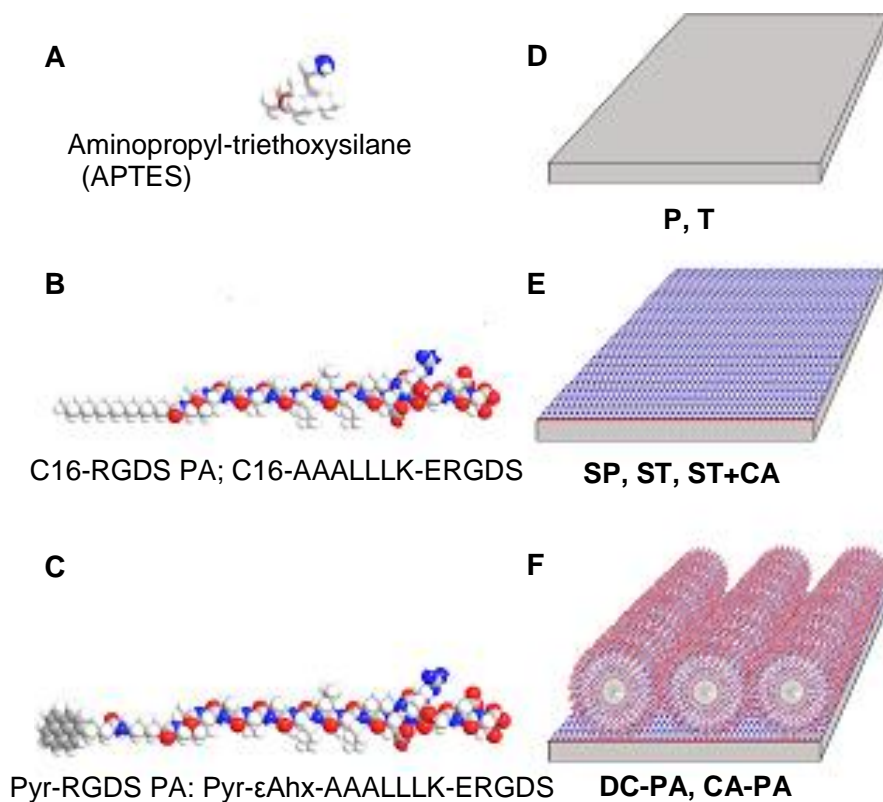
Recently, mineralization of silica with templates of PA wormlike micelles was reported. Yuwano et al. demonstrated an approach to prepare silica nanotubes by condensation of tetraethoxysilane (TEOS) on PA wormlike micelle templates followed by calcination as Figure 1-16 shows <sup>21</sup>. Wormlike micelles of the PA containing lysines or histidines were found to direct silica mineralization by providing nucleation sites and catalyzing silica polymerization on their surface.



**Figure 1-16.** (a) Chemical structure of PA1. (b) wormlike micelle of PA1. Shown is the hydrophobic core in dark gray,  $\beta$ -sheet region in blue, and the flexible region in green. (c) PA template for TEOS polymerization. (d) PA removal by calcination.

#### 4) PA wormlike micelles for surface modification and patterning

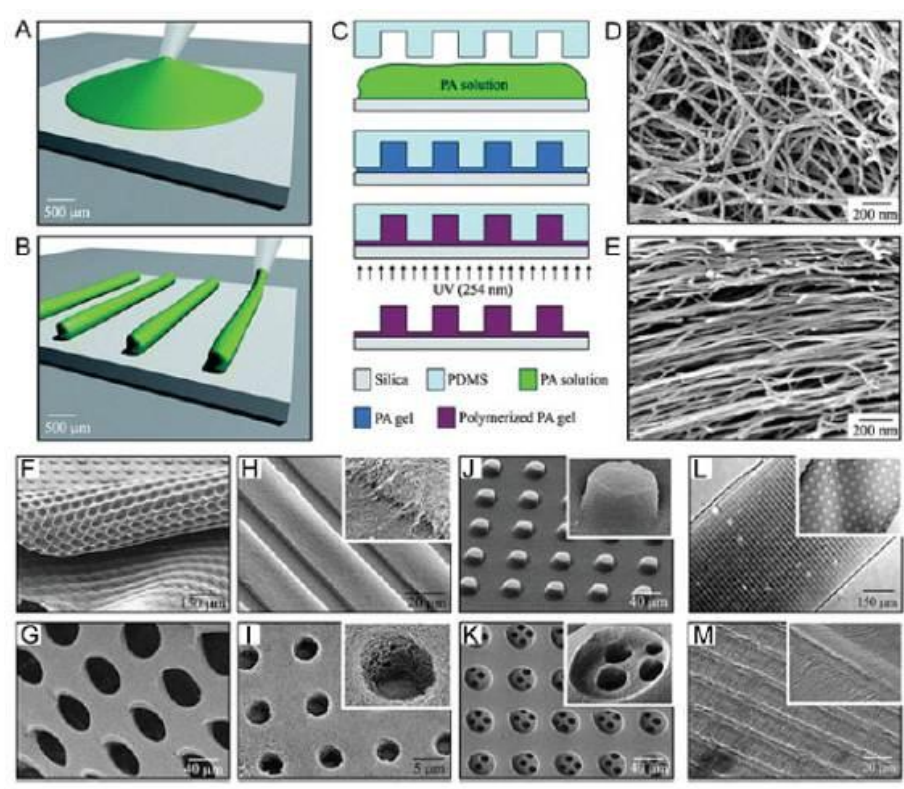
For development of implantable medical devices including stents, surface modification of metal alloy substrates with bio-active materials is required to promote cell attachment, proliferation, and possibly differentiation with keeping the mechanical properties of the bulk materials. Sargeant et al developed a method to covalently attach PA wormlike micelles on pretreated nickel–titanium substrates using an intermediary aminosilane layer as shown Figure 1-17<sup>22</sup>. The results of the study showed that the covalent binding of the PA wormlike micelles to the substrate creates robust coatings, leading to a confluent cell monolayer.



**Figure 1-17.** Chemical structure of aminopropyl-triethoxysilane (A), chemical structure of the PA (B), chemical structure of the pyr-PA (C), and images for the various nickel-titanium surfaces obtained in the process (D–F).

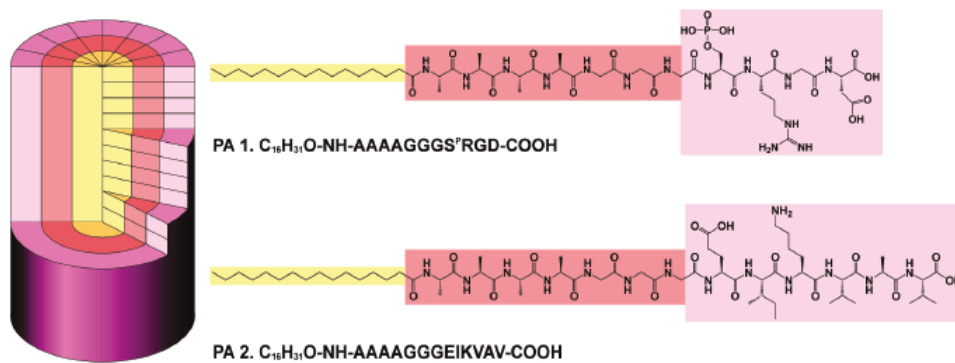
Micro-texture on the surfaces made by peptide-based patterns should be useful in molecular recognition especially for bio-sensing. Mata et al developed microfabrication techniques with using PA containing RGD and diacetylene as shown in Figure 1-18<sup>23</sup>. In the process, PA solution was covered with a mold and the PA self-assembled into wormlike micelles inside the mold under ammonium hydroxide vapor. Then, the resultant PA gel made of the PA wormlike micelles was photo-polymerized through UV irradiation and the various micro-textures of PA including channels (G), holes (I) were obtained by taking off the mold. The

micro-textures were fabricated from networking of randomly dispersed PA wormlike micelles with the process (A) or that of pre-aligned PA wormlike micelles with the process (B). When the resultant surfaces were used as cell substrates, aligned PA wormlike micelles promoted the alignment of mesenchymal stem cells, while randomly oriented micelles enhanced the osteoblastic differentiation of the cells.

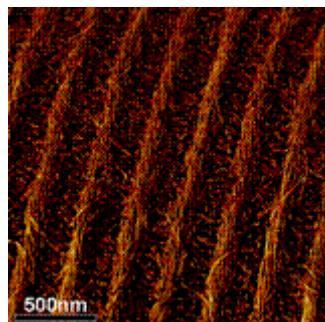


**Figure 1-18.** Fabrication techniques (A–C) and resultant PA structures (D, E). Image of dropping freshly dissolved PA with randomly oriented wormlike micelles on a silica substrate (A), image of squeezing an incubated PA solution containing aligned wormlike micelles on a silica substrate (B). process scheme of preparative method (C). SEM images of randomly oriented wormlike micelles (D), of aligned wormlike micelles (E), of various micro-textures formed from the PA wormlike micelles (F–M).

Recently, S. I. Stupp et al reported the simultaneous self-assembly, alignment, and patterning of PA wormlike micelles over wide areas by soft lithographic technique, named sonication-assisted solution embossing (SASE)<sup>24,25</sup>. Chemical structures of PA1 and PA2 are shown in Figure 1-19. In the process with this technique, PA solution was initially placed within an elastomeric stamp. Then, PA self-assembled into wormlike micelles, triggered by solvent evaporation within narrow channels of the stamp in sub-micrometer under ultrasonic agitation. The wormlike micelles were arranged parallel to the channel direction due to steric repulsion, as Figure 1-20 shows.



**Figure 1-19.** Chemical structures of PA1 and PA2, and the self-assembled structure of the PA.



**Figure 1-20.** Patterning of PA wormlike micelles by soft lithography.

## 5) Other potential applications

Some additional modifications of PA molecules were conducted to increase the robustness of the PA wormlike micelles for expanding the applications.

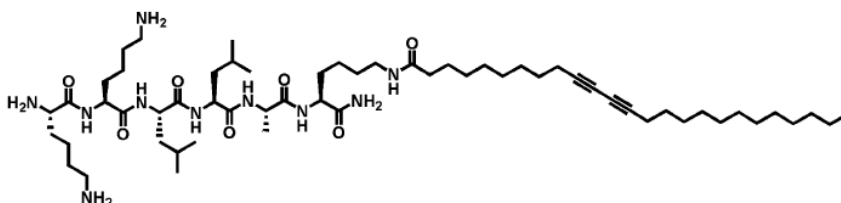
Pashuck et al controlled mechanical properties of the gel made of PA wormlike micelles by changing a number and a position of valines and alanines in the peptide of PA (Table 1-4)<sup>26</sup>. They found that valines in the peptides increased stiffness of the gel, while alanines decreased the mechanical properties. The IR results of the PA revealed that well-aligned inter-molecular hydrogen bonding along the micelle axis, existing near the hydrophobic core, conducted to high stiffness of the gel. Manipulating the mechanical stiffness of the PA gel should lead to the control of cell differentiation and cell morphology in tissue engineering.

**Table1-4.** Amino sequence of the peptides in the various PA.

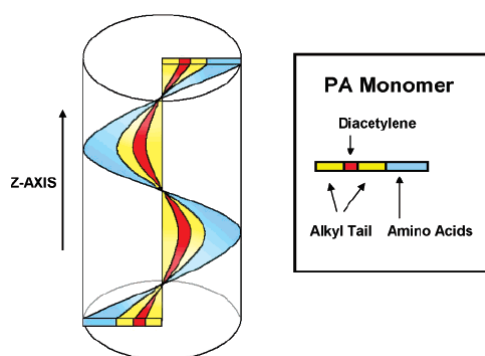
PA	$\beta$ -sheet region
PA 1	VVAAA
PA 2	VVAA
PA 3	VVVVAAAA
PA 4	VVAAAA
PA 5	VVVVAA
PA 6	AAAVVV

Another technique to enhance robustness of the PA wormlike micelles was exhibited by Hsu et al. They synthesized PA that have diacetylene-derivatized alkyl tails (Figure 1-21)<sup>27</sup>. The alkyl tails were polymerized by irradiation at 256 nm with keeping the wormlike micelle morphology. The  $\beta$ -sheet structure in the peptides induced a twisted structure in the conjugated alkyl backbone as shown in Figure 1-22. They proposed that the findings provide insight for the design of PA that form wormlike

micelles with well-controlled epitope presentation. It should open new possibilities of PA wormlike micelles for the mechanical and optical properties.



**Figure 1-21.** Chemical structure of the PA containing diacetylene group in the alkyl tail.

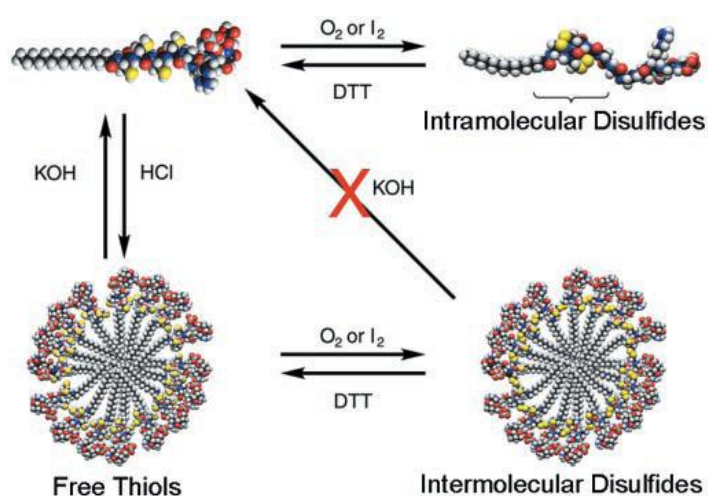


**Figure 1-22.** Schematic image of predicted structure of the PA wormlike micelles. Polymerization of diacetylene occurs along the long axis of the wormlike micelles (red) according to the  $\beta$ -sheet direction (blue).

Furthermore, to control the physical and chemical robustness of PA wormlike micelles, Hartgerink et al incorporated four consecutive cysteine residues to their PA for reversible intermolecular crosslinking<sup>28</sup>. The molecular structures are shown in Table 1-5. The PA self-assembled into wormlike micelles by acidification and disassembled at neutral and basic pH as illustrated in Figure 1-23. By oxidation of the wormlike micelles, intermolecular disulfide bonding, that stabilize the micelle structure, were formed and the wormlike micelles with disulfide bonding lost the sensitivity to pH.

**Table1-5.** Structures of PA and their charge

Molecule	N terminus	Peptide (N to C)	Charge pH 7
1	H	CCCCGGGS <sup>(PO<sub>4</sub>)</sup> RGD	-2
2	C <sub>6</sub> H <sub>11</sub> O	CCCCGGGS <sup>(PO<sub>4</sub>)</sup> RGD	-3
3	C <sub>10</sub> H <sub>19</sub> O	CCCCGGGS <sup>(PO<sub>4</sub>)</sup> RGD	-3
4	C <sub>16</sub> H <sub>31</sub> O	CCCCGGGS <sup>(PO<sub>4</sub>)</sup> RGD	-3
5	C <sub>22</sub> H <sub>43</sub> O	CCCCGGGS <sup>(PO<sub>4</sub>)</sup> RGD	-3
6	C <sub>10</sub> H <sub>19</sub> O	AAAAGGGS <sup>(PO<sub>4</sub>)</sup> RGD	-3
7	C <sub>16</sub> H <sub>31</sub> O	AAAAGGGS <sup>(PO<sub>4</sub>)</sup> RGD	-3
8	C <sub>16</sub> H <sub>31</sub> O	CCCCGGGS <sup>(PO<sub>4</sub>)</sup>	-3
9	C <sub>16</sub> H <sub>31</sub> O	CCCCGGGS <sup>(PO<sub>4</sub>)</sup> KGE	-3
10	C <sub>16</sub> H <sub>31</sub> O	CCCCGGGS <sup>(PO<sub>4</sub>)</sup> RGDS	-3
11	C <sub>16</sub> H <sub>31</sub> O	CCCCGGGSRGD	-1
12	C <sub>16</sub> H <sub>31</sub> O	CCCCGGGEIKVAV	-1



**Figure 1-23.** Schematic illustration of self-assembly and covalent capture of the PA by pH change and oxidation.



### **1.4.3 Structural analysis on PA wormlike micelles**

Recently, analytical studies on PA wormlike micelles became active for understanding the detailed hierarchical structures and for elucidating the mechanism of the micelle formation in order to facilitate and expand the design of PA that possess both bio-activity and ability to form wormlike micelles and in order to control the formation of the PA wormlike micelles. In this section, main three interactions that determine the PA micelle structure are discussed with some study results.

#### **1) Effect of alkyl tail length**

The effect of PA alkyl tail length on the formation of wormlike micelles was studied with the PA containing disulfide bounding shown in Table 1-4<sup>28</sup>. The solutions of five PA (1–5) with different alkyl tail length (no tail, C6, C10, C16, C22) were synthesized and the structures of the PA in the solutions were analyzed with TEM. The Results showed that the PA with no tail or short tail (C6) did not form gel at any pH. On the other hand, the PA with longer alkyl tail of C10, C16 and C22 formed gels by networking of the PA wormlike micelles. In fact, most part of PA that have been reported to form wormlike micelles possess C16 alkyl tails, as shown in Table 1-2. Also in this thesis, the PA with an alkyl tail of C16 was mainly used for the study on the process of wormlike micelle formation.

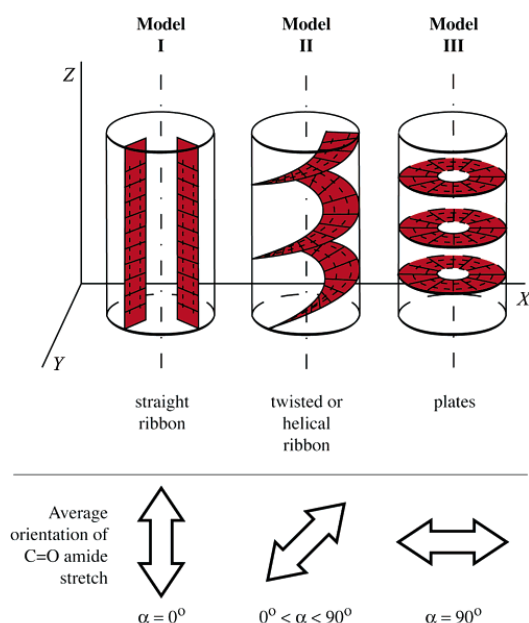
#### **2) Role of $\beta$ -sheet structure**

Because  $\beta$ -sheet structure has been observed commonly in many PA wormlike micelles, it is presumed that the intermolecular hydrogen bonding in the  $\beta$ -sheet structure plays an important role for the wormlike micelle formation. Here, three studies

on the  $\beta$ -sheet structure in the PA wormlike micelle are illustrated.

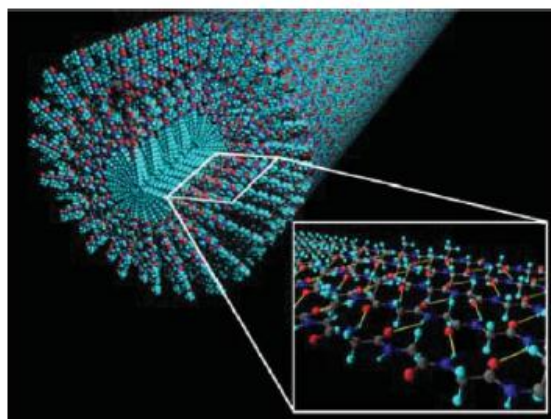
Paramonov et al studied a role of inter-molecular hydrogen bonding for wormlike micelle formation by using a series of 26 PA derivatives <sup>29</sup>. Their work demonstrated that the four amino acids closest to the hydrophobic core, that form  $\beta$ -sheet structure, are necessary for the formation of wormlike micelles. The PA without the four amino acids that have high  $\beta$ -sheet propensity favored spherical micelles instead of wormlike micelles.

They also studied a direction of the hydrogen bonding in the micelles with grazing angle and oriented transmission IR measurements. Figure 1-24 shows a schematic representation of three possible  $\beta$ -sheet interactions. According to the IR results, they suggested that model II, twisted or helical ribbon, that have combined features of model I and III, represents a realistic description of hydrogen bonding in the PA wormlike micelles.



**Figure 1-24.** Schematic representation of the possible  $\beta$ -sheet interactions

Jiang et al analyzed the internal structure of PA wormlike micelles with transmission infrared spectroscopy (IR) and polarization modulation-infrared reflection-absorption spectroscopy (PM-IRRAS)<sup>30</sup>. The PM-IRRAS results showed that peptides in PA formed  $\beta$ -sheet structure aligned parallel to a long axis of wormlike micelles and the PA were packed radially in the micelles. In the study, they also exhibited that the degree of internal order depended on the PA structures. The results suggest the correlation between the internal order of the hydrophobic core and peptide order in the shell of the micelles.



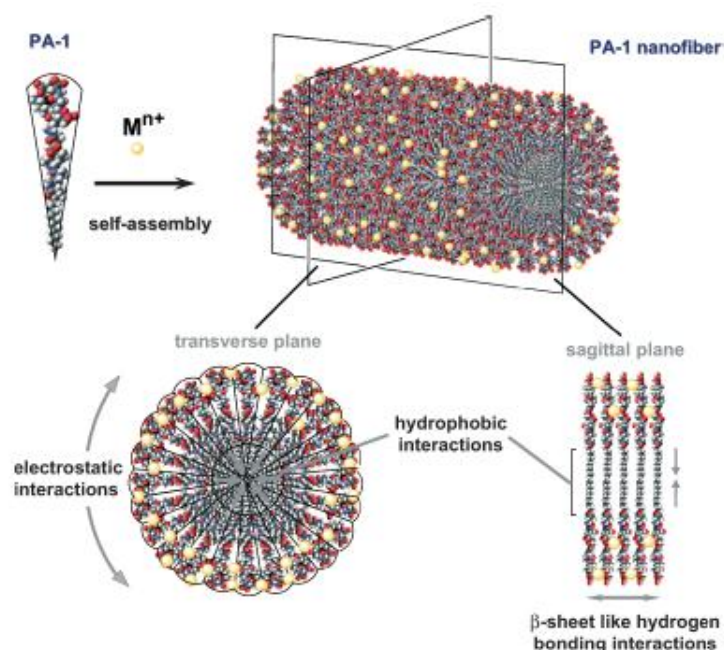
**Figure 1-25.** Schematic representation of  $\beta$ -sheets within PA wormlike micelles. In this figure, inter-molecular hydrogen bonding are represented as yellow lines, and carbon, oxygen, hydrogen and nitrogen atoms are colored grey, red, light blue and blue respectively.

The  $\beta$ -sheet formation is the most unique and attractive feature for PA as compared to other conventional surfactants, because the intermolecular hydrogen bonding provides a well-organized structure and high stability to the wormlike micelles.

### 3) Effect of electrostatic interaction

Though many PA contain charged residues in the peptides for enhancing the water solubility, it is well known that electrostatic repulsions among the charged residues in the PA induce disassociation of PA molecules. Thus, as described in the section 1-2, addition of counter ions or changing the pH for reduction of the electrostatic repulsion are required to make PA with charged residues self-assemble into wormlike micelles.

The interactions of the charged peptide amphiphile PA1 [C16-A<sub>4</sub>G<sub>3</sub>S(P)KGE-COOH] in the micelle were analyzed with oscillatory rheology, IR, and CD by Stendahl et al <sup>31</sup>. It was shown that the PA self-assembled into wormlike micelles by adding cations because of the screening of the repulsive interaction. By screening the repulsive interaction, cohesive interactions including hydrophobic interaction, ionic bridging and hydrogen bonding promote stabilization of the wormlike micelles as shown in Figure 1-26.

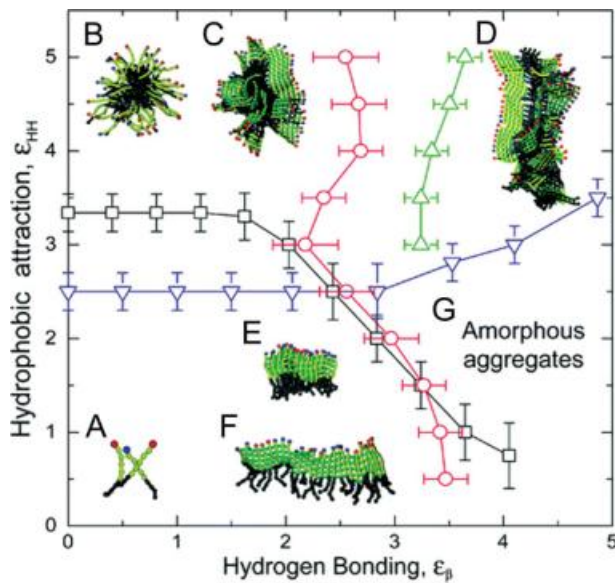


**Figure 1-26.** Schematic representation of the interactions in the PA wormlike micelles.

#### 4) Simulation

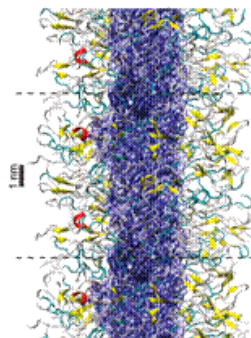
To elucidate the contribution of each interaction and the mechanism of micelle formation, “simulation” is one of the powerful means.

The micelle structures of PA were simulated by Cruz et al with the mixed Monte Carlo – stochastic dynamic method <sup>32</sup>. The simulation results have some limitations because it took into account only hydrophobic interactions and hydrogen bonding among peptides, without considering electrostatic interactions, solvent effect, and variation of dihedral angles of  $\beta$ -sheet. In their simulation, 100% hydrophobic interaction (without hydrogen bonding) produced micelles of finite size, including spherical micelles (Figure 1-27 A and B). In contrast, 100% hydrogen bonding (without hydrophobic interaction) led to gradual assembly into one-dimensional  $\beta$ -sheet structure (Figure 1-27 F). In the region where hydrophobic interaction and hydrogen bonding coexisted, the assembled structures and their kinetics were varied in accordance with the balance of two interactions. The process of the wormlike micelle formation presumed from their simulation results was that spherical micelles formed by relatively weak hydrogen bonding become instable by increasing the hydrogen bonding, and change the structure to cylindrical micelles due to the geometric frustrations by forming the  $\beta$ -sheet in the micellar shell. Thus, they exhibited that the combined effect of intermolecular hydrogen bonding of the peptides and the hydrophobic interaction of alkyl tails led to the formation of cylindrical micelles (Figure 1-27 C and D) in dilute aqueous solutions by means of the simulations.



**Figure 1-27.** Assembled structures of PA depending on the strengths of hydrogen bonding and hydrophobic interaction.

Schatz et al conducted atomistic molecular dynamics simulations to examine the formation of PA cylindrical micelles<sup>33</sup>. An amino sequence of the PA was SLSLAAAEIKVAV. The simulation results shown in Figure 1-28 indicated that the  $\beta$ -sheet structures in the SLSL region were mostly along the fiber axis, which provided a driving force to make cylindrical micelles. The results also exhibited that the epitope regions of the PA were exposed on the surface of the micelle.

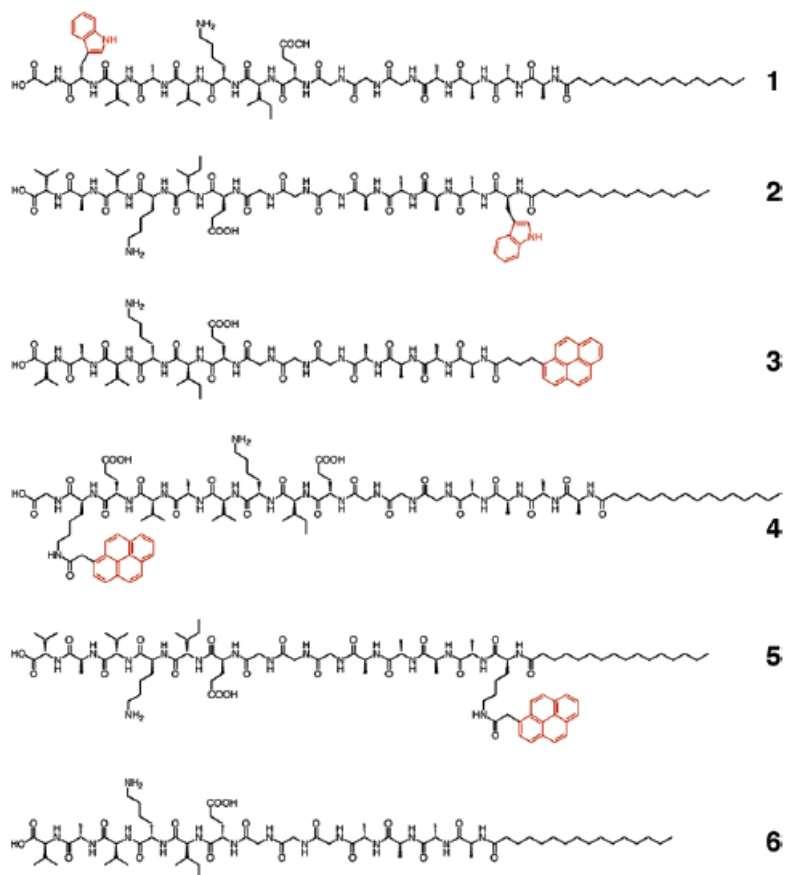


**Figure 1-28.** Snapshot of PA wormlike micell simulation at 40ns. The hydrophobic core is represented by a blue surface,  $\alpha$ -helices are in red,  $\beta$ -sheets are in yellow, turns are in cyan, and coils are in gray. Periodic boundaries of the micelles are shown in dotted lines.

## 5) Inner environment of PA wormlike micelles

Understanding the inner environment and accessibility to the inner region of the wormlike micelle is important to use the micelles as carriers.

Tovar et al. studied the accessibility of aqueous molecules to the wormlike micelles with tryptophan and pyrene fluorophores covalently attached to PA (Figure 1-29) <sup>34</sup>. In their study, tryptophan fluorescence showed that the interiors remained well-solved state even after the wormlike micelle formation, indicating existence of high degree of free volume in the micelles. In addition, they showed that fluorophores within the wormlike micelles can interact with the external environment. The study with the molecular probes showed application possibility of the PA micelles as carriers.



**Figure 1-29.** Chemical structures of PA 1~ PA 6.

## 1.5 Motivation for the thesis

As described above, various types of peptide amphiphiles were designed and synthesized to have bio-activity derived from some proteins. Thanks to their impressive achievements, practical use of the PA wormlike micelles is approaching now. Recently, since the analytical studies of the PA wormlike micelle are gradually increasing, the importance of  $\beta$ -sheet structure for the PA wormlike micelle formation is becoming clearer. However, process and mechanism of the wormlike micelle formation remain to be fully elucidated. Understanding these process and mechanism is significant to expand a freedom of the PA design and to establish more effective process to form wormlike micelles for further applications.

Therefore, here, the author investigates the process of PA wormlike micelle formation and elucidates the mechanism of the formation with a newly designed peptide amphiphile (C16-W3K) that has attractive characteristics for the structural analysis; “simple amino sequence in the peptide”, “slow speed of wormlike micelle formation”, and “no need of external trigger”. Further, the author controls the structural changes by adding some stimuli, which should open up new possibility of the PA and PA wormlike micelles.



## References

1. Kunitake, T. *Angew. Chem. Int. Ed. Engl.* **1992**, *31* (6), 709-726.
2. Berndt, P.; Fields, G. B.; Tirrell, M. *J. Am. Chem. Soc.* **1995**, *117* (37), 9515-9522.
3. Tu, R. S.; Tirrell, M. *Adv. Drug Delivery Rev.* **2004**, *56* (11), 1537-1563.
4. Israelachvili, J. N.; Mitchell, D. J.; Ninham, B. W. *J. Chem. Soc., Faraday Trans.2* **1976**, *72*, 1525-1568.
5. Yu, Y. C.; Tirrell, M.; Fields, G. B. *J. Am. Chem. Soc.* **1998**, *120* (39), 9979-9987.
6. Bitton, R.; Schmidt, J.; Biesalski, M.; Tu, R.; Tirrell, M.; Bianco-Peled, H. *Langmuir* **2005**, *21* (25), 11888-11895.
7. Hamley, I. W. *Soft Matter* **2011**, *7* (20), 9533-9534.
8. Hench, L. L.; Polak, J. M. *Science* **2002**, *295* (5557), 1014-1017.
9. Wang, Y. D.; Ameer, G. A.; Sheppard, B. J.; Langer, R. *Nat. Biotechnol.* **2002**, *20* (6), 602-606.
10. Pattison, M. A.; Wurster, S.; Webster, T. J.; Haberstroh, K. M. *Biomaterials* **2005**, *26* (15), 2491-2500.
11. Stevens, M. M.; George, J. H. *Science* **2005**, *310* (5751), 1135-1138.
12. Hartgerink, J. D.; Beniash, E.; Stupp, S. I. *Science* **2001**, *294* (5547), 1684-1688.
13. Guler, M. O.; Hsu, L.; Soukasene, S.; Harrington, D. A.; Hulvat, J. F.; Stupp, S. I. *Biomacromolecules* **2006**, *7* (6), 1855-1863.
14. Storrie, H.; Guler, M. O.; Abu-Amara, S. N.; Volberg, T.; Rao, M.; Geiger, B.; Stupp, S. I. *Biomaterials* **2007**, *28* (31), 4608-4618.
15. Beniash, E.; Hartgerink, J. D.; Storrie, H.; Stendahl, J. C.; Stupp, S. I. *Acta Biomaterialia* **2005**, *1* (4), 387-397.
16. Jun, H. W.; Paramonov, S. E.; Dong, H.; Forraz, N.; McGuckin, C.; Hartgerink, J. *D. J. Biomater. Sci. Polym. Ed.* **2008**, *19* (5), 665-676.

17. Silva, G. A.; Czeisler, C.; Niece, K. L.; Beniash, E.; Harrington, D. A.; Kessler, J. A.; Stupp, S. I. *Science* **2004**, *303* (5662), 1352-1355.
18. Niece, K. L.; Hartgerink, J. D.; Donners, J.; Stupp, S. I. *J. Am. Chem. Soc.* **2003**, *125* (24), 7146-7147.
19. Arnold, M. S.; Guler, M. O.; Hersam, M. C.; Stupp, S. I. *Langmuir* **2005**, *21* (10), 4705-4709.
20. Kim, J. K.; Anderson, J.; Jun, H. W.; Repka, M. A.; Jo, S. *Mol. Pharm.* **2009**, *6* (3), 978-985.
21. Yuwono, V. M.; Hartgerink, J. D. *Langmuir* **2007**, *23* (9), 5033-5038.
22. Sargeant, T. D.; Rao, M. S.; Koh, C. Y.; Stupp, S. I. *Biomaterials* **2008**, *29* (8), 1085-1098.
23. Mata, A.; Hsu, L.; Capito, R.; Aparicio, C.; Henrikson, K.; Stupp, S. I. *Soft Matter* **2009**, *5* (6), 1228-1236.
24. Hung, A. M.; Stupp, S. I. *Nano Lett.* **2007**, *7* (5), 1165-1171.
25. Hung, A. M.; Stupp, S. I. *Langmuir* **2009**, *25* (12), 7084-7089.
26. Pashuck, E. T.; Cui, H. G.; Stupp, S. I. *J. Am. Chem. Soc.* **2010**, *132* (17), 6041-6046.
27. Hsu, L.; Cvetanovich, G. L.; Stupp, S. I. *J. Am. Chem. Soc.* **2008**, *130* (12), 3892-3899.
28. Hartgerink, J. D.; Beniash, E.; Stupp, S. I. *Proc. Natl. Acad. Sci. U. S. A.* **2002**, *99* (8), 5133-5138.
29. Paramonov, S. E.; Jun, H. W.; Hartgerink, J. D. *J. Am. Chem. Soc.* **2006**, *128* (22), 7291-7298.
30. Jiang, H. Z.; Guler, M. O.; Stupp, S. I. *Soft Matter* **2007**, *3* (4), 454-462.
31. Stendahl, J. C.; Rao, M. S.; Guler, M. O.; Stupp, S. I. *Adv. Funct. Mater.* **2006**, *16* (4), 499-508.

32. Velichko, Y. S.; Stupp, S. I.; de la Cruz, M. O. *J. Phy. Chem. B* **2008**, *112* (8), 2326-2334.
33. Lee, O. S.; Stupp, S. I.; Schatz, G. C. *J. Am. Chem. Soc.* **2011**, *133* (10), 3677-3683.
34. Tovar, J. D.; Claussen, R. C.; Stupp, S. I. *J. Am. Chem. Soc.* **2005**, *127* (20), 7337-7345.

## **Chapter 2**

# **Wormlike Micelle Formation in Peptide Amphiphiles Driven by Secondary Structure Transformation of the Headgroups**

## 2.1 Introduction

Wormlike micelles are long, extended objects of several nanometers in diameter and micrometers in length.<sup>1</sup> Such extended objects can form entangled, fibrous networks, mimicking concentrated polymer solutions, gels or protein extra-cellular matrices and exhibiting pronounced viscoelastic behavior.<sup>2,3</sup> Micelles are both scientifically interesting, as controllable examples of self-assembly, and technologically useful objects. Spherical micelles are agents of detergency, emulsification and drug delivery; extended micelles are increasingly being explored in biomedical contexts, such as the formation of synthetic, biofunctional extracellular matrices.<sup>4,5</sup> The simplest theoretical picture for determining the geometry of aggregates is expressed in terms of the shape of the amphiphilic assemblers.<sup>6</sup> The type of assembly at a certain concentration in this picture depends on the intrinsic surfactant geometry, which is often represented by the packing parameter,  $P = V/A_0L$ , where  $V$  and  $L$  are, respectively, the volume and length of the hydrophobic tail, and  $A_0$  is the optimal surface area of the headgroup. Values of  $P$  between  $1/3$  and  $1/2$  predict cylindrical assemblies, such as wormlike micelles. The interactions among the lipid tails can be reasonably well represented by the packing parameters  $V$  and  $L$ , which are directly related to the physical size of the hydrophobic part of the molecule;  $A_0$  is more difficult to ascertain a priori. It depends not only on size, but also on interactions among the headgroups.  $A_0$  is therefore connected, for example, to electrostatic interactions in simple surfactants, or to excluded volume interactions connected with solvation in amphiphilic diblock copolymers.<sup>7</sup>

In this paper, it was presented that a class of interactions, not present in traditional amphiphiles or block copolymers, arising from structural associations among

the headgroups, can spontaneously trigger and drive the geometry of assembly from spherical to wormlike micelles. Specifically, the transition from  $\alpha$ -helices and random coils to  $\beta$ -sheets, a reorganization of the headgroup secondary structure observed in process, gives rise to a transformation of the micellar assembly from spherical to extended micelles. Other recent work<sup>8</sup> has nicely demonstrated, via synthetic variations in peptide sequence, the role that  $\beta$ -sheet formation plays in producing nanofibers consisting of cylindrical micelles of peptide amphiphiles. That work focused on the nature of the final state of the micellar solution rather than on the pathway of transformation to the final state. Velichko, et al.<sup>9</sup> have studied the trajectory of nanofiber formation in peptide amphiphiles by Monte Carlo-stochastic dynamics simulations. Their calculations anticipate transitions among different micellar states, including spherical to cylindrical, based on the interplay between hydrophobic interactions of the tails and hydrogen bonding interactions of the peptide headgroups. This paper gives new experimental data in support of those general ideas. We introduced a class of amphiphilic molecules,<sup>10-12</sup> which now falls into the broader class of PAs, in which a peptide headgroup is covalently coupled to a synthetic or natural lipid, fatty acid, or hydrophobic alkyl chain tail. Earlier work in our group<sup>13,14</sup> has shown that peptides in these conjugate molecules can adopt ordered secondary structures, both triple-helical and  $\alpha$ -helical, when the PA is present above the concentration necessary for micelles to form (the critical micelle concentration, or cmc), even when the unconjugated peptide is disordered at those same concentrations. The induction of order is due to the configurational constraints imposed by a combination of elevated local peptide concentration in the corona of the micelle, and the reduction in translational and rotational degrees of freedom caused by peptide tethering. This class

of molecules is important in its own right, as PAs are being effectively exploited in a number of laboratories for a variety of interesting functional materials <sup>8,15-18</sup> in addition to the new insights they bring to biomolecular assembly. It is specifically the interplay between the forces of micellar assembly (hydrophobic and hydrogen bonding, leading to secondary structure formation and transformation) and micellar shape. This type of self-assembly (involving hydrophobic tails) is distinct from the other interesting processes and products of self-assembly based on peptide interactions alone, <sup>18-21</sup> though clearly some peptides are themselves amphiphilic.<sup>18</sup> The physics of these different-but-related self-assembly routes requires further clarification, which is one of the objectives of the present work.

## **2.2 Experimental Methods**

### **2.2.1 Design and synthesis of the peptide amphiphile; C16-W3K**

In this work, a peptide with known  $\alpha$ -helical propensity <sup>22,23</sup> and with an axially symmetric distribution of hydrophilic lysine groups in the helical form was chosen, as shown in Figure 2-1. This peptide was termed W3K, signifying that it is an alanine peptide chain supplemented with one tryptophan (to enable fluorescence measurement of concentration) and three lysines (to render the peptide soluble in water). This symmetrical arrangement of lysines was chosen to predispose the peptide to form individual  $\alpha$ -helices in the micellar state, in contrast to the supercoiling that occurs with amphipathic helices. <sup>24</sup>

For the synthesis of C16-W3K, the peptide W3K was synthesized by Synpep Corporation and was received still coupled to the solid-phase resin. The peptide amphiphile C16-W3K is made by conjugating the peptide W3K to palmitic acid with

Fmoc solid phase peptide synthetic methods<sup>10</sup>. The conjugates were purified by High Performance Liquid Chromatography (HPLC) on a reversed-phase C4 column with gradients of acetonitrile in water with 0.1 % trifluoroacetic acid. The identity of purified conjugates was verified by MALDI-TOF (Matrix Assisted Laser Desorption Ionization - Time Of Flight) mass spectrometry.

Solution samples were prepared by adding buffer (10 mM sodium chloride and 1 mM sodium phosphate) to the synthesized conjugates C16-W3K at room temperature at a peptide concentration of about 80  $\mu\text{M}$ , determined by the optical density of tryptophan at 280 nm (well above the cmc that is at  $\sim 2 \mu\text{M}$ ).

### **2.2.2 Sample analysis**

Structures of the samples were characterized by cryogenic transmission electron microscopy (cryo-TEM), rheological measurement, circular dichroism (CD), and atomic force microscopy (AFM) and infrared (IR) spectroscopy in the attenuated total reflection (ATR) mode.

Samples for the cryo-TEM measurement were prepared by putting the peptide amphiphile solutions on lacey carbon grids in a controlled environment vitrification system (CEVS), which contained saturated water vapor to prevent evaporation of water from the sample solutions. The samples were then rapidly dropped into liquid ethane at its melting temperature and transferred into liquid nitrogen ( $-196^\circ\text{C}$ ). The vitrified samples were mounted on a cryogenic sample holder (Gatan) and examined with a JEOL TEM 1210 at an accelerating voltage of 120kV at approximately  $-175^\circ\text{C}$ . Viscosity and storage and loss moduli of the solutions were measured in an ARES-RFS rheometer operated in the cone and plate geometry (cone and plate diameter of 50mm



and cone angle of 0.04 radians) at 20°C. The gap between the cone and plate was 0.05mm. For the AFM measurement, the solution was deposited on freshly cleaved mica and kept for 20 seconds before blowing off the extra solution. Experiments were carried out with a D3000 AFM (Digital Instruments, Ltd.) in tapping mode.

CD spectra were collected with an Olis spectropolarimeter in a quartz cell (path length = 1 mm).

## **2.3 Results**

### **2.3.1 Self-assembled structure**

The cryo-TEM images of the C16-W3K solution immediately (a) and 13 days (b) after making solutions are shown in Figure 2-2. As shown in Figure 2-2 (a), the TEM image of the C16-W3K solution immediately after making solution shows existence of many discrete spherical micelle structures of diameter around 10 nm. In contrast, the image of the C16-W3K after 13 days (Figure 2-2 (c)) exhibits long nanofibrillar structures with outer diameter of ~10 nm. The images of the time-interval between initial dissolution and 13 days after dissolution, for example, Figure 2-2 (b), show mixtures of spherical and shorter extended micelle structures. The existence of such incomplete shorter “wormlike” micelle implies that the transition of the micelles structures occurs through the collision of spherical micelles and/or shorter extended micelles at least in the initial stage of the transition. The resultant nanofibrils are water soluble and have the character expected of cylindrical, wormlike micelles of the peptide amphiphiles. They do not appear to have the ribbon-like structures seen in assemblies of  $\beta$ -sheet forming peptides without hydrophobic conjugation<sup>25</sup>.

The fibril formation of C16-W3K was further confirmed by the large viscosity

change and appearance of pronounced viscoelasticity in the peptide amphiphile solution. Figure 2-3 (a) shows the viscosity of the C16-W3K solution as a function of shear rate measured by Dynamic Mechanical Analysis; immediately (original) and 13 days after making solution samples. The viscosity is constant at  $\sim 10^{-3}$  [Pa-s], almost as low as that of buffer for immediately measured sample, whereas for the sample after 13 days, the viscosity shows non-Newtonian characteristics with increased viscosity at lower shear rate. In the results of storage and loss moduli of the C16-W3K solution (Figure 2-3 (b)), for the original sample, the value of the loss modulus almost always surpasses the value of the storage modulus, which means the solution behaved more liquid-like, whereas for the sample after 13 days, the storage modulus is completely over the loss modulus, which implies that the solution is more solid-like. Further, fibrillar structures are also clearly observed in the AFM image (Figure 2-4). From the AFM image, the lengths of the fibrils are often longer than 5  $\mu\text{m}$ .

### 2.3.2 Peptide secondary structure

Peptide secondary structures in the assemblies were determined by time-dependent CD. From CD results at 25°C (Figure 2-5 (a)), it was found that the peptide W3K in the C16-W3K, changes its secondary structure from  $\alpha$ -helix and random coil to  $\beta$ -sheet with time after initial dissolution, while maintaining the solution at 25°C. The initial CD spectrum is indicative of some  $\alpha$ -helical content as indicated by the two minima at  $\sim 203$  and  $\sim 222$  nm (Figure 2-5 (a)) with a substantial random coil component ( $\sim 196$  nm). Over a period of days at 25°C, the intensity of the peak at 202 nm decreases, the peak at 220 nm shifts to 218 nm and the intensity of the peak at 218 nm continues to increase. After 13 days, the spectrum has transformed to one typical of

the  $\beta$ -sheet structure with a single minimum at 218 nm. No similar transformation of peptide secondary structure occurs with the W3K peptide alone (watery line) without conjugation to the hexadecyl chain. The CD results show that this PA molecule, which initially assembles as spheres, changes its secondary structure from a fluctuating mixture of  $\alpha$ -helix and random coil to  $\beta$ -sheet with time with no further thermal or chemical stimulus. Though some custom-made amphipathic polypeptides with alternating hydrophobic and hydrophilic residues in peptide have been known to form  $\alpha$ -helical or  $\beta$ -sheet structure depending on the conditions due to specific interactions among peptides such as hydrophobic and/or ionic interactions,<sup>26-28</sup> this alanine-based peptide was found to change its secondary structure to  $\beta$ -sheet despite the fact that the peptides, even when helical, do not present faces of differing solvent affinity. Inclusion of alanines to promote fiber formation of PAs has previously been shown. This was attributed to  $\beta$ -sheet formation along the fiber axis via intermolecular hydrogen bonding between alanines near the core-corona interface. Therefore, it appears that the stabilizing hydrogen bonding between peptides provide enough energy to overcome the tendency of each peptide to fold into an  $\alpha$ -helix.<sup>29</sup>

ATR-IR confirms the  $\beta$ -sheet structure, having a characteristic absorption band at  $1625\text{ cm}^{-1}$  (C=O stretch). Figure 2-6 shows the IR spectra of dried C16-W3K solutions 10 min, 3 days, 7 days, and 13 days after making the solution. In the IR spectrum, the peak around  $1655\text{ cm}^{-1}$  is assigned to C=O stretch in  $\alpha$ -helix and random coil and the peak at  $1625\text{ cm}^{-1}$  is assigned to C=O stretch in  $\beta$ -sheet structure. The IR spectra of C16-W3K show that the peak intensity at  $1625\text{ cm}^{-1}$  increases gradually as time passes. The IR results that exhibit the conformational transition from  $\alpha$ -helix and random coil to  $\beta$ -sheet structures as time elapse coincide with the result of CD

measurement, indicating that  $\beta$ -sheet structure of W3K was preserved after drying the solutions.

### **2.3.3 Effect of temperature on the peptide transition**

The kinetics of transformation was manipulated by changing temperature of the sample solution. Though the  $\beta$ -sheet formation takes 13 days when the peptide amphiphile solution is kept at 25°C, when the sample is incubated at 50°C, only 150 min is required to complete the transition as Figure 2-5 (b) shows. The spectra at 50°C (at 150, and 200 min) show more random coil than the spectra at 25°C in Figure 2-5 (a) (at 13 days). The accelerated transition at higher temperature indicates that  $\beta$ -sheet structure is more thermodynamically stable than  $\alpha$ -helical and random coil structure for the peptide in the PA micellar assembly.

### **2.3.4 Effect of PA alkyl tail length on the peptide transition**

Peptide Amphiphiles with different alkyl tail length (C12, C14 and C18) were synthesized for studying effect of the alkyl tail length on the peptide structural change, by conjugating the peptide W3K to lauric acid (C12-W3K), tetradecanoic acid (C14-W3K) and stearic acid (C18-W3K) with using same synthetic method as C16-W3K synthesis. Figure 2-7 (a) shows the CD spectra of C14-W3K solution at the incubation time of 0, 2, 4, 7 hours at 50°C. The spectra indicated that the peptide in C14-W3K also changed the secondary structure from  $\alpha$ -helix and random coil to mainly  $\beta$ -sheet with the incubation time. However, as compared to the CD results of C16-W3K (Figure 2-5 (b)), it was found that the speed of the transition on C14-W3K was slower than that of C16-W3K. C16-W3K underwent  $\alpha$ -to- $\beta$  transition in 150 min, while

C14-W3K took almost seven hours. The result indicated that the shorter alkyl tail of the peptide amphiphile slowed down the  $\alpha$ -to- $\beta$  transition. It was supported by the fact that the  $\alpha$ -to- $\beta$  transition required more than thirty days in C12-W3K at 25 °C, much longer than thirteen days at 25 °C in C16-W3K.

Figure 2-7 (b) shows the CD spectra of C18-W3K solution at incubation time of 0, 20, 40, 60, 180 min. Though it has been expected that the  $\alpha$ -to- $\beta$  transition in C18-W3K proceeded much faster than that of 16-W3K, there were little difference in the speed of the transition of C16-W3K and C18-W3K. The reason of the little difference was presumed that the alkyl tail of C18 has coiling of chains, while the alkyl tails of C16 and less than C16 are relatively stretched in water<sup>30</sup>.

### **2.3.5 Effect of initial micelle formation on the peptide transition**

A critical micelle concentration (CMC), a concentration at which micelles appear in the solution, of C12-W3K is much higher than that of C16-W3K. The CMC of C12-W3K was ~450  $\mu$ M, while that of C16-W3K was ~2  $\mu$ M. Though it was impossible to measure CD in the sample below the CMC in C16-W3K because the concentration was too low to measure, the CD spectrum of the sample below the CMC in C12-W3K was able to be obtained. Figure 2-8 shows the CD spectra of the samples below and above the CMC in C12-W3K at 0°C after thirty days incubation at 25°C. Though the spectrum of the sample above the CMC (red line) revealed that the peptide formed predominantly  $\beta$ -sheet structure after the  $\alpha$ -to- $\beta$  transition, the spectrum of the sample below the CMC (blue line) exhibited the  $\alpha$ -helical structure was preserved even after the thirty days. The results apparently reveal the effect of the micelle formation on the structural change in the peptide. Further, the stability of the  $\beta$ -sheet structure of the

sample above the CMC was investigated with these samples by changing temperature of the solutions (Figure 2-9). The  $\alpha$ -helical structure in the sample below the CMC was transformed to random coil, that has one broad minimum around 200 nm, reversibly by increasing the solution temperature from 0°C to 70°C. In contrast, in the sample above the CMC, just a small amount of  $\beta$ -sheet structure changed to random coil and most of the  $\beta$ -sheet remained even at 70°C. These transitions of the two samples were reversible.

## 2.4 Discussion

The data from TEM with supporting evidence from rheology and AFM, CD, and IR on the novel peptide amphiphile C16-W3K indicate that immediately after dissolution of the PA, the peptide forms a random coil structure with some helical content in the spherical micelle, while after 13 days the peptide has transformed into mainly  $\beta$ -sheet structure in the wormlike micelles that have formed concomitantly. That is, the peptide amphiphile C16-W3K changes the assembly structure from spherical to wormlike simultaneously with secondary structure changing from  $\alpha$ -helix and random coil to mainly  $\beta$ -sheet. Since there are no external stimuli triggering these transitions, the evident conclusion is that the  $\beta$ -sheet formation in the hydrophilic head-groups of the spherical micelle drives the overall transformation to wormlike micelles. The cryo-TEM snapshot of the intermediate phase of the transition, typified by Figure 2-2(b), indicates that shorter “wormlike” micelles grow by extending axially, rather than by some direct formation process of long, extended micelles. The transition is likely driven by an attraction force due to the peptide configurational transition. In terms of the packing model discussed earlier, it appears that the  $\beta$ -sheet formation has reduced the effective area per headgroup, leading to less complete coverage of the hydrophobic core

and therefore enhanced attraction. It is known that uniaxial elongation of micellar aggregates of ionic surfactants can be triggered by tuning the experimental conditions, such as increasing surfactant concentration, changing temperature, or varying salinity of a buffer. The transition mechanism in PA assemblies should be that the peptide changes the secondary structure in the micellar corona to the more stable  $\beta$ -sheet via gradual adjustment of the initial spherical structure. In this system, assembly structure and peptide secondary structure of the peptide amphiphile seem to be determined cooperatively and simultaneously in a manner similar to native protein folding.

Further, the results that the peptide W3K without an alkyl tail did not show the peptide transition and that the transition speed was manipulated by changing an alkyl tail length of the PA indicate the indispensability of an alkyl tail, which tether the peptide in the micelle shell, for the peptide transition. The necessity of the micelle formation driven by the hydrophobic interactions among the alkyl tails for the transition was also exhibited by the CD results of the samples below and above the CMC on C12-W3K.

The process of the wormlike micelle formation is presumed that the peptide transition from  $\alpha$ -helix to  $\beta$ -sheet, driven by the spherical micelle formation, triggers the micelle structural change from sphere to wormlike. In other words, the resultant hierarchical structures were formed by the delicate and time-variable balance of hydrophobic interaction of alkyl tails, intra-molecular or inter-molecular hydrogen bonding in the peptide chains, and electrostatic repulsion among positively charged lysine residues. The location of three lysine presenting angler and longitudinal symmetry in  $\alpha$ -helical structure must be another key for PA to form wormlike micelles by overcoming the electrostatic repulsion.

## 2.5 Conclusion

In an effort to better understand the factors controlling peptide amphiphile micellar shape, we synthetically linked a short peptide with an  $\alpha$ -helix-forming tendency to a hexadecyl tail. These molecules initially dissolve as spherical micelles, which can persist for hours or days, followed by transformation to wormlike micelles, which occurs simultaneously with a transition in the secondary structure of the headgroup peptides to  $\beta$ -sheet. This observation provides evidence that the extended micelle is the thermodynamically favored state sought by PA micelles in the process of forming  $\beta$ -sheet structures among the head-groups, though they are not the structures formed during the initial kinetics of assembly. Micelles of peptide amphiphiles mimic the hierarchical self-assembly found in biological systems, the complexity and richness of which are just beginning to be achieved in fully synthetic systems



## References

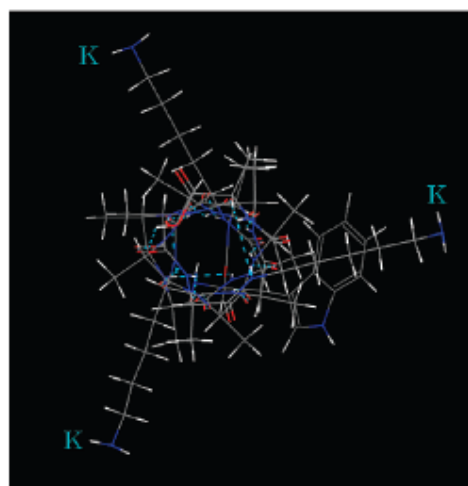
1. Keller, S. L.; Boltenhagen, P.; Pine, D. J.; Zasadzinski, J. A. *Phys. Rev. Lett.* **1998**, *80*, 2725–2728.
2. Kern, F.; Lequeux, F.; Zana, R.; Candau, S. J. *Langmuir* **1998**, *10*, 1714–1723.
3. Shikata, T.; Hirata, H.; Kotaka, T. *Langmuir* **1987**, *3*, 1081–1086.
4. Lutolf, M. P.; Hubbell, J. A. *Nat. Biotechnol.* **2005**, *23*, 47–55.
5. Hsu, L.; Cvetanovich, G. L.; Stupp, S. I. *J. Am. Chem. Soc.* **2008**, *130*, 3892–3899.
6. Israelachvili, J. N.; Mitchell, D. J.; Ninham, B. W. *J. Chem. Soc., Faraday Trans. 2* **1976**, *72*, 1525–1568.
7. Won, Y.-Y.; Bates, F. S. in *Giant Micelles: Properties and Applications*; Zana, R., Kaler, E. W., Eds.; CRC Press: Boca Raton, 2006.
8. Paramonov, S. E.; Jun, H.-W.; Hartgerink, J. D. *J. Am. Chem. Soc.* **2006**, *128*, 7291–7298.
9. Velichko, Y. S.; Stupp, S. I.; Olvera de la Cruz, M. *J. Phys. Chem. B* **2008**, *112*, 2326–2334.
10. Yu, Y.-C.; Berndt, P.; Tirrell, M.; Fields, G. B. *J. Am. Chem. Soc.* **1996**, *118*, 12515–12520.
11. Fields, G. B.; Lauer, J. L.; Dori, Y.; Forns, P.; Yu, Y.-C.; Tirrell, M. *Biopolymers* **1998**, *47*, 143–151.
12. Tu, R.; Tirrell, M. *Adv. Drug Delivery Rev.* **2004**, *56*, 1537–1563.
13. Yu, Y.-C.; Tirrell, M.; Fields, G. B. *J. Am. Chem. Soc.* **1998**, *120*, 9979–9987.
14. Bitton, R.; Schmidt, J.; Biesalski, M.; Tu, R.; Tirrell, M.; Bianco-Peled, H. *Langmuir* **2005**, *21*, 11888–11895.
15. Shimizu, T.; Masuda, M.; Minamikawa, H. *Chem. Rev.* **2005**, *105*, 1401–1444.
16. Stendahl, J. C.; Rao, M. S.; Guler, M. O.; Stupp, S. I. *Adv. Funct. Mater.* **2006**, *16*, 499–508.

17. Marques, B. F.; Schneider, J. W. *Langmuir* **2005**, *21*, 2488–2494.
18. Karmali, P. P.; Kotamraju, V. R.; Kastantin, M.; Black, M.; Missirlis, D.; Tirrell, M.; Ruoslahti, E. *Nanomedicine* **2008**, *5*, 73–82.
19. (a) Zhang, S. *Nat. Biotechnol.* **2003**, *21*, 1171–1178. (b) Zhang, S.; Holmes, T.; Lockshin, C.; Rich, A. *Proc. Natl. Acad. Sci. U. S. A.* **1993**, *90*, 3334–3338.
20. Collier, J. H.; Messersmith, P. B. *Adv. Mater.* **2004**, *16*, 907–910.
21. Woolfson, D. N.; Ryadnov, M. G. *Curr. Opin. Chem. Biol.* **2006**, *10*, 559–567.
22. Marqusee, S.; Robbins, V. H.; Baldwin, R. L. *Proc. Natl. Acad. Sci. U. S. A.* **1989**, *86*, 5286–5290.
23. Chakrabarty, A.; Kortemme, T.; Baldwin, R. L. *Protein Sci.* **1994**, *3*, 843–852.
24. (a) Yadav, M. K.; Leman, L. J.; Price, D. J.; Brooks, C. L., III.; Stout, C. D.; Ghadiri, M. R. *Biochemistry* **2006**, *45*, 4463–4473. (b) Paramonov, S. E.; Jun, H. W.; Hartgerink, J. D. *J. Am. Chem. Soc.* **2006**, *128*, 7291–7298. (c) Silva, G. A.; Czeisler, C.; Niece, K. L.; Beniash, E.; Harrington, D. A.; Kessler, J. A.; Stupp, S. I. *Science* **2004**, *303*, 1352–1355. (d) Baginska, K.; Makowska, J.; Wiczak, W.; Kasprzykowski, F.; Chmurzynski, L. *J. Peptide Sci.* **2008**, *14*, 283–289.
25. Aggeli, A.; Bell, M.; Boden, N.; Keen, J. N.; Knowles, P. F.; McLeish, T. C. B.; Pitkeathly, M.; Radford, S. E. *Nature* **1997**, *386*, 259–262.
26. Ono, S.; Kameda, N.; Yoshimura, T.; Shimaski, C.; Tsukurimichi, E.; Mihara, H.; Nishino, N. *Chem. Lett.* **1995**, *24*, 965–966.
27. Takahashi, Y.; Yamashita, T.; Ueno, A.; Mihara, H. *Tetrahedron* **2000**, *56*, 7011–7018.
28. Schenck, H. L.; Dado, G.; Gellman, S. H. *J. Am. Chem. Soc.* **1996**, *118*, 12487–12494.
29. Jonkheim, P.; van der Schoot, P.; Schenning, A. P. H. J.; Meijer, E. W. *Science* **2006**, *313*, 80–83.
30. Mukerjee, P. *Adv. Colloid Interface Sci.* **1967**, *1*, 241–275.

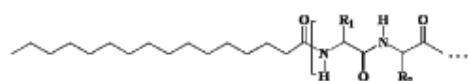
(a) WAAAAKAAAAKAAAAKA (W3K)

N-terminus C-terminus

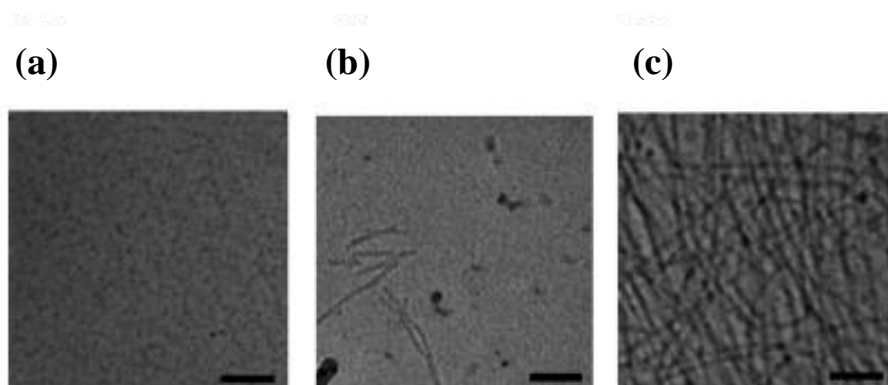
(b)



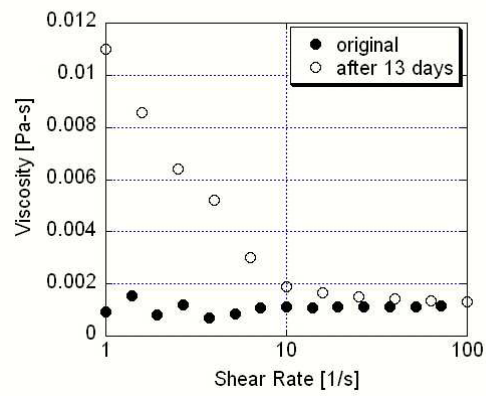
(c)



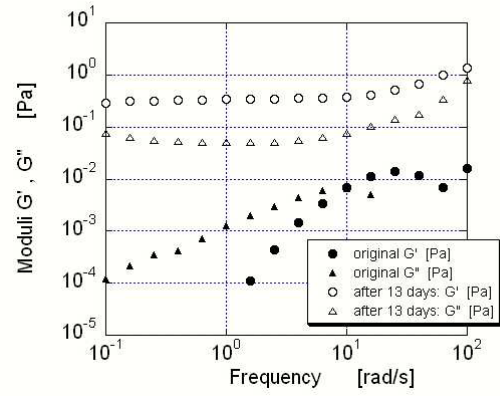
**Figure 2-1.** (a) Sequence of the peptide W3K. The peptide was chosen to contain 13 alanines to have high  $\alpha$ -helical propensity.<sup>22</sup> The other four peptides are three lysines and one N-terminal tryptophan, incorporated into the W3K peptides to introduce water solubility and to examine the accurate concentration of the peptide. The locations of three lysines in the amino sequence were determined to be distributed in an axisymmetric fashion in the peptide, presenting no angular and longitudinal asymmetry around the  $\alpha$ -helix. (b) The structure of W3K optimized by the molecular mechanics method with the COMPASS Force Field produced by Accelrys Software Inc. The image shows that three lysines are equally distributed in the peptide, presenting no angular and longitudinal asymmetry around the  $\alpha$ -helix. (c) Schematic chemical structure of the peptide amphiphile C16-W3K.



**Figure 2-2.** Cryo-TEM images of C16-W3K solutions. (a) Immediately, (b) 3 days, and (c) 13 days after making solutions. Spherical micelles of diameter  $\sim 10$  nm were scattered around the solution in Figure 2-2 (a), whereas in Figure 2-2 (c), long “nanofibrils” of similar diameter were observed. Figure 2-2 (b), the intermediate phase of the transition, shows shorter nanofibrils. Scale bars, 100 nm.

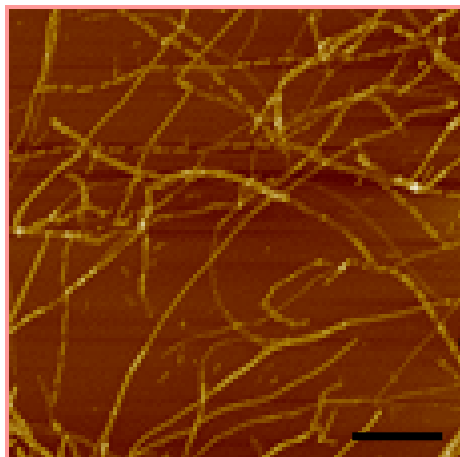


(a)

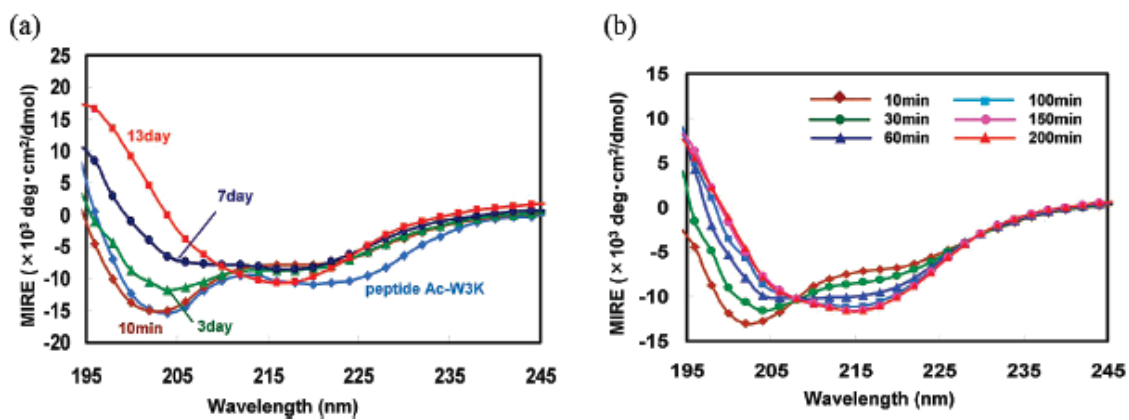


(b)

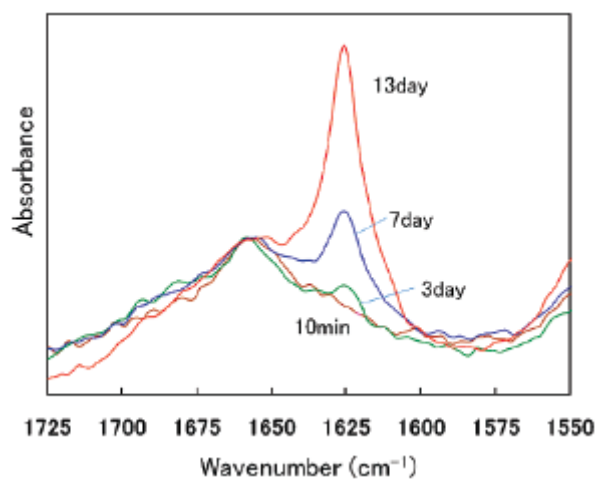
**Figure 2-3.** The results of rheological measurements of C16-W3K solutions. Viscosity (a) and storage and loss moduli (b) of C16-W3K solution immediately and 13 days after the sample preparation.



**Figure 2-4.** The AFM image of the dried C16-W3K solution 13 days after solution preparation. Scale bar = 1  $\mu\text{m}$ .

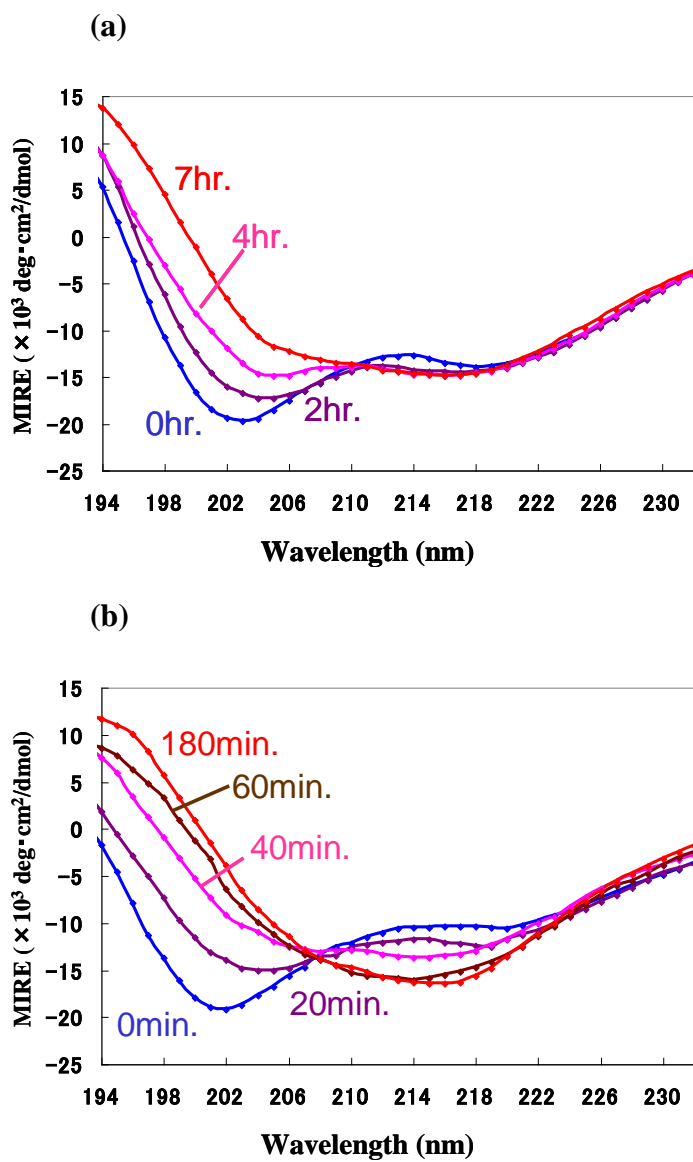


**Figure 2-5.** The CD spectra (mean integrated residue ellipticity, MIRE) of C16-W3K solutions at various times after preparation. (a) The samples were held and CD spectra obtained at 25 °C. The CD spectra evolve in a time-dependent manner from minima at ~202 and ~222 nm, representing  $\alpha$ -helical and random coil structures, to a single minimum at 218 nm, representing  $\beta$ -sheet structure. (b) The samples were held and CD spectra obtained at 50 °C. The transition is accelerated at 50°C relative to the rate at 25 °C.

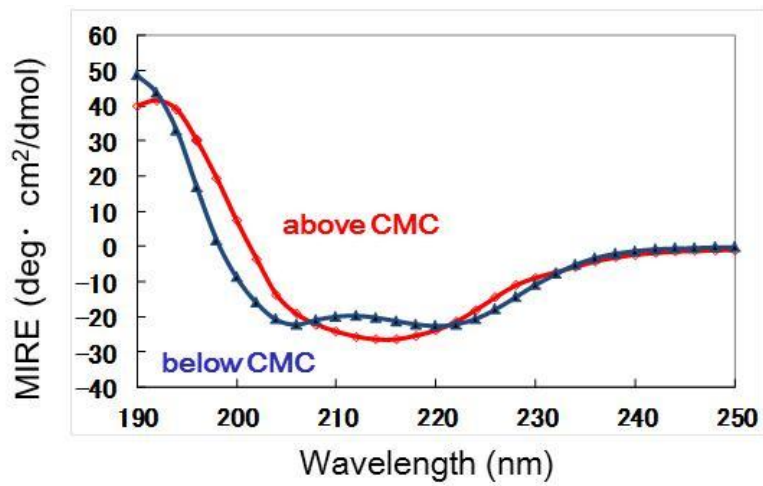


**Figure 2-6.** Time-dependent IR spectra of the dried C16-W3K solutions. Four curves are normalized at  $1655\text{ cm}^{-1}$ . The IR absorbance peak at  $1625\text{ cm}^{-1}$  is indicative of parallel  $\beta$ -sheet structure. The IR results demonstrate the increase of  $\beta$ -sheet content with time.

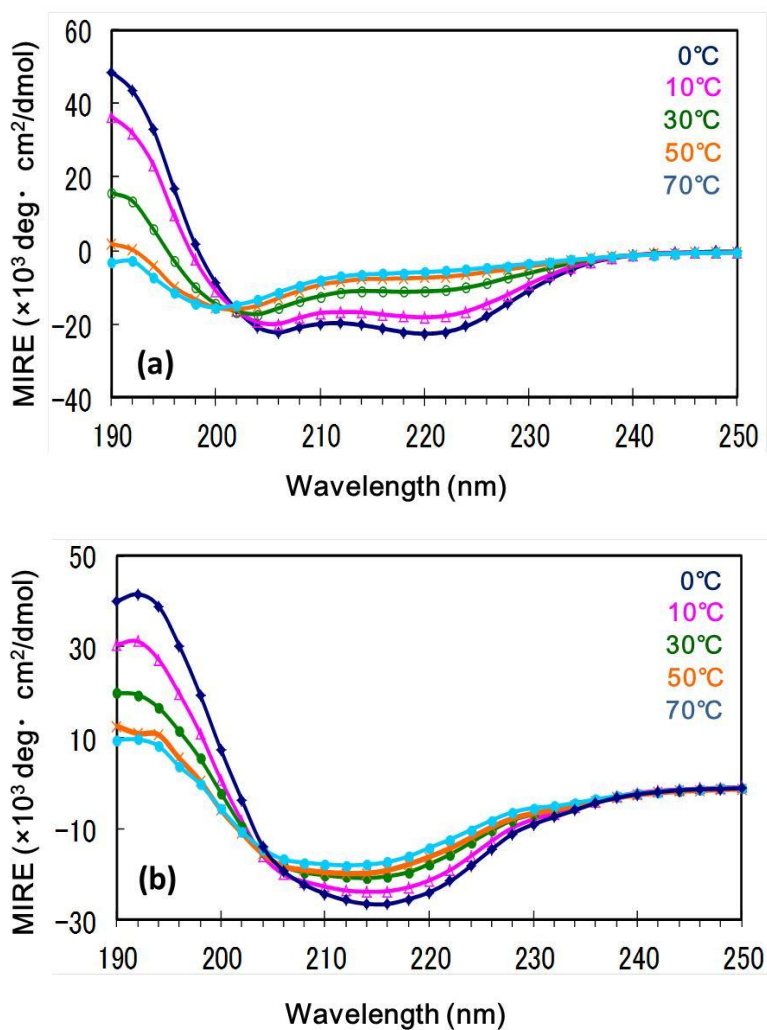




**Figure 2-7.** The CD spectra on C14-W3K (a) and on C18-W3K (b) after different incubation time at 50°C.



**Figure 2-8.** The CD spectra of the samples below and above the critical micelle concentration on C12-W3K after 30 days incubation at 25 °C, measured at 0 °C.



**Figure 2-9.** The CD spectra of the samples below (a) and above (b) the critical micelle concentration on C12-W3K after 30 days incubation at 25°C, measured at different temperature (0, 10, 30, 50 and 70°C).

## **Chapter 3**

# **Self-Assembly Process of Peptide Amphiphile Wormlike Micelles**

### 3.1 Introduction

Peptide amphiphiles (PA) are promising as molecular building blocks that can construct complex supramolecular structures in a bottom-up, modular fashion employing the wide variety of molecular designs and bioactivities that can be built into the peptide region. PA comprising hydrophilic peptides and hydrophobic alkyl tails in one molecule form various self-assembled structures, such as spherical micelles, wormlike micelles, bilayer membranes and vesicles, in a similar fashion to traditional amphiphilic molecules (such as surfactants), depending on the volume and length of the alkyl tail and surface area of the peptide head-group<sup>1</sup>. These self-assembled structures are useful as carriers and matrices because they can encapsulate and solubilize small hydrophobic molecules and can form 3D networks<sup>2-4</sup>. Of the various PA assembly structures, the “wormlike micelle” is one of the most attractive structures for the application of a functionalized artificial extracellular matrix (ECM) because the diameter of the micelle can be controlled on the nano-scale and bioactivity can be displayed on the micelle surface<sup>5-10</sup>. For example, it has been reported that PA wormlike micelles displaying the isoleucine-lysine-valine-alanine-valine (IKVAV) domain have capacity for directing neural cell differentiation<sup>7</sup>. Knowledge and technology for controlling the nano- and micro-structures of the PA assembly to give specific bioactivity of wormlike micelle are very much needed in tissue regenerative therapies. This need for understanding and ability to manipulate the formation process, not only to reach the desired final *structural* state, but also to achieve desired *processability* characteristics, such as injectability and subsequent gelation, motivates this work.

In recent years, PA that can form wormlike micelles in certain environments (pH, solvent, concentration etc.) have been developed and the presence of  $\beta$ -sheet structure is observed as a common structure in these PA<sup>11-14</sup>. Therefore,  $\beta$ -sheet formation in PA is presumed to play a key role in wormlike micelle formation. However, the studies that actually track the self-assembly processes of PA wormlike micelle are few, and the mechanism of the formation is not fully understood. In this work, the assembly process into wormlike micelles of the peptide amphiphile (C16-W3K) was studied, which has already been reported to form wormlike micelle simultaneously with  $\beta$ -sheet formation in the peptide W3K in our previous study<sup>15</sup>. The useful features of the C16-W3K for this study are simple structure, slow formation speed, and absence of a need for a specific trigger to induce the structural change. The sample was incubated at temperatures approaching 50°C to adjust the transition time to an adequate range for convenient analytical measurement. The self-assembly structures in the samples at different incubation time are analyzed with Small-Angle Neutron Scattering (SANS) and Atomic Force Microscopy (AFM).

## **3.2 Experimental methods**

### **3.2.1 Design and synthesis of the peptide amphiphile; C16-W3K**

The peptide amphiphile C16-W3K (Figure 3-1) was synthesized by covalent linkage of a peptide W3K and an alkyl tail of C16 (i.e. containing sixteen CH<sub>2</sub>) using Fmoc solid phase peptide synthetic methods<sup>16</sup>. The seventeen-residue peptide (W3K) has been designed<sup>17</sup> to contain thirteen alanines to possess high  $\alpha$ -helical propensity. Three lysines are incorporated into the peptides for introducing water solubility, presenting angular and longitudinal symmetry around the  $\alpha$ -helix axis. Samples for

analytical measurements (SANS and AFM) were prepared by adding buffer (10 mM sodium chloride and 1 mM sodium phosphate) to the C16-W3K at room temperature at concentration of 0.1 wt%., followed by 50°C incubation in a water bath.

### **3.2.2 SANS measurements**

The structural change of the micelle was studied by SANS with SANS-J-II<sup>18-20</sup> at Japan Atomic Energy Agency, JAEA, in Tokai. The time-resolved SANS measurements were performed by the T-jump method as follows: (1) the sample solution was set in the quartz cell with thickness of 10 mm at room temperature; (2) the sample cell was put into the heater block set on the optical path of incident neutron beam and regulated at 44.8°C; (3) the time-resolved SANS measurements were started when the sample was transferred into the heater block. The wavelength  $\lambda$  of the incident beam is 0.5 nm, the camera length was 2.5 m, and the accumulation time of each shot was 10 min. The two-dimensional SANS patterns obtained were averaged circularly, and corrected for absorption, the scattering from the empty cell, and the absolute intensity.

### **3.2.3 AFM measurements**

For AFM analysis, the samples were deposited on freshly cleaved mica, kept for 10 seconds at room temperature before blowing off any possible small debris on the surface. Experiments were carried out with D3000 (Digital Instruments, Ltd.) in tapping mode. 50°C incubation was performed by keeping the sample in a 50°C water bath for 10 min, 20 min, 30 min, 60 min, 120 min and 210 min.

### 3.3 Results and discussion

The structure of the peptide amphiphile C16-W3K is shown in Figure 3-1. Time-resolved SANS was used to analyze the self-assembly process of the C16-W3K in order to obtain *in situ* and continuous information <sup>21</sup>. Figure 3-2 shows the scattered intensity  $I(q)$  before and after the T-jump from room temperature to 44.8°C, plotted double-logarithmically as a function of the magnitude of the scattering vector  $q$ , defined by

$$q=4\pi \sin(\theta/2)/\lambda \quad (1),$$

where  $\theta$  is scattering angle. The SANS profile of the sample before the T-jump (Figure 3-2: open diamonds) shows that the scattering profile is proportional to  $q^{-4}$  in the region larger than  $0.7 \text{ nm}^{-1}$  and to  $q^0$  in the region smaller than  $0.3 \text{ nm}^{-1}$ , indicating spherical micelles. Though it was deduced previously <sup>15</sup> that C16-W3K form spherical micelles in the early stages of self-assembly from the cryo-TEM images, it was difficult to observe the spherical shape clearly due to its kinetic instability and smaller size relative to those of cylindrical shape. The SANS profile is direct experimental evidence for the existence of the spherical micelle as an intermediate preceding wormlike micelle formation. We conjecture that this pathway *via* the intermediate spherical state is a key factor for forming water-soluble wormlike micelle, rather than insoluble aggregates.

In contrast, the profile of the sample after 600 min (Figure 3-2: filled circles) is also proportional to the  $q^{-4}$  in the large  $q$  region, but the profile is proportional to  $q^{-1}$  for small  $q$ , indicating a locally cylindrical form of the scatterers, that is, wormlike micelles. Taken together this set of results means that structure of the micelles changes from spherical to wormlike during the incubation.



Black and red lines in Figure 3-2 show the fitting results of the SANS profiles in samples, before and 600 min. after the T-jump, respectively, to the theoretical scattering equations of sphere (Equation 2) and random oriented cylinder (Equation 3), respectively.

Sphere:

$$I(q) = CN \int_0^{\infty} P(r) \left[ \frac{4\pi r^3}{3} F_{sph}(qr) \right]^2 dr \quad (2)$$

$$F_{sph}(qr) = \frac{3}{(qr)^3} [\sin(qr) - (qr) \cos(qr)]$$

Randomly-oriented cylinder:

$$I(q) = \frac{CN}{2} \int_0^{\infty} dr \int_0^{\pi} d\beta P(r) [\pi^2 l F_{cyl}(\beta, q, r, l)]^2 \sin \beta \quad (3)$$

$$F_{cyl}(\beta, q, r, l) = \frac{2 \sin(\frac{ql}{2} \cos \beta)}{\frac{ql}{2} \cos \beta} \frac{J_1(qr \sin \beta)}{qr \sin \beta}$$

where  $r$  is a radius,  $l$  is a length of a cylinder,  $C$  is a constant independent of  $q$  and  $r$ , and  $N$  is a total number of particles.  $P(r)$  is a normalized distribution function describing a number of particles having radius  $r$ .  $P(r)$  is assumed to have the Schultz-Zimm distribution defined by:

$$P(r) = \frac{M^M}{\Gamma(M)r_0^M} r^{M-1} \exp\left(-\frac{M}{r_0} r\right) \quad (4)$$

where  $M$  is a shape factor of the distribution,  $r_0$  is a number average of  $r$ , and  $\Gamma(x)$  is the gamma function. These results exhibit that the SANS profiles before and 600 min. after the T-jump are well-fitted by the theoretical scattering equations of sphere and cylinder, respectively. The parameters obtained from the fittings are shown in Table 3-1.  $\sigma/d_0$  is a normalized standard deviation of a diameter, calculated by  $\sigma/d_0 = M^{-0.5}$ . In the fitting by Equation 3, the value of  $l$  was set to infinity. Since it can be shown that scattering from a cylinder longer than 20 nm is equivalent in this  $q$ -range, the length of the cylindrical micelle after 600 min is longer than 20 nm, but a quantitative estimate of the micelle length can not be obtained from fitting these data.

The scattering profiles of the samples during the incubation (5 min, 115 min and 315 min) show that the curves transform between the spherical one (before T-jump) and the cylindrical one (after 600 min incubation) gradually over the incubation time. As shown above, elongation of the cylindrical micelle longer than 20 nm makes no difference in this  $q$ -range. This means that the profile change over incubation time does not derive from elongation of the cylindrical micelle after that all the spherical micelles have combined into short cylinders at an early stage, since this would result in an abrupt, early transformation of the characteristic scattering from spherical to wormlike. In other words, these profiles should be interpreted as compound curves of the spherical micelles and the cylindrical micelles; the variation of the profile over time indicates the evolution of the sphere/ cylinder micelle ratio in the samples.

Therefore, the profile of the sample 115 min after T-jump (Figure 3-2: green line) was fitted by the theoretical compound equation (Equation 5) of spherical and cylindrical scattering equations.

$$I(q) = (1 - x)I_{sph}(q) + xI_{cyl}(q) \quad (5)$$

In Equation 5,  $I_{sph}(q)$  and  $I_{cyl}(q)$  are theoretical scattering forms of sphere and cylinder with the parameters shown in Table 3-1. The profile of the 115 min. incubation sample can be well-fitted by Equation 5, compound equation of  $I_{sph}(q)$  and  $I_{cyl}(q)$  (Figure 3-2: green solid line).

Figure 3-3 shows the time change of the cylindrical micelle ratio ( $x$ ) calculated by the profile fitting of Equation 5. In the fitting, all the parameters of  $I_{sph}(q)$  and  $I_{cyl}(q)$ , including the polydispersity parameter, were fixed as the values in Table 3-1. The data reveal that the ratio of the cylindrical micelle in the sample increases gradually with the incubation time and the spherical micelles remain even after long incubation time (315 min.). The remaining spherical micelle and gradual decrease of the spherical micelle may indicate that the wormlike micelle formation proceed by attachment of the sphere to the end of the short cylinder one by one (Scheme 3-1: lower image), not by simultaneous sphere combining followed by combining between cylinder and cylinder (Scheme 3-1: upper image). In our previous work, the Circular Dichroism (CD) measurement of the C16-W3K solution showed the gradual transition of the peptide secondary structure from  $\alpha$ -helix and random coil to  $\beta$ -sheet in the C16-W3K during the 50°C incubation<sup>15</sup>. The reduction of the effective area of hydrophilic headgroup in the packing parameter<sup>1</sup>, generally used to predict micelle shapes, due to the secondary structural change, specifically due to attractive hydrogen bonding in the  $\beta$ -sheet, should induce the micelle transition from sphere to wormlike.

This interpretation of the trajectory of the assembly process of C16-W3K is also supported by AFM results (Figure 3-4). AFM images were measured to examine the self-assembly structures visually in the samples of 10 min, 20 min, 30 min, 60 min, 120 min and 210 min incubation at 50°C. Though it should be noted the possibility that the assembly structures observed in AFM images could be different from the state in aqueous media for the SANS experiments because of its dried condition for the AFM measurement, the AFM images were presumed to reflect the assembly structure in aqueous media because the assembly structure is stabilized by the inter-molecular hydrogen bonding in the  $\beta$ -sheet. The stabilization of the  $\beta$ -sheet in dried state was confirmed by the IR measurement in the dried samples (data not shown).

All AFM images here show fibril-like materials, i.e. wormlike micelles. While, many block-like materials are observed in the sample of 10 min incubation. The block-like material in Figure 3-4 (a) is presumed to be an aggregate of unstable spherical micelles that have no inter-molecular hydrogen bonding (CD and IR shows little  $\beta$ -sheet in this sample) during the process of drying. The image of the sample before incubation exhibits just block-like materials, no fibril-like structure (data not shown).

The AFM images exhibit that the length of the wormlike micelles varies greatly in each sample. Even in the 210 min incubation sample, we can see some short fibrils. It is also found that number of the fibrils increases and the longest micelle length in each sample elongates with the passage of the incubation time. While the longest wormlike micelle is around 2  $\mu\text{m}$  in 10 min, it becomes about 3  $\mu\text{m}$  at 30 min. At 210 min, the longest fibrils are more than 5  $\mu\text{m}$  in length and more and bigger entangles are also observed.

Figure 3-5 shows the high magnification of the AFM image of the sample after the 210 min incubation. From the image, it was found that the wormlike micelles were tied into a braid in places, which should be crosslinking points to form gel.

From these results, it was deduced that nucleation of elongated micelles, and chain elongation of the micelles, occur simultaneously during the assembly process, consistent with both the SANA and AFM observations.

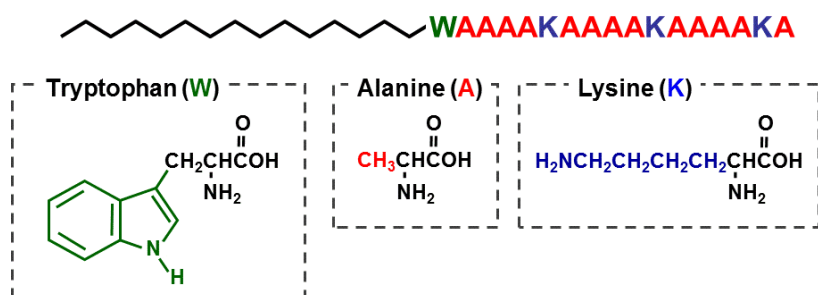
### **3.4 Conclusion**

Here, the wormlike micelle formation process of the peptide amphiphile; C16-W3K was studied with small-angle neutron scattering and atomic force microscopy. The SANS and AFM results showed that the transient spherical micelles exist in the early stage of the process and subsequently the micelle chain elongate by attachment of spherical micelles to the ends of growing cylindrical micelles in the elongated micelle formation. The understanding of the process for PA wormlike micelle formation could potentially lead to further applications of PA self-assembling materials. The trajectory we have observed here has significant implications, for example, for the rheology of the self-assembling mixture, which could, in turn, affect the utility of these materials in regenerative medicine and other expanding applications of peptide amphiphiles.

## References

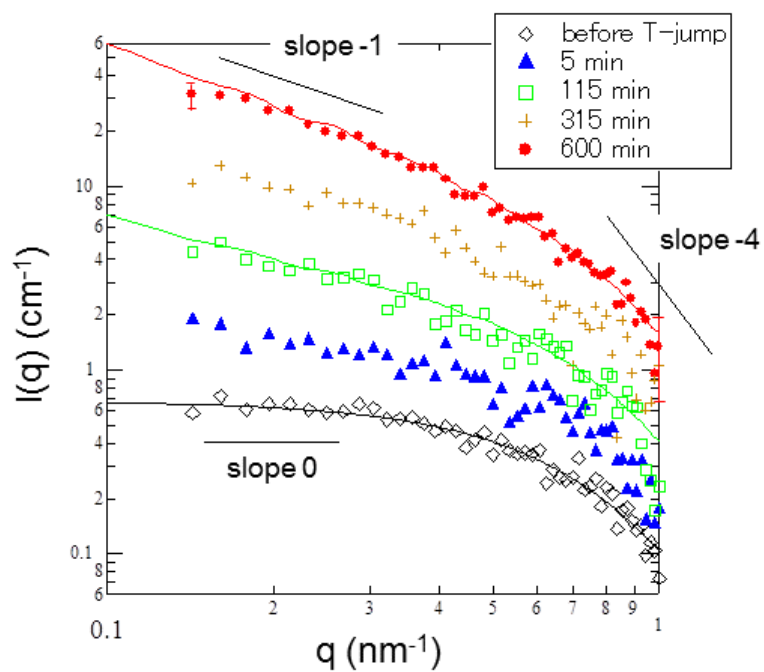
1. Israelachvili, J. N.; Mitchell, D. J.; Ninham, B. W. *J. Chem. Soc., Faraday Trans. 2* **1976**, *72*, 1525–1568.
2. Kokkoli, E.; Mardilovich, A.; Wedekind, A.; Rexeisen, E. L.; Garg, A.; Craig, J. A. *Soft Matter* **2006**, *2*, 1015-1024.
3. Cui, H.; Webber, M. J.; Stupp, S. I. *Peptide Science* **2010**, *94*, 1-18.
4. Hamley, W. *Soft Matter* **2011**, *7*, 4122-4138.
5. Hartgerink, J. D.; Beniash, E.; Stupp, S. I. *Science* **2001**, *294*, 1684-1688.
6. Hartgerink, J. D.; Beniash, E.; Stupp, S. I. *Proc. Natl. Acad. Sci. U. S. A.* **2002**, *99*, 5133-5138.
7. Silva, G. A.; Czeisler, C.; Niece, K. L.; Beniash, E.; Harrington, D. A.; Kessler, J. A.; Stupp, S. I. *Science* **2004**, *303*, 1352-1355.
8. Beniash, E.; Hartgerink, J. D.; Storrie, H.; Stendahl, J. C.; Stupp, S. I. *Acta Biomat.* **2005**, *1*, 387-397.
9. Zhang, S. *Nature Biotechnology* **2003**, *21*, 1171-1178.
10. Stevens, M. M.; George, J. H. *Science* **2005**, *310*, 1135-1138.
11. Behanna, H. A.; Donners, J. J. J. M.; Gordon, A. C.; Stupp, S. I. *J. Am. Chem. Soc.* **2005**, *127*, 1193-1200.
12. Paramonov, S. E.; Jun H-W.; Hartgerink, J. D. *Biomacromolecules* **2006**, *7*, 24-26.
13. Stendahl, J. C.; Rao, M. S.; Guler, M. O.; Stupp, S. I. *Adv. Funct. Mater.* **2006**, *16*, 499-508.
14. Paramonov, S. E.; Jun, H-W.; Hartgerink, J. D. *J. Am. Chem. Soc.* **2006**, *128*, 7291-7298.
15. Shimada, T.; Lee, S.; Bates, F.; Hotta, A.; Tirrell, M. *J. Phys. Chem. B* **2009**, *113*, 13711-13714.

16. Berndt, P.; Fields, G. B.; Tirrell, M. *J. Am. Chem. Soc.* **1995**, *117*, 9515-9522.
17. Marqusee, S.; Robbins, V. H.; Baldwin, R. L. *Proc. Natl. Acad. Sci. U. S. A.* **1989**, *86*, 5286–5290.
18. Koizumi, S.; Iwase, H.; Suzuki, J.-I.; Oku, T.; Motokawa, R.; Sasao, H.; Tanaka, H.; Yamaguchi, D.; Shimizu, H. M.; Hashimoto, T. *Physica B* **2006**, *385-386*, 1000-1006.
19. Koizumi, S.; Iwase, H.; Suzuki, J.-I.; Oku, T.; Motokawa, R.; Sasao, H.; Tanaka, H.; Yamaguchi, D.; Shimizu, H. M.; Hashimoto, T. *J. Appl. Cryst.* **2007**, *40*, 474-479.
20. Koizumi, S. *Focusing USANS Instrument Neutrons in Soft Matter (Chapter II.1.3.2)*; John Wiley & Sons, Inc.: Hoboken, New Jersey, 2011.
21. Roe, R. J. *Methods of X-ray and Neutron Scattering in Polymer Science*; Oxford University Press: Oxford, New York, 2000.



**Figure 3-1.** Chemical structure of the peptide amphiphile, C16-W3K.

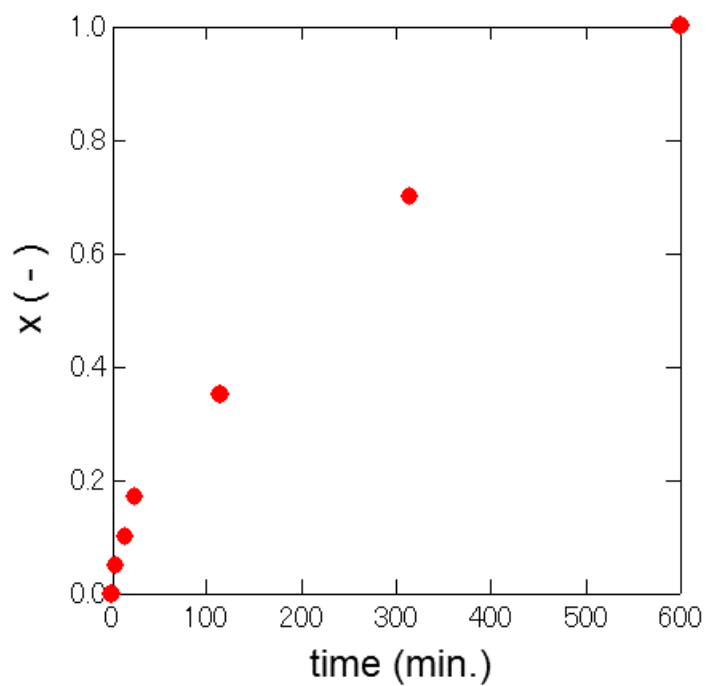




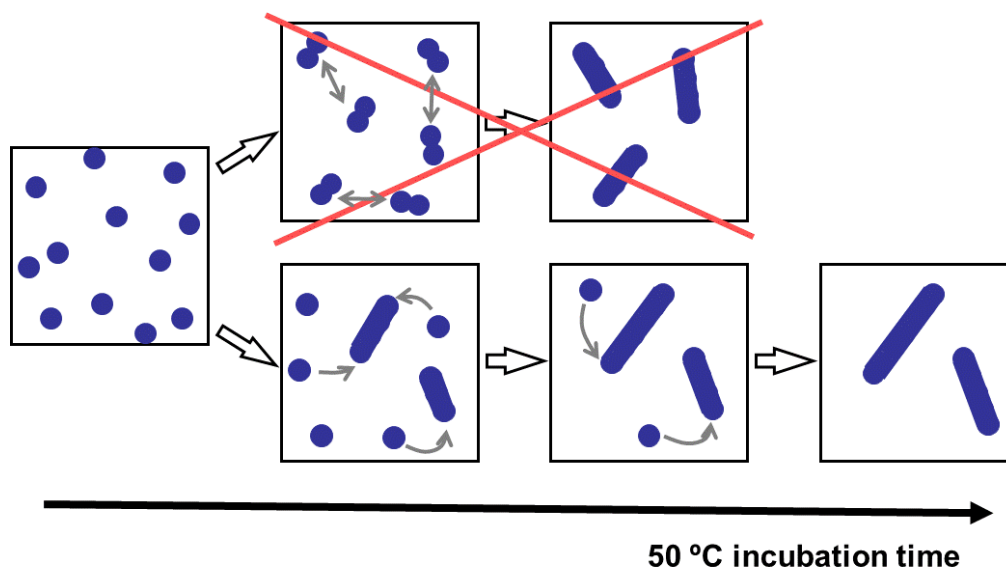
**Figure 3-2.** Time-resolved SANS profiles before and after T-jump from room temperature to 44.8°C. The symbols are measured SANS profiles, and the solid lines are theoretical scattering curves of spherical and/or cylindrical micelles. To avoid overlaps, the profiles are shifted up with factor 2.

**Table 3-1. Parameters Obtained from the Fitting of the Profiles by Equations 2 and 3.**

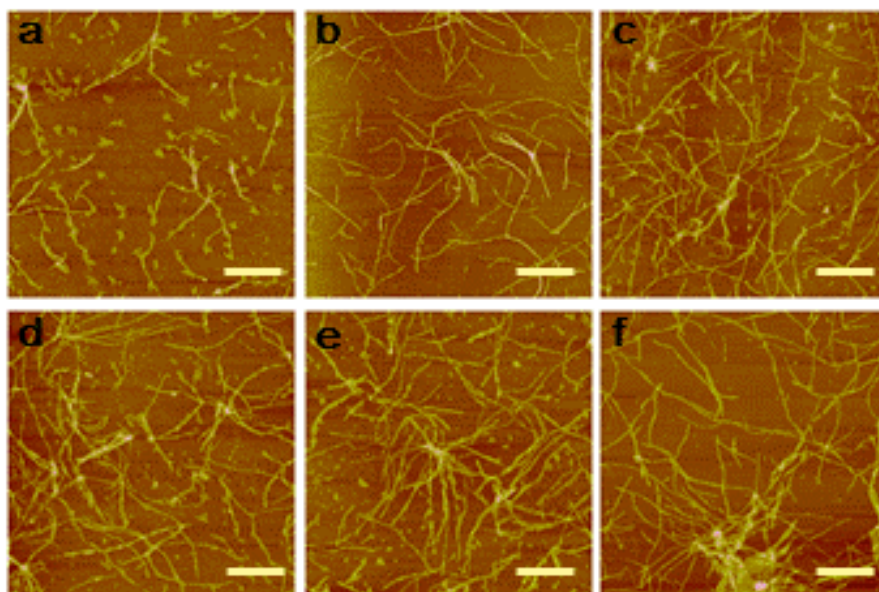
	before T-jump	600min after T-jump
micellar type	spherical	cylindrical
diameter $d_0$ (nm)	4.9	4.0
$\sigma/d_0$	0.32	0.22
cylinder length $l$ (nm)	-	>20



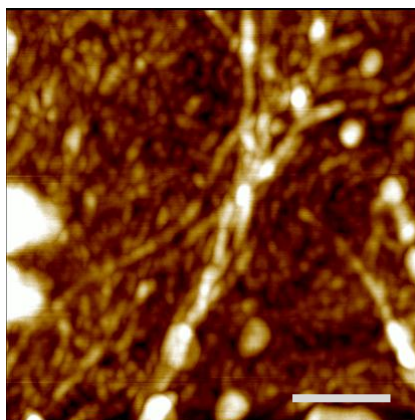
**Figure 3-3.** Cylindrical micelle evolution in the samples as a function of incubation time. The vertical axis is the fraction of cylindrical micelles in the self-assembling mixture.



**Scheme 3-1.** Self-assembly process of wormlike micelle in the peptide amphiphile C16-W3K during the 50°C incubation. Upper image exhibits the process of simultaneous sphere combining followed by combining between cylinder and cylinder, and lower image shows the wormlike micelle formation proceed by attachment of the sphere to the end of the short cylinder one by one.



**Figure 3-4.** AFM images of dried C16-W3K solution on freshly cleaved mica after 50°C incubation of (a) 10 min, (b) 20 min, (c) 30 min, (d) 60 min, (e) 120 min, (f) 210 min. scale bar, 1  $\mu\text{m}$ .



**Figure 3-5.** High magnification of the AFM image of dried C16-W3K solution after 210 min incubation at 50°C. Scale bar, 200 nm.

## **Chapter 4**

# **Wormlike Micelle Formation of Peptide Amphiphiles Induced by Fluid Mechanical Shear**

## 4.1 Introduction

Peptide amphiphiles (PA) are a class of synthetic molecules composed of a hydrophilic peptide segment (typically containing 5–30 amino acids) coupled to a hydrophobic tail (typically 10–16 carbons long), which may be single- or double-chained, natural fatty acid or lipid molecules, synthetic analogs or other hydrophobic segments. It is conceptually useful and accurate to think of these molecules as akin to, and somewhere in the molecular spectrum between, surfactants and small block copolymers.<sup>1</sup> The amphiphilicity of these molecules drives them to self-assemble in aqueous solution into structures such as spherical micelles, wormlike micelles, vesicles, monolayers, bilayers, nanotapes and ribbons due to hydrophobic interactions where the tail aggregates to minimize interactions with water.<sup>2</sup> It has been shown<sup>3–8</sup> that self-assembly of the peptide amphiphiles can induce and/or stabilize secondary structure of the peptide headgroup into triple helices,  $\alpha$ -helices, and  $\beta$ -sheets which resemble native protein molecular structures. Recapitulation of the native protein secondary structure in the peptide headgroup creates biomimetic structures, which can be employed to promote cell adhesion, spreading, migration, growth and differentiation.<sup>9–11</sup> The native secondary structure generally enhances bio-activity.<sup>12,13</sup> De novo design has been employed to select peptide sequences with propensity to form wormlike micelles, typically composed of alanine, valine or glycine amino acids.<sup>14</sup> The wormlike micelles are generally on the order of nanometres in diameter (the approximate length of two peptide amphiphile molecules) and have a polydisperse length distribution spanning many microns. In peptide amphiphiles where charged amino acids are utilized, wormlike micelle formation can be driven by pH or ion concentration changes.<sup>15</sup> It has also been shown that selfassembly into wormlike micelles is highly dependent on



hydrogen bonding and amphiphilic packing. Specifically, in one class of peptide amphiphiles,<sup>16</sup>  $\beta$ -sheet hydrogen bonds in the first four amino acids closest to the nanofiber core have been found to be necessary and sufficient to form and stabilize wormlike micelles, and disruption of those bonds will result in the formation of spherical micelles. The dimensions of the elongated wormlike micelles allow them to form entangled networks and display mechanical properties similar to those of a hydrogel.<sup>17</sup> A stable hydrogel can be operationally defined as having a storage modulus ( $G'$ ) to loss modulus ( $G''$ ) ratio of greater than 1 at a dynamic frequency of 10 Hz.<sup>18</sup> In this work, a peptide amphiphile system termed C16-W3K was used, which has been previously shown to transform with time (on the order of days) from spherical to wormlike micellar assemblies.<sup>19</sup> The C16-W3K molecule is a 17-amino acid chain composed of thirteen alanines (A), with a tryptophan (W) (to allow fluorescence measurements of concentration), and three spatially separated lysines (K) (to increase solubility in water) attached to a 16-carbon alkyl tail (Figure 4-1).<sup>19,20</sup> This arrangement of amino acids was chosen in particular due to the repeated alanine stretches and symmetrical arrangement of lysines that predisposes the peptide to form individual  $\alpha$ -helices.<sup>21</sup> Previous work demonstrates that the PA will first form spherical micelles and then over time (days at 25°C and hours at 50°C) undergo a transition to wormlike micelles with  $\beta$ -sheet character in the headgroup.<sup>19</sup> Here, it was shown that this transition can be driven by fluid shear stress, effectively and instantaneously. It was found that at a specific shear rate ( $100 \text{ s}^{-1}$ ) the system experiences an irreversible jump in viscosity, and in subsequent rheological tests, shows gel-like behavior. The measurements presented here show an abrupt transition at the micro-scale (the fibril formations) as well as on a molecular scale (the conformational  $\alpha$ -helix to  $\beta$ -sheet

transition) in the peptide amphiphile solution. A bioactive system, such as the one presented here, in which the gelation transition is driven by shear force, could be useful as an injectable matrix or scaffold for supporting tissue regeneration. Many peptide amphiphile systems have been investigated for use as matrices for applications such as bone, blood vessel or nerve tissue engineering.<sup>22,23</sup> However, most of these systems require nanofiber formation control by way of temperature or solution changes.<sup>24</sup> The present system transforms itself nearly instantaneously to a gel-like state in simple shear flow on exceeding a critical shear rate, which might be applied during the injection process itself.

## **4.2 Experimental methods**

### **4.2.1 Synthesis and material preparation**

Peptides were obtained as synthesized on resin, with side groups fully protected, from Synpep Corporation (Dublin, CA). Synthesis reagents N-hydrobenzotriazole (HOBt) and 2-(1H-benzotriazole-yl)-1,1,3,3-tetramethyl uroniumhexafluorophosphate (HBTU) were purchased from Novabiochem. All other chemical reagents were purchased from Sigma-Aldrich. The peptide amphiphile C16-W3K (Figure 4-1) was made by conjugating the peptide to palmitic acid using the Fmoc solidphase peptide-synthetic methods. All peptide amphiphiles were deprotected and cleaved using a mixture of 95% by volume trifluoroacetic acid (TFA)/water solution. The peptides were then precipitated in cold methyl-tert-butyl-ether. The conjugates were purified by reverse phase high performance liquid chromatography (RP-HPLC) on a C4 column with gradients of acetonitrile in water with 0.1% trifluoroacetic acid (TFA). The identity of purified conjugates was verified by MALDI-TOF (Matrix Assisted Laser Desorption

Ionization—Time of Flight) mass spectrometry. Purified samples were then lyophilized, resuspended by adding buffer (10 mM sodium chloride with 1 mM sodium phosphate; pH=7.4) at room temperature at a PA concentration of 700  $\mu\text{M}$  (well above the CMC 2  $\mu\text{M}$ ), and used immediately for analysis. The samples were soluble instantly in the buffer, and it was not necessary to stir the samples to dissolve the PA. All the following experiments were carried out in a similar fashion to prevent any sort of shear history before the experiments. At this neutral pH, the lysines in the PA are positively charged.

#### **4.2.2 Rheological measurements**

Rheological measurements were carried out using an ARES-RFS rheometer (TA Instruments) with a cone and plate geometry (50 mm in diameter with the cone angle of 0.04 rad) at 20°C. The gap between the cone tip and the plate was kept constant at 0.05 mm. In each experiment, a new solution of the peptide amphiphile was prepared so that the time evolution of the solution could be neglected. Each testing required a sample volume of 1.4 ml. A unidirectional shear rate sweep was used to determine viscosity as a function of shear rate (ranging from 1 to 1000  $\text{s}^{-1}$ ). Amplitude sweeps were performed to determine the linear viscoelastic range. Storage modulus  $G'$  and loss modulus  $G''$  were determined using an oscillatory frequency sweep over the frequency range of  $0.1 \text{ Hz} < \omega < 100 \text{ Hz}$ .

#### **4.2.3 Cryogenic transmission electron microscopy**

Cryogenic transmission electron microscopy (cryo-TEM) was performed to characterize the self-assembled structures of the peptide amphiphiles in buffer before and after rheological testing. Samples for the cryo-TEM measurement were prepared by

putting the peptide amphiphile solutions on lacey carbon grids in a controlled environment vitrification system, which contained saturated water vapor to prevent the evaporation of water from the sample solutions. The samples were then rapidly dropped into liquid ethane kept at its melting temperature (-182°C) before transferring into liquid nitrogen (-196°C). The vitrified samples were mounted on a cryogenic sample holder (Gatan) and examined with a JEOL TEM 1210 at an accelerating voltage of 120 kV at -175°C.

#### **4.2.4 Atomic force microscopy**

Atomic force microscopy (AFM) was performed on samples before and after rheological testing. Samples were deposited on freshly cleaved mica, kept for 10 seconds at room temperature before blowing off any possible small debris on the surface. Experiments were carried out with the D3000 AFM (Digital Instruments, Ltd) in tapping mode.

#### **4.2.5 Circular dichroism**

The peptide secondary structure was studied by circular dichroism (CD) on an Ollis spectropolarimeter. The diluted peptide amphiphile solutions before and after the rheological testing were used for the CD measurements. Data were collected from 190 nm to 250 nm at 1 nm intervals. All reported spectra are the result of averaging three scans.

#### 4.2.6 Infrared spectroscopy

Infrared (IR) spectra were obtained with a Nicolet Magna-IR by the Attenuated Total Reflection (ATR) method. Samples for the IR measurements were dried on a germanium (Ge) plate for one hour at room temperature.

### 4.3 Results

#### 4.3.1 Rheological testing

Figure 4-2 shows the first scan of the viscosity versus shear rate measurement for the C16-W3K solution using unidirectional shear. For shear rates ranging from  $10^0$  to  $10^2 \text{ s}^{-1}$ , the viscosity was constant ( $10^{-3} \text{ Pa s}$ ), near the value for pure water. In this range, viscosity was independent of shear rate; the solution behaved as a Newtonian fluid.<sup>18</sup> At the shear rate of  $10^2 \text{ s}^{-1}$ , an abrupt increase in viscosity was observed, which implies that a phase transition has occurred in the peptide solution. After the critical shear rate, the solution demonstrated shear-thinning behavior, indicating a network formation of entangled fibers. The results show that the micelles change their structure to become wormlike micelles by shear and form entangled networks at the shear rate of  $10^2 \text{ s}^{-1}$ . Figure 4-3 shows the viscosity of the C16-W3K solution at the shear rate ranging from  $10^0$  to  $10^3 \text{ s}^{-1}$  of the first, second and third scans of a single sample. The viscosity of the second cycle increased dramatically, nearly 1000 times higher at the shear rate of  $1 \text{ s}^{-1}$  than the viscosity during the first scan (i.e. initial solution). The third cycle closely reproduces the second one, indicating no further structural change. From these results, it was presumed that the solution irreversibly changed from a very dilute suspension of spherical micelles, rheologically indistinguishable from water, into a highly viscous solution with entangled wormlike micelles, during the rheological

testing.

In Figure 4-4, the results of the oscillatory frequency sweep are shown for the solution before and after the rheological testing. Before the transition, the storage modulus ( $G'$ ) and the loss modulus ( $G''$ ) were too low to be detected, indicating that the liquid behaved as Newtonian fluid. The storage modulus ( $G'$ ) and the loss modulus ( $G''$ ) of the sample after the testing were higher by one-thousand fold to ten-thousand fold than those of the sample before the testing. Above the frequency of 100, the loss modulus became higher than the storage modulus with  $G' \sim \omega^2$  and  $G'' \sim \omega$ , indicating that the sample behaved as viscoelastic liquid. The oscillatory shear presumably lowered the transition frequency of the PA solution, showing viscoelastic features with an obvious correlation between PA, inducing a possible networking caused by the generation of short wormlike structures above the frequency of  $10^0$ . Such transitional structures with the shorter wormlike micelles have already been reported by Shimada et al.<sup>19</sup> After the transition, the storage modulus was constant and higher than the loss modulus throughout the range of frequency, indicating that, at this stage, the solid elastic-like behavior dominated the viscous components. In addition, the modulus was relatively independent of frequency across the range tested, characteristic of a soft networked elastic solid, in this case, a hydrogel. The transition from liquid-like to solid-like structure and properties (a sol–gel transition) derives from the wormlike micelle formation of C16-W3K in the solution, leading to the possible entanglement of the elongated wormlike micelles, which resemble entangled polymers raising the modulus of the solution. It was therefore presumed that the applied shear during the rheological testing induced the transition of the micelle structures in the solution from spherical to wormlike micelles, and thus creating non-Newtonian and gel-like properties.

### 4.3.2 Micellar structures

The micellar structures were analyzed by cryo-TEM and AFM measurements. In the cryo-TEM images, while the C16-W3K solution before the rheological testing (Figure 4-5 (a)) showed no fibril-like structure, the solution after the rheological testing (Figure 4-5 (b)) exhibited many long fibrillar structures, i.e. wormlike micelles.

The results indicate that shear force induced wormlike micelle formation in C16-W3K solution through the rheological testing. In the previous work, it was reported that the wormlike micelle formation of the C16-W3K takes 13 days at 25°C and just short micelles were observed in 3 days in the condition of no external stimuli. In contrast, during the rheological testing, the wormlike micelle formation occurs immediately. Further, in the image of the sample after the testing (Figure 4-5 (b')), some entanglements were observed. The entanglements establish the networks, in which water can be contained, leading abrupt increase in viscosity of the solution after the testing. The cryo-TEM image after the testing supports the results of the rheological testing.

Figure 4-6 shows the AFM result of a sample after the rheological testing. The image confirmed the existence of fibril-like structures. The image of the sample before the testing exhibited just small aggregates and no fibril (data not shown). The critical difference between cryo-TEM and AFM measurements is that the AFM images are obtained under dry conditions. Therefore, the fibrillike structures in the AFM image indicate the wormlike micelles are preserved and stable upon drying of the sample. The high stability of the wormlike micelle is one of the features of our PA micelles, which may be caused by the peptide secondary structure in the peptide region.

### 4.3.3 Peptide secondary structures

CD and IR were used to study the peptide secondary structure in the peptide headgroup. Figure 4-7 shows the CD spectra of the peptide amphiphile solutions measured before (red) and after (blue) the rheological testing. The CD spectrum of the sample before rheological testing exhibited two minima at 204 nm and 222 nm, indicating that initially, the C16-W3K formed  $\alpha$ -helical and random-coil secondary structures in solution. In contrast, the spectrum measured after the rheological testing presented a typical spectrum of the  $\beta$ -sheet structure in the solution, with a single minimum at 218 nm. Thus it was found that the sample experienced a transition in molecular conformation from  $\alpha$ -helical with random coil structures to predominantly  $\beta$ -sheet structures during the rheological testing. IR spectra of the samples before and after the rheological testing are shown in Figure 4-8. The IR absorbance at  $1625\text{ cm}^{-1}$ , which was assigned to the C=O stretch in the  $\beta$ -sheet structure, appears after the rheological testing, indicating the  $\beta$ -sheet formation through the rheological testing. As the IR spectra were measured under dry conditions, this result shows that the  $\beta$ -sheet secondary structure of C16-W3K was also preserved after sample drying.

Through the CD and IR measurements, it was found that, in addition to the wormlike micelle formation, the peptide W3K in C16-W3K simultaneously changed the secondary structure from predominantly  $\alpha$ -helix with random coils to mainly  $\beta$ -sheet during the rheological testing. Our previous work showed that the  $\beta$ -sheet formation also takes days at  $25^{\circ}\text{C}$ . However in this experiment with rheological testing, the secondary structural change occurs in a short time, indicating that the  $\alpha$ -helix and random coil to  $\beta$ -sheet transition in the peptide is also induced by the mechanical shear in the rheological testing. Although some polypeptides have already been reported to



undergo  $\alpha$ -helix to  $\beta$ -sheet transitions triggered by external stimulation such as changes in pH or redox, the microscopic  $\alpha$ -helix to  $\beta$ -sheet transition in polypeptides induced by macroscopic forces such as fluid mechanical shear has not been reported, to our knowledge. Since the direct effect of macroscopic mechanical shear on the peptide secondary structure in the molecular scale cannot be reasonable, it is presumed that the micellar structural change induced by shear triggers the peptide structural change.

#### **4.4 Discussion**

Our peptide amphiphile C16-W3K showed an abrupt increase in viscosity and gelation at certain shear rate during the rheological testing. And the cryo-TEM and AFM images revealed that the macroscopic transition was caused by the wormlike micelle formation and entanglement of the elongated micelles. It is known that some dilute cationic surfactant systems, such as CTAB (hexadecyltrimethylammonium bromide) and CTAT (cetyltrimethylammonium p-toluensulfonate), also exhibit the abrupt increases in viscosity at a critical shear rate during rheological testing and the structures formed under shear have been studied by using small angle neutron scattering with shear, light scattering, birefringence and cryo-TEM.<sup>25-32</sup> In these studies, the common requirements for the surfactant systems are (1) concentration which is very low, but above the CMC, where partially wormlike micelles can be formed and (2) strong electrostatic repulsion in the charged micelles. In our experiments, since the concentration C16-W3K is low but above its CMC and it has three lysines which are positively charged at pH=7.4, our C16-W3K system matches the requirements. The wormlike micelles of other cationic surfactants formed by induction of shear are stable just under the shear stress and disappear again when the shear force is stopped.

However, our results indicate that our PA wormlike micelles remain after shear is removed. Further, the wormlike micelles are also stable when the solution is dried, as seen in AFM measurements. It is presumed that the irreversibility and the high stability of the micelles come from the intermolecular hydrogen bonding in the  $\beta$ -sheet structure of the peptide existing in the micelle shell. The CD and IR results clearly show the new  $\beta$ -sheet formation through the rheological testing. The micelle structure and the peptide secondary structure are determined cooperatively to minimize the whole energy of the system. In some PA systems, induction and stabilization of peptide secondary structures by micelle formation have been reported.<sup>3-8</sup> The micelle formation changes the local environment around the peptides in the PA, affecting the peptide secondary structures. The similar process may happen in our C16-W3K system. The W3K is stable in  $\alpha$ -helix and random coil when the C16-W3K forms spherical micelle. However, when the micelle structure is forced to change by mechanical shear to be wormlike, the peptides may adjust the secondary structure to  $\beta$ -sheet that is most stable in the new environment. Such structural controls may lead to bottom-up designs of mechanically triggered self-assembling systems for various applications. In the field of biomaterials, a hydrogel made of biocompatible nano-fibrils, which can be readily produced with peptide amphiphiles<sup>33,34</sup> can be used as an artificial extracellular matrix for tissue engineering and as a therapeutic injectable gel. In nature, the protein secondary structure is governed by local hydrogen bonding as well as non-local interactions such as hydrophobic and ionic interaction. The dynamic process of protein folding aims to minimize the free energy of the protein by reducing unfavorable interactions. The detailed investigation of the conformational transitions in our designed peptide amphiphile may well provide useful information about how mechanical force influence protein folding in nature.

## **4.5 Conclusion**

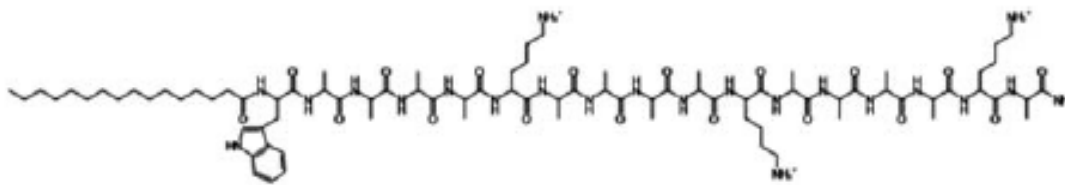
In this work, a novel method to induce multi-scale supramolecular structures in our peptide amphiphile solution through mechanical shear was introduced. The solution changes its viscosity due to the gelation, and at the same time manipulating the second-order structure on a molecular scale. The results should broaden the field of application for self-assembling supramolecular peptides.

## References

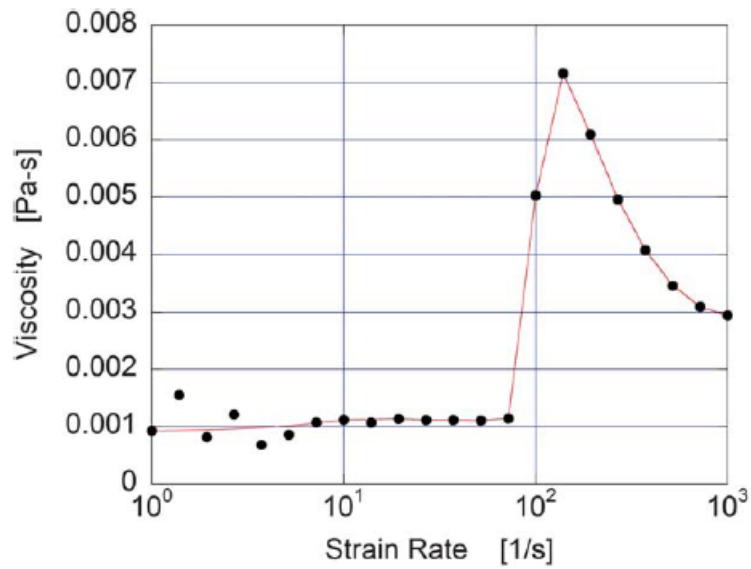
1. Hartgerink, J. D.; Beniash, E.; Stupp, S. I. *Proc. Natl. Acad. Sci. U. S. A.* **2002**, *99*, 5133–5138.
2. Tu, R.; Tirrell, M. *Adv. Drug Delivery Rev.* **2004**, *56*, 1537–1563.
3. Yu, Y. C.; Berndt, P.; Tirrell, M.; Fields, G. B. *J. Am. Chem. Soc.* **1996**, *118*, 12515–12520.
4. Fields, G. B.; Lauer, J. L.; Dori, Y.; Forns, P.; Yu, Y. C.; Tirrell, M. *Biopolymers* **1998**, *47*, 143–151.
5. Yu, Y. C.; Roontga, V.; Daragan, V. A.; Mayo, K. H.; Tirrell, M.; Fields, G. B. *Biochemistry* **1999**, *38*, 1659–1668.
6. Pakalns, T.; Haverstick, K. L.; Fields, G. B.; McCarthy, J. B.; Mooradian, D. L.; Tirrell, M. *Biomaterials* **1999**, *20*, 2265–2279.
7. Forns, P.; Lauer-Fields, J. L.; Gao, S.; Fields, G. B. *Biopolymers* **2000**, *54*, 531–546.
8. Malkar, N. B.; Lauer-Fields, J. L.; Juska, D.; Fields, G. B. *Biomacromolecules* **2003**, *4*, 518–528.
9. Dori, Y.; Bianco-Peled, H.; Satija, S. K.; Fields, G. B.; McCarthy, J. B.; Tirrell, M. *J. Biomed. Mater. Res.* **2000**, *50*, 75–81.
10. Berndt, P.; Fields, G. B.; Tirrell, M. *J. Am. Chem. Soc.* **1995**, *117*, 9515–9522.
11. Winger, T. M.; Ludovice, P. J.; Chaikof, E. L. *Biomaterials* **1996**, *17*, 437–441.
12. Tu, R. S.; Marullo, R. M.; Pynn, R.; Bitton, R.; Bianco-Peled, H.; Tirrell, M. V. *Soft Matter* **2010**, *6*, 1035–1044.
13. Missirlis, D.; Farine, M.; Kastantin, M.; Ananthanarayanan, B.; Neumann, T.; Tirrell, M. V. *Bioconjugate Chem.* **2010**, *21*, 465–475.
14. Zhang, S. *Nat. Biotechnol.* **2003**, *21*, 1171–1178.

15. Hartgerink, J. D.; Beniash, E.; Stupp, S. I. *Science* **2001**, *294*, 1684–1688.
16. Paramonov, S. E.; Jun, H. W.; Hartgerink, J. D. *J. Am. Chem. Soc.* **2006**, *128*, 7291–7298.
17. Kern, F.; Lequeux, F.; Zana, R.; Candau, S. J. *Langmuir* **1994**, *10*, 1714–1723.
18. Mezger, T. *The Rheology Handbook: For Users of Rotational and Oscillatory Rheometers*, Vincentz Network, Hanover, Germany, **2006**.
19. Shimada, T.; Lee, S.; Bates, F. S.; Hotta, A.; Tirrell, M. *J. Phys. Chem. B* **2009**, *113*, 13711–13714.
20. Marqusee, S.; Baldwin, R. L. *Proc. Natl. Acad. Sci. U. S. A.* **1987**, *84*, 8898–8902.
21. Marqusee, S.; Robbins, V.; Baldwin, R. L. *Proc. Natl. Acad. Sci. U. S. A.* **1989**, *86*, 5286–5290.
22. Sargeant, T. D.; Guler, M. O.; Oppenheimer, S. M.; Mata, A.; Satcher, R. L.; Dunand, D. C. *Biomaterials* **2007**, *29*, 161–171.
23. Hosseinkhani, H.; Hosseinkhani, M.; Khademohosseini, A.; Kobayashi, H.; Tabata, Y. *Biomaterials* **2005**, *27*, 5836–5844.
24. Mart, R. J.; Osborne, R. D.; Stevens, M. M.; Ulijn, R. V. *Soft Matter* **2006**, *2*, 822–835.
25. Walker, L. M. *Curr. Opin. Colloid Interface Sci.* **2001**, *6*, 452–456.
26. Berret, J. F.; Corrales, R. G.; Oberdisse, J.; Walker, L. W.; Lindner, P. *Europhys. Lett.* **1998**, *41*(6), 677–682.
27. Ohlendorf, D.; Interthal, W.; Hoffmann, H. *Rheol. Acta* **1986**, *25*, 468–486.
28. Wunderlich, I.; Hoffmann, H.; Rehage, H. *Rheol. Acta* **1987**, *26*, 532–542.
29. Oda, R.; Panizza, P.; schmutz, M.; Lequeux, F. *Langmuir* **1997**, *13*, 6407–6412.
30. Mackintosh, C. F.; Safran, A. S.; Pincus, A. P. *Europhys. Lett.* **1990**, *12*, 697–702.
31. Truong, M. T.; Walker, L. M. *Langmuir* **2002**, *18*, 2024–2031.

32. Liu, C.; Pine, D. J. *Phys. Rev. Lett.* **1996**, *77*, 2121–2124.
33. Kokkoli, E.; Madrilovich, A.; Wedekind, A.; Rexeisen, E. L.; Garg, A.; Craig, J. A. *Soft Matter* **2006**, *2*, 1015–1024.
34. Hamley, W. *Soft Matter* **2011**, *7*, 4122–4138.

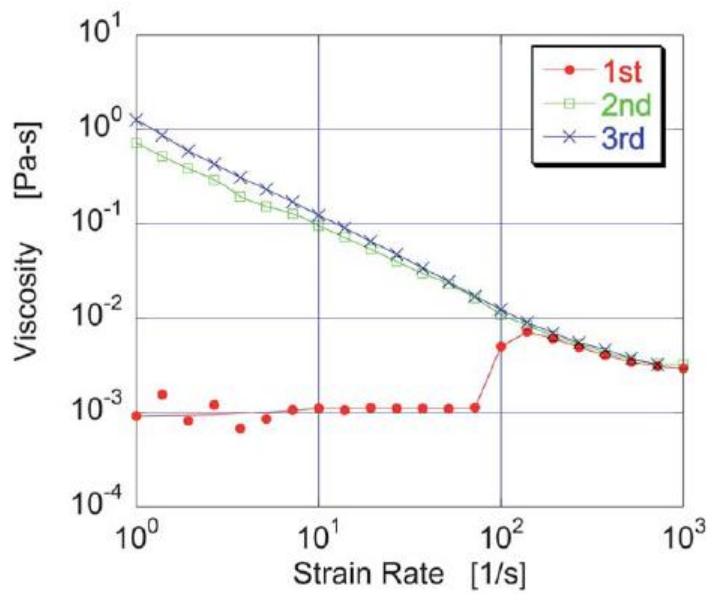


**Figure 4-1.** Synthetic peptide amphiphile C16-W3K.

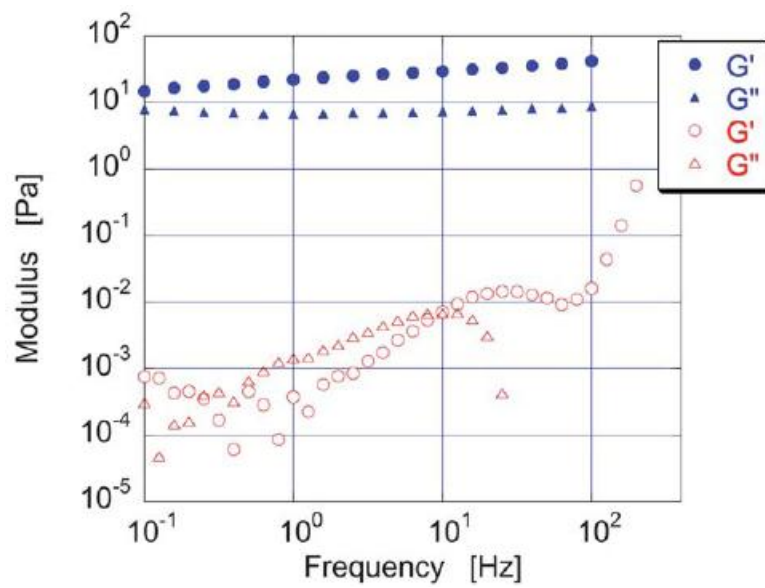


**Figure 4-2.** The viscosity of the C16-W3K solution as a function of strain rate measured by rheology. A rapid increase in viscosity was found at the strain rate of 100 s<sup>-1</sup>.

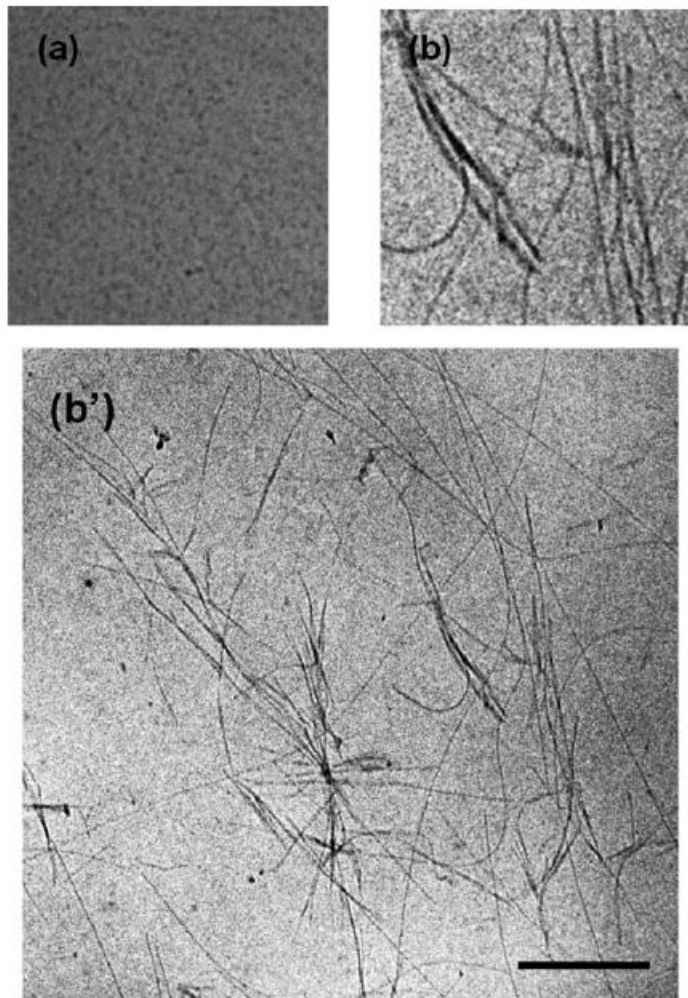




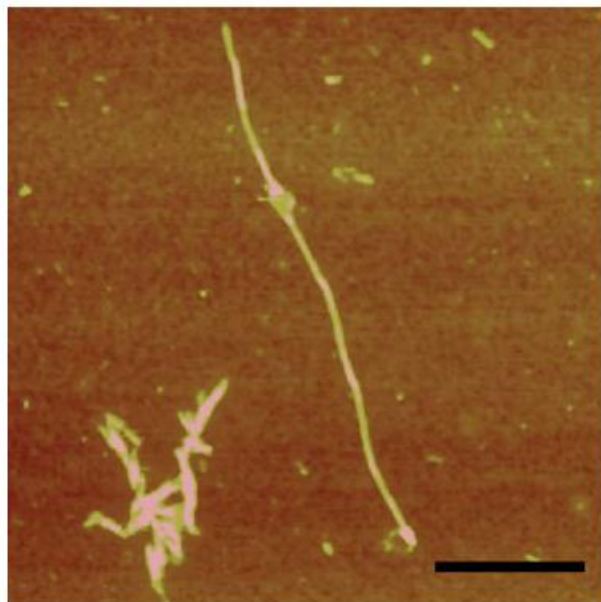
**Figure 4-3.** Viscosity measurements of the C16-W3K solution in the first, second and third cycles of testing from one sample. The abrupt transition was observed only during the first cycle. The succeeding two cycles almost traced the same viscosity line. The viscosity of the second and the third cycles increased by nearly 1000 times at a strain rate of  $1 \text{ s}^{-1}$ .



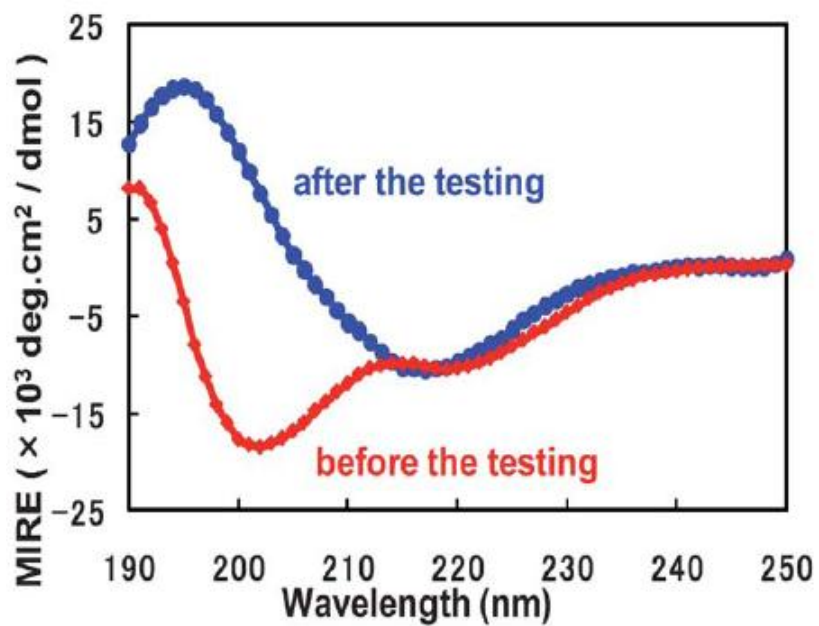
**Figure 4-4.** Oscillatory testing of C16-W3K solutions before (open symbols) and after (closed symbols) the transition was induced by the simple shear test.



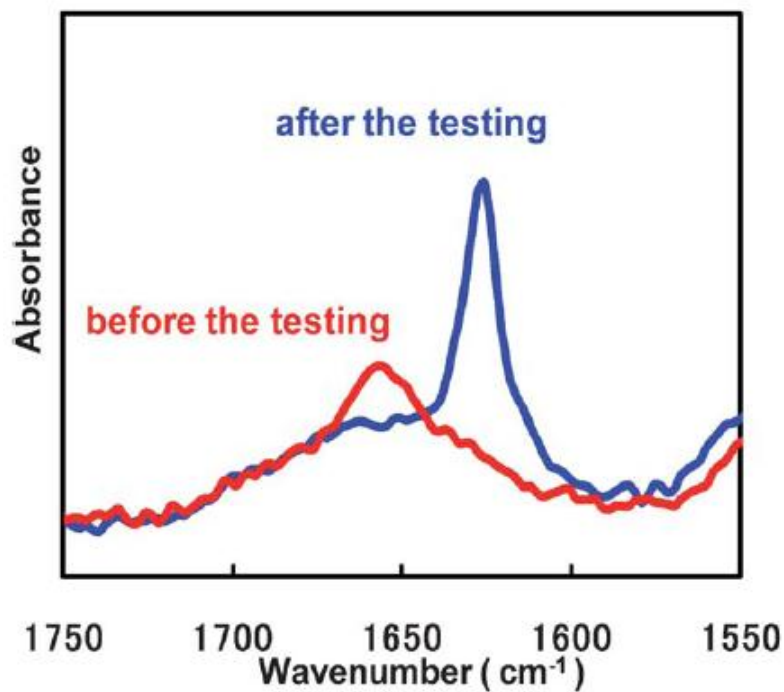
**Figure 4-5.** Cryo-TEM images of PA solution (a) before and (b) after the rheological testing. The sides of (a) and (b), and the scale bar in (b') represents 500 nm.



**Figure 4-6.** AFM image of the dried C16-W3K solution on mica after the rheological testing. The scale bar in the figure represents 500 nm.



**Figure 4-7.** The CD spectra of the C16-W3K solution measured before the rheological testing (red) and after the rheological testing (blue). The red curve has its peaks at 204 nm and 222 nm representing  $\alpha$ -helical and random coil structures and the blue curve has its peak at 218 nm representing the  $\beta$ -sheet structure.



**Figure 4-8.** The IR spectra of C16-W3K solutions before the rheological testing (red) and after the rheological testing (blue). The IR absorbance peak at 1625 cm<sup>-1</sup> indicates the  $\beta$ -sheet structure.

## **Chapter 5**

### **Disassembly of Peptide Amphiphile Wormlike Micelles Induced by Trifluoro Ethanol**

## 5.1 Introduction

The wormlike micelles of peptide amphiphiles (PA) are actively studied for the potential applications, especially in biological and medical fields. Artificial scaffold in regenerative medicine is one of the most attractive applications for the PA wormlike micelles <sup>1, 2, 3</sup>. Recently, further applications of PA wormlike micelles including bio-modification of metal for implantable medical devices <sup>4</sup>, carriers for drugs and carbon nanotubes <sup>5,6</sup>, and molecular recognition for bio-sensing <sup>7</sup> came under the spotlight. For these applications, reversible control of the micelle formation is crucial because dissociation of the micelle enable release of the inclusions, such as drugs, from the micelles and change of surface bio-activity at an appropriate timing. However, because the PA wormlike micelles are generally stable due to the intermolecular hydrogen bonding in the peptide shell, the PA wormlike micelles could not be dissociated by dilution of the solution to a concentration below the critical micelle concentration or by drying up the solvent from the sample solution.

Here, 2,2,2-trifluoroethanol (TFE) was chosen as a candidate of an agent that would induce dissociation of the wormlike micelles by breaking the intermolecular hydrogen bonding because TFE is known to induce and/or stabilize  $\alpha$ -helical structure in peptides and proteins that have an intrinsic propensity to form  $\alpha$ -helical structure (intramolecular hydrogen bonding) in aqueous media <sup>8-12</sup>. For example, TFE was used to analyze the intermediate state of protein folding in  $\beta$ -lactoglobulin <sup>10</sup>. Though  $\beta$ -lactoglobulin consists mainly of  $\beta$ -sheet structure in native state, it changed the peptide secondary structure from  $\beta$ -sheet to  $\alpha$ -helix by adding TFE to the solvent.



It was already reported by us that our designed PA (C16-W3K), containing an alanine-based peptide head-group (WAAAKKAAAKKAAAKA : W3K), formed wormlike micelles gradually with incubation time, coincidentally with the change of peptide secondary structure from  $\alpha$ -helix to  $\beta$ -sheet<sup>13</sup>. The secondary structure and micellar structure changes were irreversible because the wormlike micelles were stabilized by the inter-molecular hydrogen bonding in the  $\beta$ -sheet. In this study, the structural changes of the C16-W3K by adding TFE were investigated to achieve the reversible transitions.

Moreover,  $\beta$ -sheet and fibrillar aggregates formation in proteins has been received much attention on the grounds that unsolved serious diseases, such as Alzheimer's disease and mad cow disease. Our results of the study may provide insights about the solution approach for the diseases.

## 5.2 Experimental methods

The peptide amphiphile C16-W3K was synthesized by conjugating the peptide W3K to palmitic acid with modified Fmoc solid phase peptide synthetic methods, followed by purification with reverse-phase HPLC. The initial sample for the study, already forming wormlike micelle with  $\beta$ -sheet structure, was prepared by dissolving the C16-W3K into an aqueous buffer (1 mM sodium phosphate and 10 mM sodium chloride: pH=7.4) and keeping the solution at 50°C for one day. The peptide concentration of the sample was 100  $\mu$ M. Before adding TFE to the solution, the existence of the wormlike micelles and  $\beta$ -sheet structure in the sample were confirmed with atomic force microscopy (AFM) and circular dichroism (CD), respectively. Then, TFE was added to the solution to the TFE concentration between 10 % and 25 % and

the samples were stirred for one day at room temperature before structural analysis with AFM and CD.

## **5.3 Result**

### **5.3.1 Effect of TFE on the peptide secondary structure**

The change of the peptide secondary structure by adding TFE was studied with CD. Figure 5-1 shows the CD results of the solution with 0 %, 10 %, 20 % and 25 % TFE. Before adding TFE (i.e. 0 % TFE), the CD spectrum showed one minimum at 218 nm, indicating that the peptide W3K was forming predominantly  $\beta$ -sheet structure. From the result, the existence of  $\beta$ -sheet in the initial sample was confirmed. Though the spectrum showed minor difference by adding 10 % TFE, the spectrum dramatically changed from one minimum at 218 nm to two minima at 205 nm and 222 nm, that is a typical spectrum for  $\alpha$ -helical structure, as a concentration of TFE increased from 10 % to 20 % and 25 %. The spectrum of the sample with 25 % TFE revealed that C16-W3K form predominantly  $\alpha$ -helical structure in this sample, and the  $\alpha$ -helical content of the 25 % TFE sample was higher than that of the 20 % TFE sample. The results indicate that the 25 % TFE induced the secondary structure change of W3K in C16-W3K from  $\beta$ -sheet to  $\alpha$ -helix, while 10 % TFE was not effective for the peptide transition.

### **5.3.2 Effect of TFE on the micelle structure**

The micelle structural change of PA by adding TFE was studied with using AFM. For the AFM measurement, the solution was deposited on freshly cleaved mica and kept for 20 seconds before blowing off the extra solution. Figure 5-2 (a)-(d) show the AFM images of dried C16-W3K solution with 0 %, 10 %, 20 % and 25 % of TFE.

In the AFM image of the sample without TFE (a), many long fibrils with ~10nm in width were observed. The existence of fibril structures in the AFM image of the dried sample revealed that the fibrillar structure, i.e. wormlike micelles, was stable even after the solution was dried up. The existence of the wormlike micelles in the initial sample was affirmed by the AFM image.

Though the network of the fibrillar structure was still observed at 10 % of TFE (b), the long fibrils disappeared while some shorter ones still existed at the 20 % TFE sample (c). When the concentration of TFE was increased up to 25 %, almost all the fibrils were vanished and some aggregates were observed. The aggregates were presumed to be the aggregates formed from unstable spherical micelles during the process of drying up. On the basis of these AFM results, it is obvious that TFE with the concentration of 25 % can disassemble almost all the wormlike micelles of C16-W3K.

#### **5.4 Discussion**

The CD and AFM results of the TFE-added samples indicated that TFE triggered the conformational change from  $\beta$ -sheet to  $\alpha$ -helix and the dissociation of the wormlike micelles. The effect of TFE concentration on the peptide conformational transition and the dissociation of micelles have a same tendency that more than 20 % TFE is effective to these changes. The simultaneous changes of peptide conformation in the W3K and micelle structure of C16-W3K may suggest the significant correlation between  $\beta$ -sheet structure and worm-like micelles. Paramonov et al. has studied a role of hydrogen bonding in PA self-assembly into wormlike micelles with a series of N-methylated PA derivatives, demonstrating the importance of  $\beta$ -sheet hydrogen bonding in the closest amino acids of the micelle core for wormlike micelle formation<sup>14</sup>.

Our results showing a strong correlation between  $\beta$ -sheet and wormlike micelles may be another clear evidence that demonstrates the importance of  $\beta$ -sheet hydrogen bonding in the peptide head-group for PA wormlike micelle formation.

The effect of TFE has been explained partly by decreased polarity of a solvent that weakens the hydrophobic interaction (non-local). In the environment, secondary structures of peptides are mainly determined by local hydrogen bonding. Therefore, the result that TFE induced the  $\beta$ -sheet to  $\alpha$ -helix transition in our PA indicated that the peptide W3K has a propensity to form  $\alpha$ -helical structure when it is organized by only a local interactions and the  $\beta$ -sheet structure of our PA was based on non-local hydrophobic interaction among alkyl tails. In other words, it may demonstrate that the alkyl tails of the PA play a significant role in provoking  $\beta$ -sheet formation as discussed before.

As for the TFE concentration, CD and AFM results showed that 20 % and 25 % TFE were much more effective than 10 % TFE to trigger the transitions. The similar result, indicating the effectiveness of around 20 % TFE for the  $\beta$ -sheet to  $\alpha$ -helix transition, has been reported on  $\beta$ -lactoglobulin and on melittin by Goto et al.<sup>10,11</sup>. They presumed the reason for the TFE's unexpectedly high potential for inducing and stabilizing the  $\alpha$ -helical structure at this concentration is the existence of TFE cluster. The TFE cluster in water was studied by Kuprin et al. with small angle X-ray scattering and the examination has shown that TFE forms micelle-like clusters with a maximum at about 30 %<sup>15</sup>. Goto et al. suggested that the clustering of TFE is an important factor enhancing the effects of TFE and the concentration slightly below the concentration where TFE form clusters is the most effective<sup>10,11</sup>.

Recently, it was reported that TFE also induced amyloid-fibril formation and the same concentration (around 20 %) was effective in this case<sup>16</sup>. It is interesting that TFE induces both fibril de-formation of a PA wormlike micelles and fibril formation of amyloid fibrils. It was presumed that in our PA wormlike micelles, because the defective clusters of hydrophobic TFE molecules provided a local relatively less-polar environment that weakens hydrophobic interactions and strengthens local hydrogen bonding, the inter-molecular hydrogen bonding in  $\beta$ -sheet were substituted by intra-molecular hydrogen bonding in  $\alpha$ -helical structure, resulting in the de-formation of the wormlike micelles. On the other hand, the hydrophobic interaction between the TFE defective cluster and the hydrophobic region of an amyloid protein may facilitate the gathering of hydrophobic region of the amyloid protein, resulting in acceleration of the fibril formation.

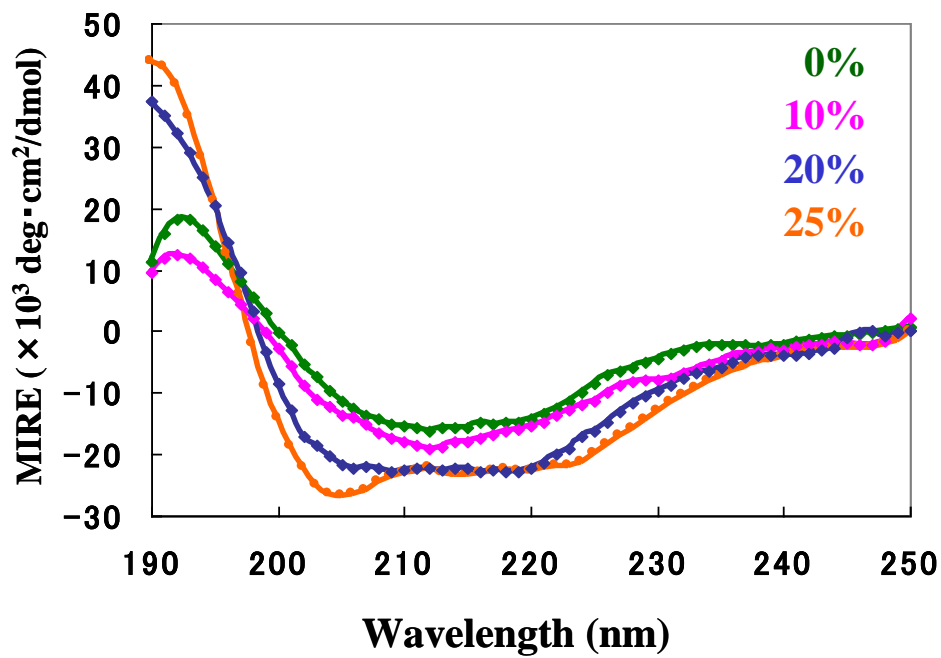
## **5.5 Conclusion**

The results in this work clearly show that 25% TFE induce the dissociation of the PA wormlike micelles and the peptide transition from  $\beta$ -sheet to  $\alpha$ -helix. The dissociation of the wormlike micelles of the peptide amphiphile would expand the potential applications of the PA wormlike micelles as intelligent carriers and surface modification that can be controlled by specific external stimuli. The system would also become a good model to understand the mechanism of the structural changes of proteins.

## References

1. Beniash, E.; Hartgerink, J. D.; Storrie, H.; Stendahl, J. C.; Stupp, S. I. *Acta Biomaterialia* **2005**, *1* (4), 387-397.
2. Jun, H. W.; Paramonov, S. E.; Dong, H.; Forraz, N.; McGuckin, C.; Hartgerink, J. D. *J. Biomater. Sci. Polym. Ed.* **2008**, *19* (5), 665-676.
3. Silva, G. A.; Czeisler, C.; Niece, K. L.; Beniash, E.; Harrington, D. A.; Kessler, J. A.; Stupp, S. I. *Science* **2004**, *303* (5662), 1352-1355.
4. Sargeant, T. D.; Rao, M. S.; Koh, C. Y.; Stupp, S. I. *Biomaterials* **2008**, *29* (8), 1085-1098.
5. Kim, J. K.; Anderson, J.; Jun, H. W.; Repka, M. A.; Jo, S. *Mol. Pharmaceutics* **2009**, *6* (3), 978-985.
6. Arnold, M. S.; Guler, M. O.; Hersam, M. C.; Stupp, S. I. *Langmuir* **2005**, *21* (10), 4705-4709.
7. Mata, A.; Hsu, L.; Capito, R.; Aparicio, C.; Henrikson, K.; Stupp, S. I. *Soft Matter* **2009**, *5* (6), 1228-1236.
8. Shiraki, K.; Nishikawa, K.; Goto, Y. *J. Mol. Biol.* **1995**, *245*, 180-194.
9. Hirota, N.; Mizuno, K.; Goto, Y. *Protein Sci.* **1997**, *6*, 416-421.
10. Hong, D-P; Hoshino, M.; Kuboi, R.; Goto, Y. *J. Am. Chem. Soc.* **1999**, *121*, 8427-8433.
11. Luo, P.; Baldwin, L. *Biochemistry* **1997**, *36*, 8413-8421.
12. Povey, J. F.; Smales, C. M.; Hassard, S. J.; Howard, M. J. *J. Struct. Biol.* **2007**, *157*, 329-338.
13. Shimada, T.; Lee, S.; Bates, F.; Hotta, A.; Tirrell, M. *J. Phys. Chem. B* **2006**, *113*, 13711-13714.

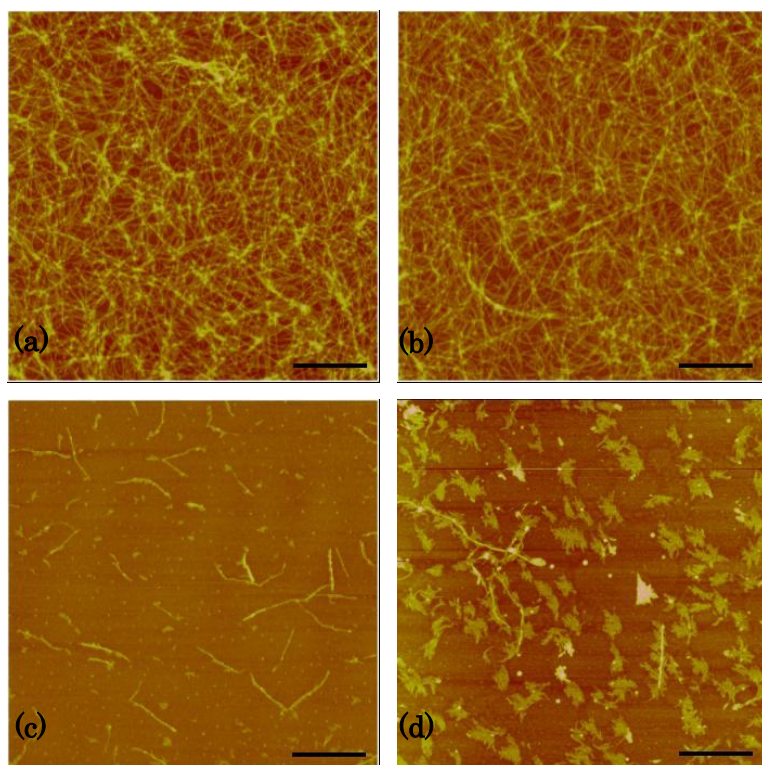
14. Paramonov, S. E.; Jun, H. W.; Hartgerink, J. D. *J. Am. Chem. Soc.* **2006**, *128*, 7291-7298.
15. Kuprin, S.; Graslund, A.; Ehrenberg, A.; Koch, M. H. *J. Biochem. Biophys. Res. Commun.* **1995**, *217*, 1151-1156.
16. Yamaguchi, K.; Naiki H.; Goto, Y.; *J. Mol. Biol.* **2006**, *363*, 279–288.



**Figure 5-1.** CD spectra on C16-W3K solution with 0 %, 10 %, 20 %, 25 % of TFE.

The CD spectra changed by adding TFE to the sample solution.





**Figure 5-2.** AFM images of the dried C16-W3K solution on mica with 0% (a), 10% (b), 20% (c) and 25% (d) of TFE. Scale bar, 1  $\mu\text{m}$ . TFE with the concentration of 25 % disassembled almost all the wormlike micelles of C16-W3K.

## **Chapter 6**

# **A Novel Method of Silica Nanotubes by Utilizing Self-Assembly and Disassembly of Peptide Amphiphiles**

## 6.1 Introduction

Silica nanotubes have received broad attention due to the potential applications not only in catalysis but also in medical and biological fields, such as DNA sensing<sup>1</sup> and drug-carriers,<sup>2</sup> by modifying the outer surface and by encapsulating functional molecules in the inner pore. For these applications, control of the microstructure and bio-modification of the surfaces of nanotubes are important. Silica nanotubes are normally prepared from soluble silica species by so-called templating method by using collagen fibers,<sup>3</sup> organic gel filaments,<sup>4,5</sup>  $\beta$ -sheet peptides,<sup>6,7</sup> etc., as rod-like templates. However, because calcination around 500-600°C is required to remove such organic templates, all the organic components are burn off and the microstructures of silica tubes are varied. Therefore, milder methods for removing templates are required in order to make good use of the organic components and silica microstructures.

Here a new soft preparative method of silica nanotubes by utilizing self-assembly and disassembly of peptide amphiphiles (PA) is proposed. PA are surfactants that have peptide chains in the hydrophilic regions, and some of the PA are known to self-assemble into wormlike micelles.<sup>8-12</sup> Wormlike micelles of PA with homogeneous and tunable diameter have peptides on the surface that can form secondary structures ( $\alpha$ -helix,  $\beta$ -sheet, etc.) and exhibit bioactivity. Consequently, the micelles are well-suited as templates for preparing silica nanotubes. More importantly, self-assembled templates can be softly removed by disassembly.

Recently, Yuwano et al. reported the preparation of silica nanotubes with PA templates having lysines or histidines.<sup>13</sup> In the study, they found that any catalyst is not required in the system because the amine moieties in lysines or histidines work as a

catalyst for hydrolysis and condensation of silicon alkoxides. Though their study has exhibited advantages of PA micelles as templates, calcination was inevitably conducted in the process to remove PA wormlike micelles. Generally, PA wormlike micelles are structurally stable as compared to wormlike micelles of conventional surfactants because the  $\beta$ -sheet structure, based on intermolecular hydrogen bonding, stabilizes micelle structures. Thus, it is difficult to dissociate the wormlike micelles by increasing temperature of micelle solutions or adding alkyl alcohols to remove templates.

It has been found that 2,2,2-trifluoroethanol (TFE) disassemble the wormlike micelles of peptide amphiphile C16-W3K by changing the peptide secondary structure from  $\beta$ -sheet to  $\alpha$ -helix.<sup>14</sup> C16-W3K, consisting of a C16 alkyl tail and a peptide W3K [WAAAAKAAA KAAA KA] (W: tryptophan, A: alanine, and K: lysine) that has a high  $\alpha$ -helical propensity,<sup>15</sup> has been reported to form wormlike micelles in an aqueous buffer solution with forming a  $\beta$ -sheet structure, as reported by us.<sup>16</sup> Because C16-W3K has three lysines, that can act catalytically, and forms wormlike micelles at physiological pH (pH=7.4), it is expected to be an ideal template for preparation of silica nanotubes. In addition, the slow speed of the micelle formation, which is characteristic of C16-W3K, facilitates the control of the wormlike micelles. If the template can be removed by disassembly of wormlike micelles by TFE, preparation of silica nanotubes without calcination should be achieved.

## 6.2 Experimental methods

The peptide amphiphile C16-W3K was synthesized by Scrum Inc. by covalently bonding of the peptide W3K to the alkyl tail of C16. The molecular weight of the C16-W3K was verified by MALDI-TOF mass spectrometry. Here a new method

for the preparation of silica nanotubes by utilizing self-assembly and disassembly of C16-W3K was proposed as shown in Scheme 6-1. Step (i) is the formation process of C16-W3K wormlike micelles, and step (ii) depicts the preparation of wormlike micelles coated with silica by hydrolysis and condensation of silica precursors. Step (iii) shows the process for removing the C16-W3K wormlike micelle template.

As the first step of the process, the templates of the wormlike micelles were prepared. The template samples were prepared by adding C16-W3K to a buffer solution (pH=7.4) at a peptide concentration of about 125  $\mu$ M, and subsequently by incubating the solution at 50°C for 1, 2, 5, 10, and 20 min to get short wormlike micelles. Networking of long wormlike micelles causes the gelation of the PA solution, which makes it difficult to mix PA and silica precursors homogeneously. Short micelles are eligible to prepare detached silica nanotubes which are appropriate for the characterization. Because wormlike micelles of C16-W3K elongate with incubation time, the length of the wormlike micelle can be controlled by changing the incubation time. At the second step, Tetramethoxysilane (TMOS) was added to the solutions immediately after the incubation at 50°C and the mixtures were stirred at room temperature for two days. TMOS was chosen as a silica precursor because of its high hydrolysis rate. Neither acid nor base catalyst was added and the molar ratio of TMOS to C16-W3K was 1, 2, 3, 5, and 20. As the final step to prepare silica nanotubes, TFE was added to the solution to remove the templates. The concentration of TFE employed in solutions was 25%, because the value is most effective to dissociate C16-W3K wormlike micelles, as reported previously.<sup>14</sup> The solution was stirred for one day at

room temperature. When the solution was left for a while after centrifugation, glittering precipitates were obtained in the solution.

### 6.3 Results and discussion

Resultant structures of the samples after the step (ii) were observed with transmission electron microscopy (TEM) without staining. The image of only the sample, prepared with C16-W3K incubated for 10 min and at the TMOS/PA molar ratio of one, shows mainly fibrous structures with a diameter of ~40 nm (Figure 6-1 (a)). The fibrous materials have no branch and have uniform diameter. A small amount of membrane-like materials, presumed to be extra C16-W3K, were observed among the fibrils. The fibrous materials were presumed to be wormlike micelles coated with silica judging from its diameter. The images of the samples prepared with C16-W3K incubated for 1 min, 2 min, and 5 min show inhomogeneous structures including aggregated structures and very short fibrils. The sample with C16-W3K incubated for 20 min was too viscous to mix the PA with TMOS homogeneously. Consequently, incubation time of 10 min is appropriate to prepare the templates of C16-W3K wormlike micelles. In the TEM images of the samples that have higher TMOS/PA molar ratios than one under the same incubation time (10 min), not only fibrous silica but also aggregated silica was observed. Figure 6-1 (b) shows the TEM image of the sample (TMOS/PA = 3). Because it is difficult to isolate the wormlike micelles coated with silica from the mixture, the TMOS/PA molar ratio of one was found to be suitable for the process. Even though C16-W3K was incubated only for 10 min before adding TMOS, the length of the fibrils was longer than 200 nm. This suggests that the PA wormlike micelles were elongated during the condensation of hydrolyzed species of

TMOS due to the neutralization of the negatively charged hydrolysed TMOS and positively charged lysines in the W3K at the ends of the micelles. Though the incubation at 50°C was applied here to make wormlike micelles, it has been found that C16-W3K also form wormlike micelles at room temperature, though spending longer than 10 days.<sup>16</sup> Thus, if the appropriate incubation time at room temperature can be found, all the process should be performed at room temperature, which may facilitate establishment of the preparation system for silica nanotubes.

The IR spectrum (KBr disc method) of the precipitates after the step (iii) is shown in Figure 6-2. The IR spectrum shows two characteristic absorption bands at 1105  $\text{cm}^{-1}$  and 1165  $\text{cm}^{-1}$ , assignable to the Si-O-Si stretching vibration. The broad bands at 3400  $\text{cm}^{-1}$  and 950  $\text{cm}^{-1}$  are assigned to SiOH. Though very small sharp bands at 1630  $\text{cm}^{-1}$  and 2930  $\text{cm}^{-1}$  are assigned to C=O and CH<sub>2</sub> in C16-W3K, respectively, the bands should be due to a small amount of C16-W3K that remained on the washed nanotubes. Because the silica coated wormlike micelles are dispersed and can not be isolated from the solution before adding TFE, it is inappropriate to directly compare the IR spectra of the samples before and after adding TFE. The washed sample virtually does not contain C16-W3K inside and outside of the nanotubes because the IR bands due to C16-W3K are so small.

The TEM image of the precipitate (Figure 6-3) shows the fibrils with an outer diameter of about 30~40 nm, judging from the TEM image. In the image at low magnification of the sample (Figure 6-3 (a)), the membrane-like materials of C16-W3K observed in Figure 6-1 (a) vanished and the fibrous materials can be observed more clearly. In the fibrils, the linear areas of a light color with a diameter of ~10 nm were observed (Figure

6-3 (b)). Because the TEM image was taken without staining, it was difficult to determine whether the PA templates were removed or not by the comparison between Figure 6-1 (a) and Figure 6-3. However, as the IR result indicates that the precipitates consist of mainly silica, the fibrils can be regarded as silica nanotubes. Because the inner pore diameter of ~10 nm, observed in the TEM image, roughly corresponds to the diameter of C16-W3K wormlike micelles measured by contrast variation SANS (Small Angle Neutron Scattering),<sup>17</sup> it is reasonable to conclude that silica layers are constructed on the outer surface of PA micelles.

In the process, hydrolyzed TMOS was condensed exclusively on the micellar surface due to the catalytic amino acids of W3K. Because the peptide forms relatively stretched structure ( $\beta$ -sheet) in the shell of the wormlike micelles, it is presumed that the outermost lysine mainly serve as a catalyst. Even though the wormlike micelles were covered with silica before adding TFE, it was surmised that TFE can reach the interior from the ends or through the defects in silica layers and dissociate the PA wormlike micelles. The remarkable effect of TFE on the structural changes is explained by the presence of the hydrophobic TFE clusters.<sup>18-20</sup>

These IR and TEM results described above exhibit that the PA wormlike micelles inside the nanotubes can be removed by adding TFE, and silica nanotubes are prepared successfully without calcination. The TEM image exhibits relatively thicker silica walls if we consider the TMOS/PA ratio. The detailed explanation is not possible but we may propose the following scheme. The PA solution is composed of monomeric PA, PA spherical micelles, and wormlike micelles. The initial hydrolysis and condensation of TMOS may occur randomly. Further condensation of dissolved silica species should preferentially occur on initially deposited silica which is thought to be



mainly located on wormlike micelles because the catalytic lysine sites are denser on wormlike micelles. The control of wall thickness of silica nanotubes prepared with PA templates by changing the molar ratio of PA and TEOS, and volume fraction of ethanol in the solvent has been reported,<sup>21,22</sup> though there are differences between their study and ours in various points including PA types, silica precursor, solvent, and template removal method, etc.

The results of the same procedure with the spherical micelles of C16-W3K in the sample without incubation showed no fibrous or spherical silica formation, which may be caused by the destabilization of the spherical micelles due to the interaction between the peptides and TMOS. It is presumed that stabilization of the micelles by  $\beta$ -sheet is important for the PA templates that are formed by the balance of various interactions.

The new method described here has several advantages including the use of a physiological pH of the solution, no need of catalysts, and an absence of a high temperature process. Further, with this method through mild conditions, relatively expensive peptide amphiphiles can be reused and encapsulated drugs in the self-assembled templates can remain in the silica nanotubes after removing the templates. It is known that silicatein filaments and their subunits govern the enzymatic and structurally controlled synthesis of silica *in vivo* at ambient temperature and at near-neutral pH in a marine sponge,<sup>23, 24</sup> which is similar to our system that the PA wormlike micelles serve as catalytic templates for the formation of silica layers at room temperature and at pH=7.4 *in vitro*. The new preparative method reported here should be also fascinating as a model for understanding the mechanism of biomineralization.

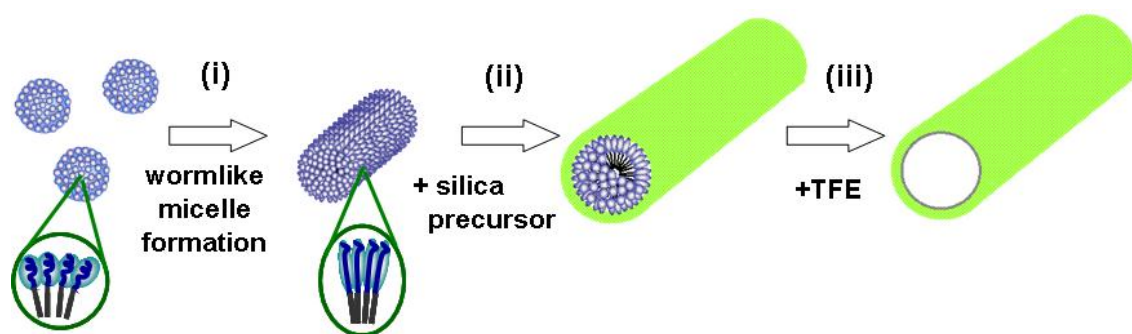
## **6.4 Conclusion**

In conclusion, structural changes of peptide amphiphiles with TFE are utilizable for the preparation of silica nanotubes with avoiding structural deterioration by thermal treatment. Because of the peptide secondary structure in the outer surface of the template and the mild condition of the preparation processes, the resultant silica nanotubes may exhibit structural uniqueness and open up new possibilities for these silica nanotubes in bio-applications.

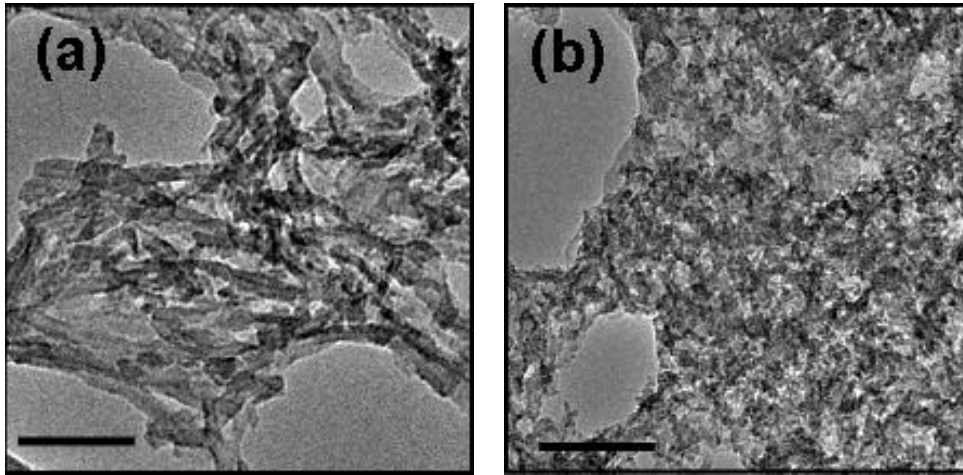
## References

1. Fan, R.; Karnik, R.; Yue, M.; Li, D.; Majumdar, A.; Yang, P. *Nano Lett.* **2005**, *5*, 1633-1637.
2. Martin, C. R.; Kohli, P. *Nat. Rev. Drug Discovery* **2003**, *2*, 29-37.
3. Ono, Y.; Kanekiyo, Y.; Inoue, K.; Hojo, J.; Nango, M.; Shinkai, S. *Chem. Lett.* **1999**, *28*, 475-476.
4. Ono, Y.; Nakashimada, K.; Sano, M.; Kanekiyo, Y.; Inoue, K.; Hojo, J.; Shinkai, S. *Chem. Commun.* **1998**, *14*, 1477-1478.
5. Jung, J. H.; Park, M.; Shinkai, S. *Chem. Soc. Rev.* **2010**, *39*, 4286-4302.
6. Meegan, J. E.; Aggeli, A.; Boden, N.; Brydson, R.; Brown, A. P.; Carrick, L.; Brough, A. R.; Hussain, A.; Ansell, R. J. *Adv. Funct. Mater.* **2004**, *14*, 31-37.
7. Acar, H.; Garifullin, R.; Guler, M. O. *Langmuir* **2011**, *27*, 1079-1084.
8. Hartgerink, J. D.; Beniash, E.; Stupp, S. I. *Science* **2001**, *294*, 1684-1688.
9. Silva, G. A.; Czeisler, C.; Niece, K. L.; Beniash, E.; Harrington, D. A.; Kessler, J. A.; Stupp, S. I. *Science* **2004**, *303*, 1352-1355.
10. Tovar, J. D.; Claussen, R. C.; Stupp, S. I. *J. Am. Chem. Soc.* **2005**, *127*, 7337-7345.
11. Paramonov, S. E.; Jun, H. W.; Hartgerink, J. D. *J. Am. Chem. Soc.* **2006**, *128*, 7291-7298.
12. Hamley, W. *Soft Matter* **2011**, *7*, 4122-4138.
13. Yuwano, V. M.; Hartgerink, J. D. *Langmuir* **2007**, *23*, 5033-5038.
14. Shimada, T.; Tirrell, M. in *Peptide Science 2006*, ed. by H. Mihara, **2007**, p382-383.
15. Marqusee, S.; Robbins, V. H.; Baldwin, R. L. *Proc. Natl. Acad. Sci. U. S. A.* **1989**, *86*, 5286-5290.
16. Shimada, T.; Lee, S.; Bates, F. S.; Hotta, A.; Tirrell, M. *J. Phys. Chem. B* **2009**, *113*, 13711-13714.

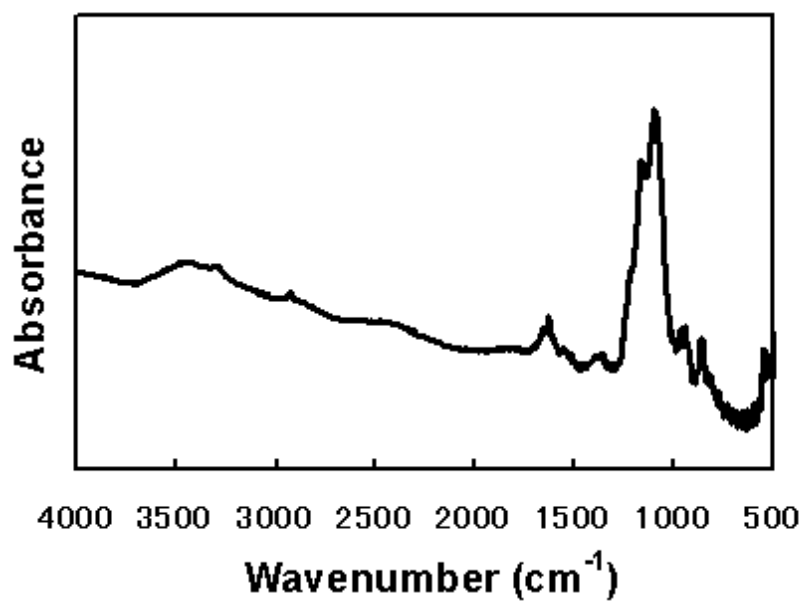
17. Sakamoto, N.; Shimada, T. *Abstracts of Papers, Presented at the Technical Seminar on Industrial Use of Neutrons*, Miraikan, Tokyo, Feb 13, **2008** .
18. Kuprin, S.; Graslund, A.; Ehrenberg, A.; Koch, M. H. J. *Biochem. Biophys. Res. Commun.* **1995**, *217*, 1151-1156.
19. Hong, D-P.; Hoshino, M.; Kuboi, R.; Goto, Y. *J. Am. Chem. Soc.* **1999**, *121*, 8427-8433.
20. Shiraki, K.; Nishikawa, K.; Goto, Y. *J. Mol. Biol.* **1995**, *245*, 180-194.
21. Ji, Q.; Iwaura, R.; Shimizu, T. *Chem. Lett.* **2004**, *33*, 504-505.
22. Ji, Q.; Iwaura, R.; Shimizu, T. *Chem. Mater.* **2007**, *19*, 1329-1334.
23. Shimizu, K.; Cha, J.; Stucky, G. D.; Morse, D. E. *Proc. Natl. Acad. Sci. U. S. A.* **1998**, *95*, 6234-6238.
24. Cha, J. N.; Shimizu, K.; Zhou, Y.; Christiansen, S. C.; Chmelka, B. F.; Stucky, G. D.; Morse, D. E. *Proc. Natl. Acad. Sci. U. S. A.* **1999**, *96*, 361-365.



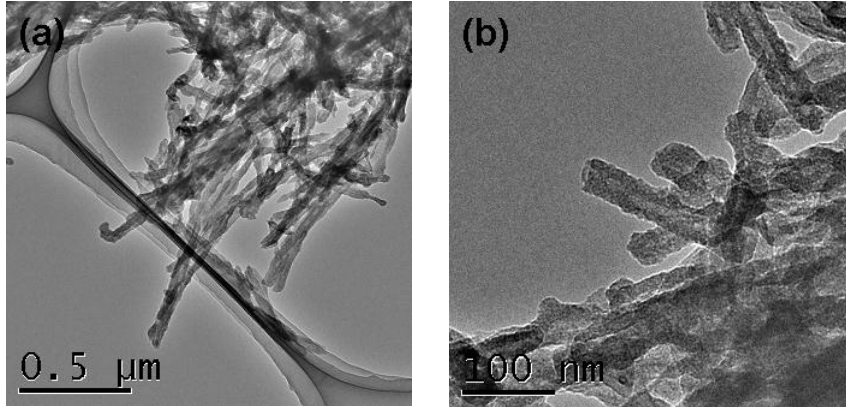
**Scheme 6-1.** Schematic of the formation of silica nanotubes. Step (i) is the formation process of C16-W3K wormlike micelles, and step (ii) depicts the preparation of wormlike micelles coated with silica by hydrolysis and condensation of silica precursors. Step (iii) shows the process for removing the C16-W3K wormlike micelle template by adding TFE to the solution.



**Figure 6-1.** TEM images (without staining) of (a) silica coated C16-W3K incubated for 10 min and the TMOS/PA molar ratio is one and (b) incubated for 10 min and the TMOS/PA molar ratio is three. Scale bar, 100nm.



**Figure 6-2.** IR spectrum of the precipitates after the step (iii).



**Figure 6-3.** TEM images (without staining) of the precipitates (a) at low magnification and (b) at high magnification after the step (iii).



## **Chapter 7**

### **Conclusions and Future prospects**

## 7.1 Conclusions

In this thesis, the author describes the study results on the formation processes of wormlike micelles derived from peptide amphiphiles. In this chapter, important conclusions from this study are summarized.

Chapter 2 describes the study results of the time-dependent changes of peptide secondary structure and micelle structure of newly designed peptide amphiphile C16-W3K [W3K:WAAAAKAAA KAAA KA (W=tryptophan, A=alanine, K=lysine)] in a buffer (pH=7.4) with a circular dichroism (CD), an infrared spectroscopy (IR), a cryo-transmission electron microscopy (cryo-TEM) and an atomic force microscopy (AFM). The results showed that C16-W3K gradually form wormlike micelles in 13 days at 25°C with simultaneously changing the secondary structure from  $\alpha$ -helix and random coil to  $\beta$ -sheet. In addition, the result of dynamic viscoelastic measurement revealed the gelation of the solution with the formation of the wormlike micelles. Since these results exhibit the cooperative progression of wormlike micelle formation and  $\beta$ -sheet formation, it is presumed that  $\beta$ -sheet is one of the key factors for PA to form wormlike micelles. Further, it was found that the hierarchical transitions can be controlled by changing the solution temperature and by modifying the alkyl tail length of PA.

Chapter 3 exhibits the study results of the formation process of C16-W3K wormlike micelles at 50°C with small angle neutron scattering (SANS). The SANS results showed that the transient spherical micelles exist at the early stage of the process and subsequently the micelle chain elongate by attachment of spherical micelles to the ends of growing cylindrical micelles during the wormlike micelle formation. The process presumed from SANS results was supported by the AFM results of the samples

with different incubation time. The intermediate spherical state mainly driven by the hydrophobic interactions of alkyl tails and subsequent  $\beta$ -sheet formation in the shell of the micelles may allow the C16-W3K to form water-soluble wormlike micelle, instead of insoluble fibers.

Chapter 4 shows induction of the wormlike micelle formation of C16-W3K and gelation of the solution by simple mechanical shear. When shear was applied to C16-W3K solution gradually, the solution dramatically underwent gelation at the critical shear rate of about 100 [1/s]. Cryo-TEM and AFM results of the sample after the gelation revealed the wormlike micelle formation, and CD and IR results also showed the  $\beta$ -sheet formation in the sample. The effect of macroscopic mechanical shear on the peptide secondary structure clarifies the strong correlation between  $\beta$ -sheet formation, wormlike micelle formation and gelation.

Chapter 5 describes a new method to dissociate the C16-W3K wormlike micelles by adding 2,2,2-Trifluoroethanol (TFE) that is known to induce the  $\alpha$ -helical structure in some proteins. The wormlike micelles were dissociated by adding TFE with the structural change in the peptide from  $\beta$ -sheet (inter-molecular hydrogen bonding) to  $\alpha$ -helix (intra-molecular hydrogen bonding).

Chapter 6 shows a novel method to prepare silica nanotubes with the catalytic templates of C16-W3K wormlike micelles. In the method, the hierarchical structural changes of PA by addition of TFE were utilized for the preparation of silica nanotubes from silica-micelle complexes with avoiding structural deterioration that is normally caused by thermal treatment. This method is advantageous for the preparation of silica nanotubes because of reusability of peptide template, possible replication of the surface of  $\beta$ -sheet structure, and very mild conditions.

These results in Chapter two to six clearly exhibits the importance of the intermediate spherical micelles mainly driven by the hydrophobic interaction among alkyl tails, and the subsequent  $\beta$ -sheet formation in the peptide shell driven by intermolecular hydrogen bonding for the formation of the PA wormlike micelles. Further, in these studies, the elongation process of the wormlike micelles were presumed and it was shown that the micelle formation can be controlled by the solution temperature, alkyl tail length of PA, mechanical shear and addition of TFE. The findings on the process should be crucial, not only to reach the desired final structural state, but also to achieve desired processability, which lead to advancement in self-assembling materials triggered by specific stimuli for medical applications.

## 7.2 Future prospects

The understanding of the process of the PA wormlike micelle formation could potentially lead to further applications of PA self-assembling materials, including artificial scaffolds, drug carriers, cosmetics, bio-modification and organic/inorganic hybrid materials.

By using this well-organized PA system as a scaffold in regenerative medicine, the mechanism of the cell signaling in the scaffold should become clearer, which enable control of the cell signaling. Mechanically triggered self-assembling systems described in Chapter 4 should be useful as a therapeutic injectable gel.

Another interesting direction of PA applications is the formulation of organic-inorganic hybrid materials with templates of the PA wormlike micelle. Because of the peptide secondary structure and bio-activity of the peptide in the outer surface of the templates, the resultant materials may exhibit structural uniqueness and open up new possibilities of these materials in bio-applications. The PA designed to cleave between a peptide and an alkyl tail has potential to prepare the silica nanotube whose inner surface is totally covered with functional peptide.

In the field of proteomics, self-assembled structures of the biomimetic peptide amphiphiles should be useful model systems for the characterization and elucidation of the biological and physiological phenomena including the correlation between the secondary and tertiary structures of the protein domains and functions. The further investigation on the transitions of hierarchical structures in the peptide amphiphiles should also provide important information about how external stimuli, such as mechanical force and environment change, influence the protein folding in nature.

## List of publications

1. Tomoko Shimada, Naoki Sakamoto, Ryuhei Motokawa, Satoshi Koizumi, Matthew Tirrell. “Self-Assembly Process of Peptide Amphiphile Worm-like Micelles”

*J. Phys. Chem. B*, **116**, 240-243, 2012

2. Tomoko Shimada, Yasuhiro Tamura, Matthew Tirrell, Kazuyuki Kuroda

“A Novel Preparative Method of Silica Nanotubes by Utilizing Self-Assembly and Disassembly of Peptide Amphiphiles”

*Chem. Lett.*, **41**, 95-97, 2012

3. Tomoko Shimada, Katie Megley, Matthew Tirrell, Atsushi Hotta

“Fluid mechanical shear induces structural transitions in assembly of a peptide–lipid conjugate”

*Soft Matter*, **7**, 8856-8861, 2011

4. Tomoko Shimada, Sangwoo Lee, Frank Bates, Atsushi Hotta, Matthew Tirrell

“Wormlike Micelle Formation in Peptide-Lipid Conjugates Driven by Secondary Structure Transformation of the Headgroups”

*J. Phys. Chem. B*, **113**, 13711-13714, 2009

5. Tomoko Shimada, Matthew Tirrell

“Control of the  $\alpha$ -helix to  $\beta$ -sheet Transition and the Self-assembly Structural Change in the Peptide Amphiphile”

*Peptide Science* 2006 ed. by H. Mihara, 382-383, 2007

## Oral Presentations

島田智子、坂本直紀、高田堅介、堀田篤、元川竜平、小泉智

“ペプチド両親媒性分子のひも状ミセル形成プロセスの解析”

第 57 回 高分子学会年会, 横浜 (2008 年 5 月)

島田智子、堀田篤、ティレル マシュー

“ペプチド両親媒性分子の階層構造転移”

第 55 回 高分子討論会, 富山 (2006 年 9 月)

Tomoko Shimada, Atsushi Hotta, Matthew Tirrell

“Fibril Formation on an alanine-based peptide attached to an alkyl tail”

231st National ACS Meeting, Atlanta, USA (March 2006)

Tomoko Shimada, Matthew Tirrell

“ $\alpha$ -Helix to  $\beta$ -Sheet transitions of novel short peptides conjugated to lipids induced by aggregation”

230 th National ACS Meeting, Washington D.C., USA (August 2005)

## **Acknowledgement**

The present dissertation is the collection of the studies which have been carried out under the direction of Prof. Kazuyuki Kuroda, Department of Applied Chemistry at Waseda University and the direction of Prof. Matthew Tirrell, Material Research Laboratory at University of California Santa Barbara. The author expresses the greatest acknowledgement to Prof. Kazuyuki Kuroda, Prof. Matthew Tirrell, Prof. Hiroyuki Nishide, Prof. Yoshiyuki Sugahara and other professors at applied chemistry, Waseda University for all their guidance in the completion of this work. The author admires their passion for chemistry and their personal characters. The author would like to thank everyone in the Prof. Kuroda's Gr. and Prof. Tirrell's group, past and present, for a friendly and supportive research environment.

The author would like to acknowledge and thank Dr. Hotta (Keio University) for his research supports, especially rheological testing, which are very crucial in carrying this research forward.

The author expresses the special thanks to all the collaborators, Dr. Naoki Sakamoto, Dr. Ryuhei Motokawa, Dr. Satoshi Koizumi, Mr. Yasuhiro Tamura, Ms. Katie Megle, Dr. Sangwoo Lee and Prof. Frank Bates.

The author also expresses her sincere gratitude to Asahi Kasei Co. for the financial support.

February, 2012

Tomoko Shimada